Theses and dissertations

1-1-2012

Assessing The Clinical Application Of The Van Herk Margin Formula For Lung Radiotherapy

Gillian Ecclestone
Ryerson University

Recommended Citation

ASSESSING THE CLINICAL APPLICATION OF THE VAN HERK MARGIN FORMULA
FOR LUNG RADIOTHERAPY

By

Gillian Ecclestone

B.M.R.Sc. Medical Radiation Sciences,

McMaster University, 2010

A thesis

presented to Ryerson University

in partial fulfillment of the

requirements for the degree of

Master of Science

in the Program of

Biomedical Physics

Toronto, Ontario, Canada, 2012

© Gillian Ecclestone 2012

Author's Declaration

I hereby declare that I am the sole author of this thesis. This is a true copy of the thesis, including any required final revisions, as accepted by my examiners.

I authorize Ryerson University to lend this thesis to other institutions or individuals for the purpose of scholarly research

I further authorize Ryerson University to reproduce this thesis by photocopying or by other means, in total or in part, at the request of other institutions or individuals for the purpose of scholarly research.

I understand that my thesis may be made electronically available to the public.

Assessing the clinical application of the van Herk margin formula for lung radiotherapy

Master of Science, 2012

Gillian Ecclestone

Biomedical Physics

Ryerson University

ABSTRACT

In radiation therapy treatment planning, margins are added to the tumour volume to ensure that the correct radiation dose is delivered to the tumour in the presence of geometrical uncertainties. The van Herk margin formula (VHMF) was developed to calculate the minimum margin on the target to provide full coverage by 95% of the prescribed dose to 90% of the population. However, this formula is based on an ideal dose profile model that is not realistic for lung radiotherapy. The purpose of this study was to investigate the validity of the VHMF for lung radiotherapy with accurate dose calculation algorithms and respiratory motion modeling. Ultimately, the VHMF ensured sufficient target coverage, with the exception of small lesions in soft tissue; however, the derived PTV margins were larger than necessary. A novel planning approach using the VHMF was tested indicating the need to account for tumour motion trajectory and plan conformity.

Acknowledgments

I would like to sincerely thank my supervisor Dr. Emily Heath for her time, patience and dedication to this project as well as my personal academic development. Her commitment to innovation within the medical physics community is truly inspiring and is something I will strive to emulate for the remainder of my career.

I would also like to thank Dr. Jean-Pierre Bissonnette for agreeing to supervise me at Princess Margaret Hospital where I was provided with the resources required to conduct this thesis project. His invaluable advice and experienced opinion was a key necessity in my success and it was a privilege to work for him.

Special thanks to James Stewart at Princess Margaret Hospital who provided all of my training and technical support for using ORBIT treatment planning software and Dr. Catherine Beauchemin who helped me create the data fitting scripts for this study.

Lastly, I would like to acknowledge the continual support of my family who has provided endless encouragement and kept me well fed throughout the completion of my Masters Degree.

Table of Contents

LIST OF TABLES

LIST OF FIGURES

xii

LIST OF SYMBOLS AND ABBREVIATIONS

VHMF – van Herk Margin Formula

CT – Computed Tomography

GTV – Gross Tumour Volume

CTV – Clinical Target Volume

ITV – Internal Target Volume

PTV – Planning Target Volume

TV – Treated Volume

OAR – Organ at Risk

MLC – Multi leaf collimator

3DCRT – Three Dimensional Conformal Radiation Therapy

IMRT – Intensity Modulated Radiation Therapy

σ – Standard deviation of random geometrical errors

σ_m – Standard deviation of random organ motion

σ_s – Standard deviation of random setup error

$\sum$ – Standard deviation systematic geometrical errors

$\sum_m$ – Standard deviation systematic organ motion

$\sum_s$ – Standard deviation systematic setup error

$\sum_d$ – Standard deviation delineation error

CN – Conformation Number

V_{95} – Volume of the treatment target receiving 95% of the prescribed dose

IV_{95} – Volume of the 95% isodose value

CHAPTER 1

INTRODUCTION AND BACKGROUND

1.1 Introduction to Lung Cancer

It is currently estimated that 40% of Canadian women and 45% of Canadian men will develop cancer in their lifetime[1]. In 2011 alone, the Canadian Cancer Society expected 177 800 new cases of cancer in Canada and 75 000 cancer deaths with over one-quarter of them accredited to lung cancer alone[1]. Lung cancer stems from uncontrolled cell growth of lung tissue that leads to the rapid formation of harmful malignant lesions[2]. It is currently the second most common cancer in Canada and continues to be the leading cause of cancer death for both men and women with a five-year relative survival ratio of only 16%[1].

Lung cancer is separated into two main categories, Non-Small Cell Lung Cancer which is most common and Small Cell Lung Cancer the less common of the two. Both are treated with combinations of surgery, chemotherapy and radiotherapy, depending on the patient's baseline health and stage of disease. People diagnosed with lung cancer often present with many respiratory co-morbidities such as Chronic Obstructive Pulmonary Disease (COPD) and are therefore are not always ideal surgical candidates. Consequently, chemotherapy and radiotherapy (often performed concurrently) are at the forefront of the radical treatment of lung cancer with a curative intent.

1.2 External Beam Radiation Therapy

External beam radiation therapy (EBRT) delivers ionizing radiation to a targeted point within a patient (the tumour) from an external source. The term "dose" or "absorbed dose"

refers to a physical quantity relating the amount of energy imparted by ionizing radiation to a small mass of matter. The unit of dose is the Gray (Gy), where 1 Gy is the absorption of 1 Joule of energy per 1 kg mass of matter. The goal of EBRT is to deliver a high dose of radiation to kill the cancer cells by destroying their DNA while sparing the surrounding normal healthy tissues. Malignant tumour cells specifically have been shown to be very sensitive to the adverse effects of ionizing radiation and are therefore preferentially killed over normal cells in the process.

A radiotherapy treatment regime is administered over several weeks and consists of many daily treatments where a fraction of the total dose is delivered. The dose is fractionated to allow normal cells in the path of the radiation beam time to recover from any repairable radiation induced DNA damage. Repair mechanisms are absent in tumour cells. Thus, fractionation permits for a higher dose to be delivered to the tumour than is possible if the total dose was delivered in one treatment. Radiation doses are chosen specifically to kill the malignant tissue without exceeding the dose tolerances of surrounding normal tissue that will cause severe complications. The prescribed radiation dose also depends on many patient-specific factors such as whether radiation is the primary modality used to treat the cancer, if it is delivered in conjunction with surgery or chemotherapy, the stage of the disease and the baseline health of the patient. A typical dose and fractionation regime for the potentially curative treatment of patients with unresectable Non-Small Cell Lung Cancer is 2 Gy per fraction delivered daily to a total dose of 60–66 Gy. Limited stage Small Cell Lung Cancer patients undergoing radiotherapy receive doses with an upper limit of 40–45 Gy with 1.8–2 Gy delivered per treatment[2].

1.2.1 The Linear Accelerator

The radiation beams used for EBRT are produced by linear accelerators (linacs) as depicted in *Figure 1.1*. Linacs produce high energy x-rays through the radiative interactions of electrons accelerated to high kinetic energies in the range of 4–25 MeV. The electrons are produced by an electron gun and accelerated to their desired speed via an accelerating waveguide. They then enter the treatment head and strike a target of high atomic number, producing the treatment beam which consists of a Bremsstrahlung x-ray spectrum characterized by the nominal accelerating potential[3]. Typical x-ray beam energies employed in lung radiotherapy range from nominal accelerating potentials of 4–10 Megavolts (MV)[4].

Subsequently, the treatment beam is collimated, filtered and monitored within the treatment head of the linac in order to produce a clinically useful radiation beam which delivers a uniform dose distribution at a specified depth in water. The treatment beam is collimated by adjustable jaws in head of the machine plus an extra collimation system at the distal portion of the treatment head consisting of several narrow abutting tungsten leaves. This is required to produce fields or irregular shape. This is termed a Multileaf Collimator (MLC) and will be discussed in further detail in *Section 1.4*

During treatment, the patient is positioned on an adjustable carbon fibre (or other radiolucent material) couch beneath the treatment head of the linac. The treatment head is mounted on a rotational gantry that is capable of moving 360° around the treatment couch in order to treat the patient from multiple angles. The axis of rotation of the gantry, collimator and couch is at a fixed point within the treatment room 100 cm below the target within the treatment head. The intersection of the three axes of rotation is termed the isocentre. Patients

are either positioned so that their skin surface is at the machine isocentre, which is termed a Source-to-Skin Distance (SSD) technique, or so that the isocentre is within the treatment target, which is termed a Source-to-Axis Distance (SAD) technique. Linacs are calibrated by Medical Physicists to deliver a specific radiation dose at the isocentre with a high degree of accuracy and treatment plans are designed around this point. The machine output is measured in monitor units (MU) in which individual machines are calibrated to deliver a specific absorbed dose per MU (usually 1Gy/MU).
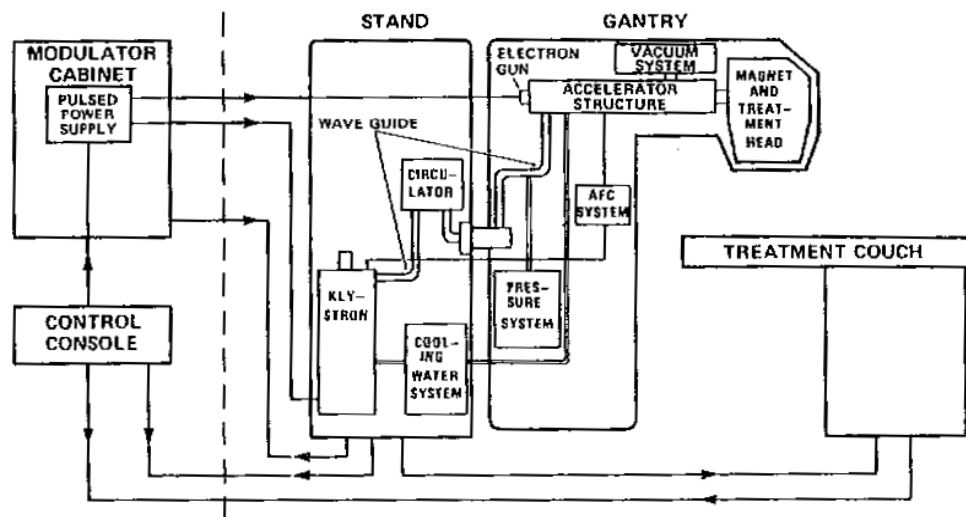
Figure 1.1: Simplified block diagram of the components of a linear accelerator. Taken from Karzmark et al[3].

1.3 The Radiation Therapy Process

The journey from diagnosis to the radiation therapy treatment room requires much planning and many steps involving many healthcare professionals. After a cancer diagnosis and the decision to treat with radiation has been made the patient undergoes the first step of treatment planning which is termed "treatment simulation". In this step, the diseased area is imaged and localized for treatment plan design.

4

Simulation employs Computed Tomography (CT) to build a computer model of the patient. In this step, the treatment position and any treatment accessories required for patient comfort and immobilization are chosen and documented by the simulator staff. Although the specific treatment position is subject to the mobility of the patient, typical radical lung treatments require the patient to be in a supine position with their arms above their head.

The patient is then positioned on the CT simulator couch in their treatment position. A CT scan is acquired for tumour localization in the chosen position. After the tumour is localized on the CT scan, permanent marks (tattoos) are placed on the patient skin along two orthogonal axes that intersect at the center of the tumour. These marks are used to guide the positioning of the patient for treatment and to ensure that the isocentre of the linac is aligned with the center of the treatment target each day.

Once the CT simulation stage is complete, the three dimensional (3D) CT dataset is imported into specialized treatment planning software where the CT images are segmented to delineate the tumour and surrounding organs, the treatment beams are placed on the patient and the dose to the tumour and surrounding anatomy is calculated. In this stage, treatments are designed to ensure that an optimal dose distribution within the patient is achieved. Current treatment planning software uses complex dose calculation algorithms that accurately model the dose deposition process to calculate the dose within the patient based on tissue attenuation information provided by the CT image.

It should be noted that the dose grid is set by the treatment planner and is independent of the CT dataset in terms of resolution and location. A fine dose grid gives more accurate

spatial resolution, in terms of dose display however there is a trade-off between high resolution and computation time[5].

1.3.1 Treatment Planning and ICRU Criteria

In 1993, the International Commission on Radiation Units and Measurements (ICRU) issued report number 50 (ICRU-50)[6], titled "Prescribing, Recording, and Reporting Photon Beam Therapy". This was followed by report number 62 (ICRU-62)[7] as a supplement to ICRU-50 in 1999. The goal of these reports is to ensure consistency in specifying and reporting radiation doses in radiation therapy to provide meaningful data for assessing the results of treatments. Thus, the ICRU-50 and ICRU-62 reports instil a worldwide standard for radiation therapy treatments. They provide guidelines to promote the use of a common language for specifying and reporting the doses in radiation therapy, as well as the volumes in which they are prescribed.

The volumes which need to be identified prior to the construction of any radiotherapy treatment plan depicted in *Figure 1.2* are defined to ensure that the entire tumour receives a high and uniform dose while sparing dose to the surrounding normal tissue. The first of crucial target volume to be defined is the "Gross Tumour Volume" (GTV) which is described by ICRU-50 as *"The gross palpable or visible/demonstrable extent and location of malignant growth."*[6] In other words, the GTV is the visible primary tumour and any bulky disease that is observed. GTV volumes can be based on prior diagnostic and functional imaging such as CT, magnetic resonance imaging (MRI), positron emission tomography (PET) and ultrasound as well as pathology reports and clinical examination[2].

The second target volume, termed the "Clinical Target Volume" (CTV), is defined by the ICRU as *"the tissue volume that contains a demonstrable GTV and/or sub-clinical microscopic malignant disease, which has to be eliminated. This volume thus has to be treated adequately in order to achieve the aim of therapy, cure or palliation."*[6] Therefore, the CTV is created by adding a margin determined by the radiation oncologist to the GTV to account for any microscopic extension of the disease into the surrounding normal tissue. The width of the margin added to the GTV for lung radiation therapy is dependent on many patient specific factors such as the diagnosis and stage of the diseases, and is usually around 5-8mm[2].

The final target volume for which the treatment plans are designed around is termed the "Planning Target Volume" (PTV). The PTV is a geometrical concept described by ICRU-50 to help *"select appropriate beam arrangements, taking into consideration the net effect of all possible geometrical variations, in order to ensure that the prescribed dose is actually absorbed in the CTV"*[6]. Thus, a margin is added on to the CTV to account for positional uncertainties of the CTV that may occur during treatment due to internal organ motion or slight positional variations from the treatment plan. As per ICRU-62, the PTV margin contains the Internal Margin (IM) which accounts for internal physiological movements and variations in size, shape and position of the CTV during treatment, plus a Setup Margin (SM) that accounts for patient setup variations[7]. The combination of the CTV and the IM creates a sub-volume called the Internal Target Volume (ITV). The ITV accounts for the motion of the CTV within the patient, however does not account for setup uncertainties.

The use of ITVs is controversial in lung radiotherapy in the creation of the PTV margins to ensure the CTV is treated along all points of the respiratory cycle. The large PTV

margins frequently seen in lung radiation therapy are often a result of the size of the ITV if the tumour has a large range of motion. Although large PTV margins restrict the maximum prescribed dose due to normal tissue toxicities, smaller more conservative margins pose the risk of tumour under dosage and geographical miss. Therefore, the ITV approach is widely used in radiation therapy despite the fact that it has shown to be larger than the required margin for a suitable radiation therapy treatment because it is conservative [7].

Furthermore, the ICRU requires every "Organ at Risk" (OAR) to be delineated and identified for every treatment plan. OARs are defined as surrounding organs that possess sensitivities to radiation that may significantly influence the prescribed dose and treatment planning[6]. Specific organs have dose tolerances in which serious complications will occur if they are exceeded. These tolerances are based on the 1991 report by Emami *et al.*[8]. This report provides partial volume irradiation tolerances for several organs based on an extensive literature search and opinions of experienced clinicians. Crucial OARs in lung radiotherapy are the spinal cord, healthy lung tissue, heart and esophagus.

In order to report doses in a way that is consistent amongst cancer centres, a clearly defined point within the patient must be established to specify where the dose is prescribed to. The dose at this point termed the "ICRU Reference Point" should always be reported as well as the maximum and minimum doses in the PTV. The ICRU Reference Point is recommended to be placed in the central part of the PTV at the intersection of the beams and must be representative of the dose distribution throughout the PTV. Its location should be in an area where accurate dose calculation is achievable therefore excluding the build-up region and areas of steep dose gradients[6].

Additional definitions in reporting dose include the Treated Volume (TV), Irradiated Volume (IR), maximum dose, minimum dose and hot spots. The Treated Volume refers to a volume of tissue surrounded by a specified isodose value pertinent to achieve the treatment goal whereas the Irradiated Volume refers to the volume of tissue receiving a dose significant compared to the normal tissue tolerance[6]. The terms maximum dose and hot spots are often mistakenly used interchangeably as both require a minimum diameter of 15 mm to be clinically relevant according to the ICRU. However, the term maximum dose refers to the highest dose within the PTV and hot spots refer to areas outside the PTV. The ICRU definition of minimum dose has no volume restriction and refers to the lowest dose inside the PTV volume.

According to the ICRU, in order for a treatment plan to be acceptable, it must be reproducible, the highest dose must be located within the target volume, the lowest dose must be located outside the target volume and the dose to organs at risk must be kept to a minimum and below tolerance. The dose within the PTV must be uniform to within -5% to +7% of the dose prescribed at the ICRU reference point. Therefore, it is crucial that the PTV receive no less than 95% of the prescribed dose in order for the plan to be clinically acceptable[6].
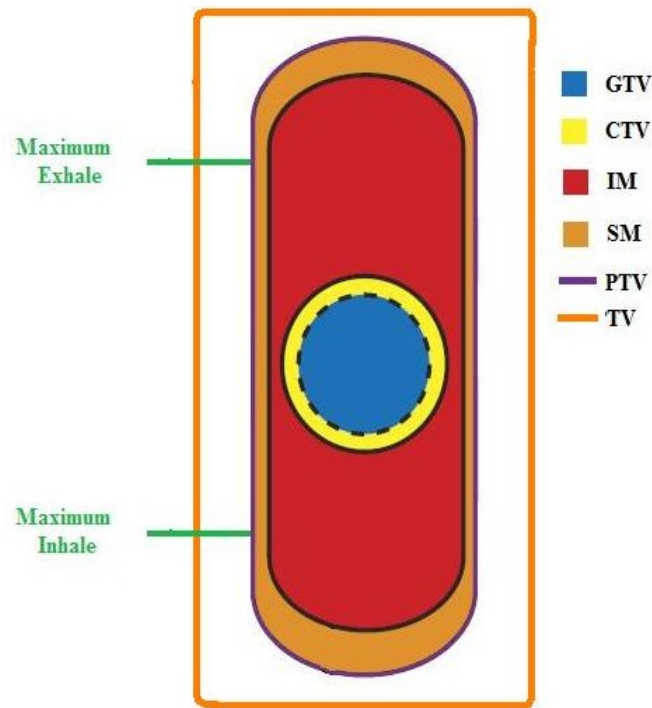
Figure 1.2: Illustration of the ICRU definitions of treatment planning volumes adapted from Wolthaus et al.[9]

1.4 Major Technological Advances in Radiation Therapy

Within the past decade, the technology behind radiation therapy instrumentation has advanced tremendously in a short amount of time, leading to significant improvements in the accurate localization and treatment of disease. The invention of the Multileaf Collimator (MLC) revolutionized conventional field shaping permitting the fast and easy production of complex and irregular field shapes[10]. An MLC is an extra collimation system at the distal portion of the treatment head consisting of several narrow abutting tungsten leaves. Each MLC leaf is motorized and individually controlled allowing the treatment fields to be shaped around the target itself. MLCs can contain anywhere from 60-120 leaf pairs of widths ranging from 1mm to 1cm depending on the linac design[4].

1.4.1 Three Dimensional Conformal Radiation Therapy

The birth of multi-leaf collimation along with the use of Computed Tomography (CT) in treatment planning gave rise to one of the most common treatment planning techniques used today, Three Dimensional Conformal Radiation Therapy (3DCRT). Prior to the invention of 3DCRT, treatment field shapes were limited to squares and rectangles which produce dose distributions with box shaped high dose region around the target. However, with the introduction of the MLC into the treatment head, high dose regions are now able to be shaped to conform to the target[11]. Treatment planners use the CT data acquired in the simulation to conform the high dose region to the target in all three planes, hence the term "Three Dimensional Conformal Radiation Therapy". This technique can drastically reduce the volume of normal tissue irradiated in comparison to the two dimensional conventional radiation therapy treatment techniques used prior[10]. This has been extremely significant in lung radiotherapy and has lead to a reduction in adverse side effects from treatment, dose escalation and in turn better local disease control.

1.4.2 Intensity Modulated Radiation Therapy

Following the birth of 3DCRT, a new type of radiation therapy treatment technique was invented termed Intensity Modulated Radiation Therapy (IMRT). IMRT differs from 3DCRT as it modulates the photon fluence of the linac during a treatment as opposed to keeping it constant which occurs in conventional treatments. Photon fluence is defined as the number of photons incident on a small sphere, divided by its cross-sectional area and integrated over time[4]. Thus, IMRT employs radiation beams with non-uniform intensities to produce dose distributions more conformal than 3DCRT techniques[10]. IMRT plans can be delivered by two different techniques employing multi-leaf collimators. In "step and shoot" IMRT, each

treatment field is divided into multiple segments which are delivered individually. In "dynamic" or "sliding window" IMRT, the intensity modulation is achieved by moving the MLC leaves independently in and out of the field at varying speeds while the beam is on[12]. IMRT requires the implementation of an inverse treatment planning method in contrast to conventional "forward" planning. Inverse treatment planning requires the treatment planner to input the goals of the treatment in terms of the desired dose to the target and surrounding organs into a treatment planning program. Using an optimization engine, the treatment planning program then finds the optimal radiation beam intensity distributions which satisfy the user specified goals[12].

1.4.3 On Board Imaging and IGRT

Basic linacs now include a retractable imaging panel and image administration software at the treatment console to take digital planar x-ray images with the treatment beam which are termed portal images[4]. Verification that the patient's position on the treatment couch reproduces the planning position is performed by comparing portal images acquired prior to the treatment to a set of reference images, called digitally reconstructed radiographs (DRRs), acquired from projections along each beam direction through the planning CT dataset obtained from simulation. Pre-treatment imaging is a useful quality assurance tool that has drastically reduced the frequency and magnitude of setup errors, allowing for reduced PTV margins[13]. Unfortunately, the high energy of the treatment beam yields poor quality images only capable of illustrating bony anatomy. Portal imaging enabled Image Guided Radiation Therapy (IGRT) which has become more prevalent in recent years[14].

The latest generation of linacs have a kilovoltage (kV) x-ray tube and detector mounted on the gantry orthogonal to the treatment head, sharing the same isocentre[15]. The kV projection and fluoroscopic images produced enable high quality and real time imaging with improved soft tissue visualization compared to MV portal imaging[14]. On-board kV imaging improves the ability to direct the radiation beams on the tumour for greater treatment accuracy. The acquisition of multiple projection images, coupled with tomographic reconstruction methods enables the creation of 3D volumetric images termed Cone Beam CT (CBCT)[16]. Due to the large longitudinal Field of View (FOV) of the kV source, the projections can be acquired in a single gantry rotation and yields a pre-treatment CT dataset that can be compared with the planning CT data. The ability to acquire volumetric images in the treatment room allows for a full three dimensional assessment of the target position with soft tissue visualization to provide the highest degree of treatment accuracy yet.

1.5 Introduction to the van Herk Margin Formula (VHMF)

With the improved ability to quantify and characterize random and systematic errors in the target position, many researchers have attempted to use this information to derive formulations that infer the correct PTV margin size for use in treatment planning. Margin recipes are formulations that calculated the required PTV margin to provide adequate CTV dose coverage in the presence of errors for specific patient populations. They have been derived from dose-coverage probabilities, physical and biological considerations[13].

A widely used dose-coverage probability based margin recipe was proposed by van Herk *et al*. that ensures a minimum CTV dose of 95% of the prescribed dose to 90% of the population[17]. A unique feature of this margin recipe is that random and systematic errors are

separated in the formula due to their different impacts on the dose distribution[13]. Random errors are assumed to blur the dose distribution while systematic errors result in a shift of the dose distribution relative to the CTV. The van Herk margin formula (VHMF) is written as:

$$M = 2.5\Sigma + 1.64(\sigma - \sigma_p) \tag{1}$$

Where $\sum$ is the standard deviation (SD) of all systematic errors, σ is the SD of random errors and σ_p is the width of the treatment beam penumbra as defined later in *Section 2.1*. The margin formula was derived from an idealized dose model by finding the geometrical margin required to ensure that the CTV is fully covered by 95% of the prescribed dose as the dose distribution was blurred and shifted to model the random and systematic errors inherent in the treatment and planning process.

1.6 Thesis objectives and organization

Although the VHMF should be applicable to any treatment site, there are assumptions in the dose model used to derive the formula that may limit its accuracy in lung radiotherapy. These assumptions affect the accuracy of modeling dose distribution in lung tissue as well as the modeling of effects of respiratory motion on dose distribution. Therefore, the motivation for this work stems from these assumptions that oversimplify a realistic treatment scenario and may pose limitations when applying the VHMF to lung radiotherapy. For example, the construction of this model does not take into account target size, tissue density or plan conformity and assumes the dosimetric effects of motion can be modeled with a convolution.

The objective of this thesis is to investigate the validity of the VHMF in lung radiotherapy. Accurate dose calculation algorithms and realistic respiratory motion modeling

were used to evaluate the impact of assumptions made in the derivation of the VHMF that some feel limit its application to lung radiotherapy. In Chapter 2, the physics radiation beams relevant to the understanding of this thesis is outlined as well as a detailed explanation of the VHMF and hypotheses of this work. Chapter 3 outlines the materials and experimental methods used to investigate the VHMF for lung radiotherapy. Chapter 4 presents and discusses the results of these investigations. Finally, a summary of the findings of this thesis is provided in Chapter 5 as well as suggestions for future work.

CHAPTER 2

PHYSICS OF RADIATION THERAPY, THE VAN HERK MARGIN FORMULA AND HYPOTHESIS

This chapter provides an overview of radiation therapy physics as it pertains to the properties of typical dose distributions obtained in lung tissue. An overview of the challenges introduced by respiratory motion in radiation therapy and current approaches to its management is also discussed. Finally, a detailed explanation of the VHMF is presented as well as previous work done by other groups investigating its application in radiotherapy. Thus, at the end of this chapter the oversimplifications made in the derivation of the VHMF should be clear, validating our concern in its safe application to lung radiotherapy and further justifying the objectives of this study.

2.1 Dosimetric characteristics of a radiation beam

The dosimetric characteristics of a radiation beam vary with the type of radiation, energy as well as the linac design and the medium through which the radiation passes. Radiation beams produced by an individual linac need to be characterized to enable accurate beam modelling for dose calculation. It should be noted that all beams are characterized in water which has similar radiological properties to soft tissue and thus they are considered equivalent in radiation therapy[18].

One of the most basic characterizations of a clinical radiation beam is the amount of dose deposited along the longitudinal axis of the beam. This is defined as the central axis depth dose curve which is a graphical representation of the dose variation as a function of depth in tissue, measured along the central axis of the beam[12]. Central axis depth dose curves provide

relevant information such as the surface or skin dose, the depth in tissue where the maximum dose point occurs (d_{max}) as well as the rate of dose falloff as a function of depth along the central axis. The dose is most often displayed as a percentage of the maximum dose. Central axis depth dose curves also allow one to characterize the build-up region of a radiation beam which is the area between the skin and d_{max}. *Figure 2.1a* displays several central axis depth dose curves representing beams of various energies. Although all the curves have the same general shape, it is clear that as the beam energy increases, the depth of d_{max} increases, the skin dose decreases and the rate of dose falloff decreases.

One shortcoming of a central axis depth dose curve is that the distribution of dose across the transverse axes of the field is not displayed. Instead, this can be displayed through the construction of a beam profile. A beam profile is a graphical representation of the beam intensity as a function of transverse distance from the central axis[12] as displayed in *Figure 2.1b*. Profiles also indicate the "flatness" of the beam which refers to the variation of dose along the transverse axis of the beam at a given depth and is important to monitor for quality assurance purposes. The hatched lines indicate the dosimetric field edge which is defined at the point lateral to the central axis of the beam where 50% of the dose is delivered. The region at the edge of the beam over which the dose changes rapidly as a function of distance from the central axis is termed the penumbra. The penumbra is caused by the physical construction of the treatment machine (geometric penumbra), the scatter from and transmission through the collimation system (transmission penumbra) and the scattering of radiation within the tissue (scattered penumbra)[12]. It should also be mentioned that profiles are not limited to describing a single beam and may be generated for treatment plans that include a combination of many

17

beams. This is done by plotting the dose along a single plane of the three dimensional distribution of dose.
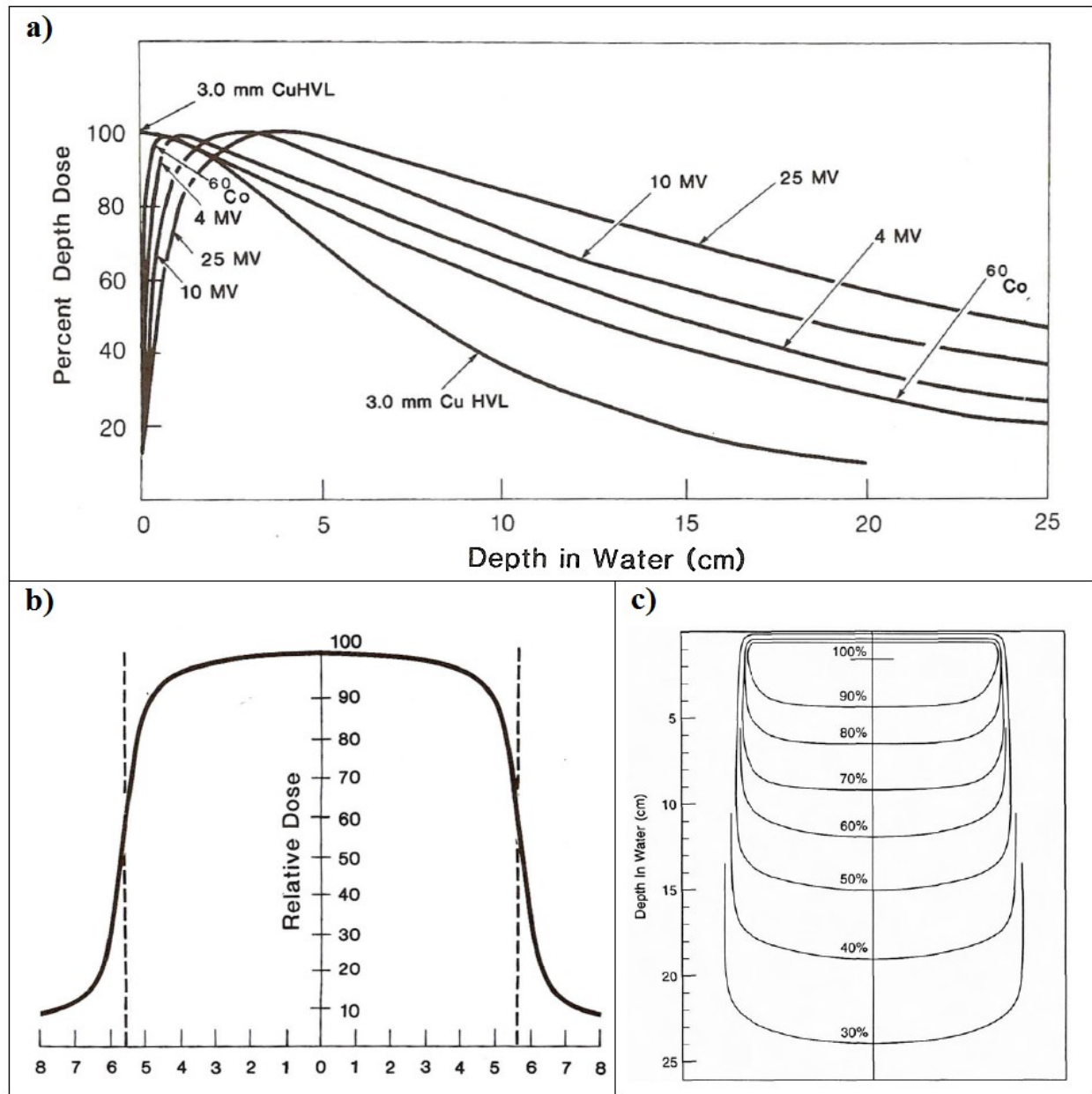
Figure 2.1: a)Central axis depth dose curves of multiple beam energies[12]. b)Typical Co-60 beam profile.[12] c)Typical 6MV isodose chart[3]. a) and b) taken from Khan[12], c) taken from Karzmark et al.[3]

Isodose charts combine depth dose and profile information to describe the variation in dose as a function of depth as well as transverse distance from the central axis. Lines are drawn through points receiving equal dose, termed isodose lines. Isodose charts contain a set of isodose curves, usually drawn at equal increments of the percentage depth dose (*Figure2.1c*)[3].

2.1.1 Dosimetric characteristics of radiation beam combinations

The characterization of a single radiation beam is extremely important for clinically accurate dose calculation in treatment planning. For most radical treatment plans, a combination of two or more beams is used to concentrate the high dose region to the target volume which is usually located centrally within the patient. The distribution of dose for multiple beams can be obtained by the linear addition of the overlapping isodose charts of the individual beams as shown in *Figure 2.2*. The dose for treatment plans with multiple beams is most often normalized so that the 100% dose level occurs at the isocentre and the dose at all other points within the distribution are relative to this. The most basic multi-beam arrangement is termed a parallel opposed pair (POP) that involves two identical beams positioned 180° from one another, providing a more uniform dose distribution at the centre of the patient. A POP dose distribution has a characteristic hourglass shape with the maximum dose occurring at the entrance and exit point of the beams and the minimum dose occurring in the centre as shown in *Figure 2.2c*.
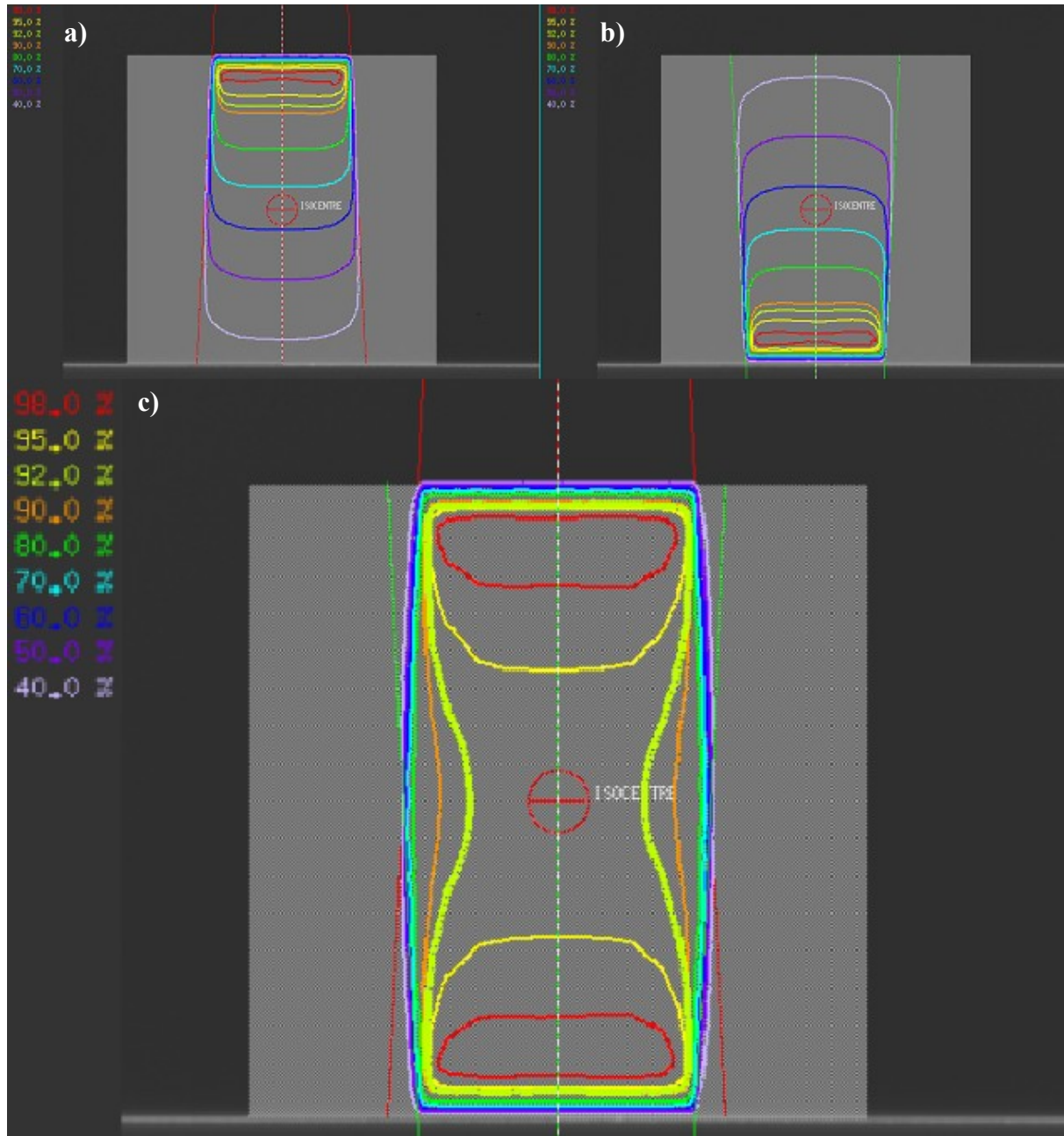
Figure 2.2: A POP dose distribution is constructed on a water phantom in Pinnacle treatment planning software (Philips Healthcare, Andover, MA). The combination of the anterior field in a) and posterior field in b) produced the POP dose distribution in c).

When two POPs are positioned orthogonally to each other, the high dose region at the

centre of the patient forms a box shape creating a common beam configuration termed a four

field box (*Figure 2.3*). This shape can also be achieved with three beams; however the high

dose "box" will be located closer to the surface of the patient along the central axis of the unopposed beam. The shape of the high dose area can be modified by altering the number of beams, their angles and the amount of radiation delivered by each beam relative to one another (termed beam weighting). The optimal beam configuration for a treatment plan is dependent on the treatment site, the required shape of the high dose area and the presence of surrounding sensitive organs.
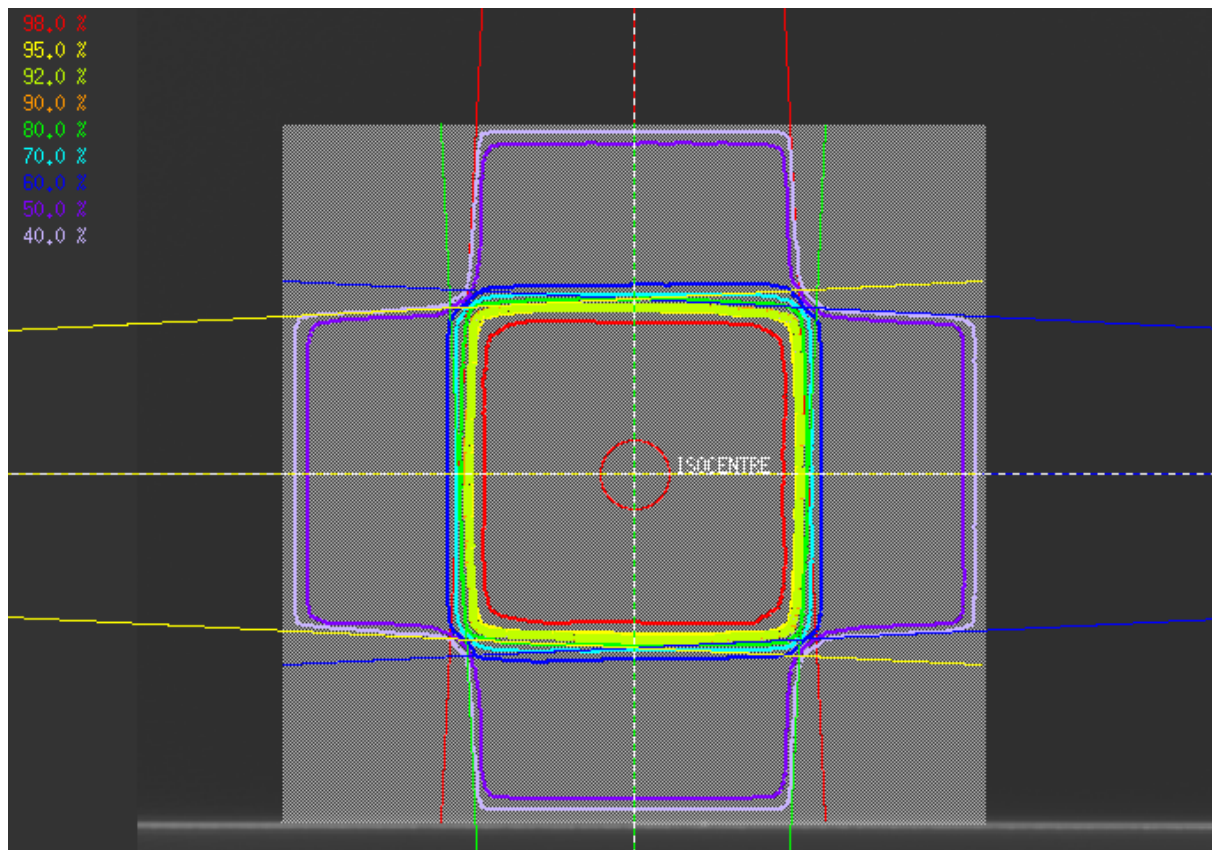
Figure 2.3: Dose distribution for a 4-field box technique constructed on a water phantom in Pinnacle treatment planning software.

Lung tissue is very sensitive to radiation and therefore it is important to spare the healthy contralateral lung from any unnecessary radiation dose when treating lung cancer.

Consequently, 2-5 beam configurations avoiding the healthy lung are most commonly employed in the radiotherapy of lung cancer including POPs and three field boxes.

2.1.2 Dosimetric characteristics of a radiation beam in lung tissue

The dosimetric characteristics of a radiation beam are heavily influenced by the composition of the medium through which it passes. Lung tissue has a much lower density of 0.15-0.35 g/cm^3 compared to that of soft tissue which is around 1 g/cm^3 [19]. Thus, the ability to deliver adequate absorbed dose to lung malignancies is complicated by the increased photon transmission, decreased field flatness and increased penumbra width observed in lung radiotherapy[18, 20]. The physical process behind these phenomena is Compton scattering which is the primary photon interaction in the megavoltage energy range of radiation therapy[21]. Compton scattering occurs when the incoming x-ray photon transfers energy to an atomic electron in the incident medium. The electron is ejected with some kinetic energy and the incident photon scatters, with the remaining energy, at another angle. Since lung tissue has a lower density than soft tissue, the Compton electrons are able to travel further in the medium before losing their energy by collisional interactions[12]. If the increased electron range is comparable to the field size, a significant number of Compton electrons scatter out of the radiation field boundary. It has been shown that this so-called lateral electronic disequilibrium seen in lung tissue, depicted in *Figure 2.4b*, causes a widening of the penumbra region of the beam resulting in a lower dose at the field edge and decreased field flatness. This phenomenon may cause under dosage at the periphery of lung tumours if not accounted for and is especially apparent for small lesions that require small field sizes comparable to the Compton electron range in lung tissue[22].
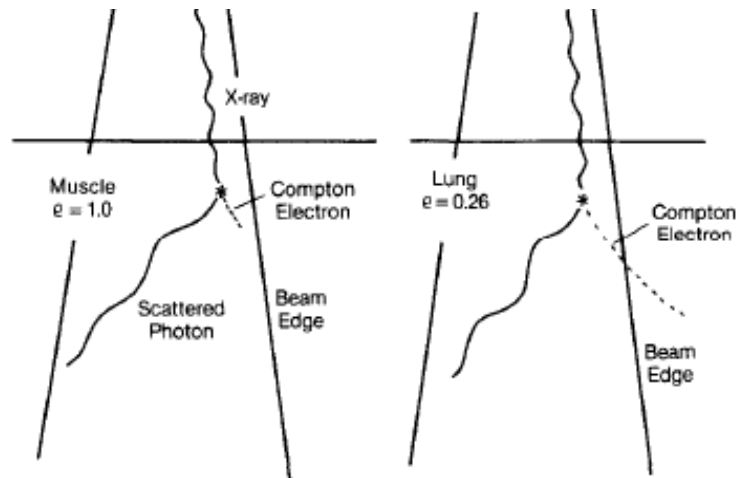
Figure 2.4: Depiction of Compton interactions within a treatment beam for a) soft tissue and b) lung where the Compton electron leaves field showing an electron deficit. Taken from Ekstrand et al. [21].

Lateral disequilibrium is overcome in practice by accurate dose calculation software that correctly models these effects so they can be compensated for in the planning process. The use of high beam energies in lung radiotherapy is avoided as well as the use of very small fields that have shown to experience a loss of CPE and pose a risk of tumour under dosage. Accounting for tissue density effects in the dose calculation process also ensures calculation of the correct number of MUs to compensate for the decreased photon attenuation in lung tissue.

2.2 Respiratory motion and its management in lung radiotherapy

The treatment of a moving tumour remains one of the most complicated problems in radiation therapy to date and a number of solutions have been proposed. An average healthy person at rest breathes 12-15 times per minute[23]. Inspiration occurs with the contraction of the diaphragm and intercostal muscles in between the ribs resulting in the expansion of the lungs with air while expiration is passive due to elastic recoil[23]. Therefore, the expansion and contraction of the thoracic cavity during respiration causes deformation in the surrounding anatomy including any malignant lesions located within the lung. Respiratory-induced tumour

motion can be modeled by an asymmetric periodic function displayed in *Figure 2.5* where more time is spent at exhale than inhale[24].
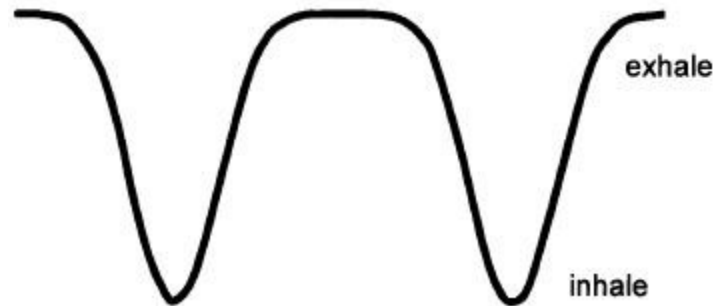
Figure 2.5: Periodic asymmetric function modelling respiratory motion Adapted from Seppenwoolde et al. [24].

The average magnitude of tumour motion is greatest in the cranial-caudal direction due to the motion of the diaphragm and is normally minimal in the lateral and anterior-posterior planes[24]. Typical motion magnitudes vary depending on the location within the lung, as tumours with the greatest peak-to-peak amplitudes are usually located in the lower lobes of the lung, closest to the diaphragm which drives respiratory motion[24]. Typical maximum motion amplitudes of tumours are in the vicinity of 12 mm in the cranial-caudal direction and 5 mm in the lateral as well as the anterior-posterior directions[24]. Despite the large variability, typical motion amplitudes range from 5-8mm, 3-9mm and 2-3mm in the cranial-caudal, lateral and anterior-posterior directions respectively for middle and lower lobe tumours[25]. However, this is very dependent on the tumour location as well as the density and elasticity of the lungs.

The management of respiratory motion during treatment is approached in many different ways and depends on the technology available and expertise of the treatment staff. The most common form of motion management is achieved during treatment planning by designing PTV margins that include an ITV to fully encompass the CTV position at maximum

inhale and exhale. Others believe planning on the tumour's time averaged position is the more beneficial. More recent attempts to manage respiratory motion focus on the treatment execution phase by developing technology that determines the tumour location and turns on the beam when it is in a specific location. The evolution of planning and delivering treatments using detailed motion information is in full development leading to more accurate treatments with reduced PTV margins. An overview in the different approaches is outlines in the following sub-sections.

2.2.1 Motion encompassing methods

The most straightforward method to compensate for respiratory motion is to design a PTV margin that accurately accounts for the tumour motion. Margin recipes such as the VHMF discussed previously is one method of designing accurate PTV margins in which individual patient and population statistics are inputted into a formula that calculates the PTV margin required. Another conservative approach is to create an ITV by adding a margin to the CTV to encompass the full range of tumour motion. Motion encompassing methods require an accurate estimation of the range of motion. This is usually done in the CT simulation process with either inhale and exhale breath hold CT or more now commonly four-dimensional computed tomography (4DCT)[26,15].

Another way of obtaining a tumour encompassing volume without the unwanted motion blur is to perform two CT scans with the patient holding their breath at inhale and exhale, respectively[26]. The tumour encompassing volume can be obtained by fusing tumour contours on the inhale and exhale image sets. Another approach is to combine the inhale and exhale images into one image representing the extent of tumour motion, similar to the slow-CT

approach with the maximum intensity projection tool[27]. The maximum intensity projection is an image post processing tool available in most commercial software that creates the tumour encompassing volume by selecting image voxels with the highest density value in a region of interest encountered in each dataset throughout the respiratory cycle. Unfortunately, the inhale and exhale breath-hold CT method heavily relies on the patient's ability to hold their breath which can be extremely difficult for individuals with co-morbidities such as Chronic Obstructive Pulmonary Disease and the tumour position on each scan is not indicative of its maximum and minimum free breathing position. It also requires twice the amount of scanning time as two separate 3DCT images are required[26].

A major contribution to the advancement of lung radiation therapy treatment plan design has been the invention of four-dimensional computed tomography (4DCT) [28]. In 4DCT, the respirations of the patient are recorded during the CT scan acquisition to correlate each resulting image slice with a respiratory phase. All the slices are then sorted based on the respiratory phase and interpolated to yield several, typically 10, 3DCT datasets at specific respiratory phases as seen in *Figure 2.6*. The use of 4DCT allows for the characterization of patient specific respiratory motion trajectory[9]. Contour fusions as well as the maximum intensity projection tool described earlier may also be used on 4DCT datasets for the construction of tumour encompassing volumes such as ITVs.
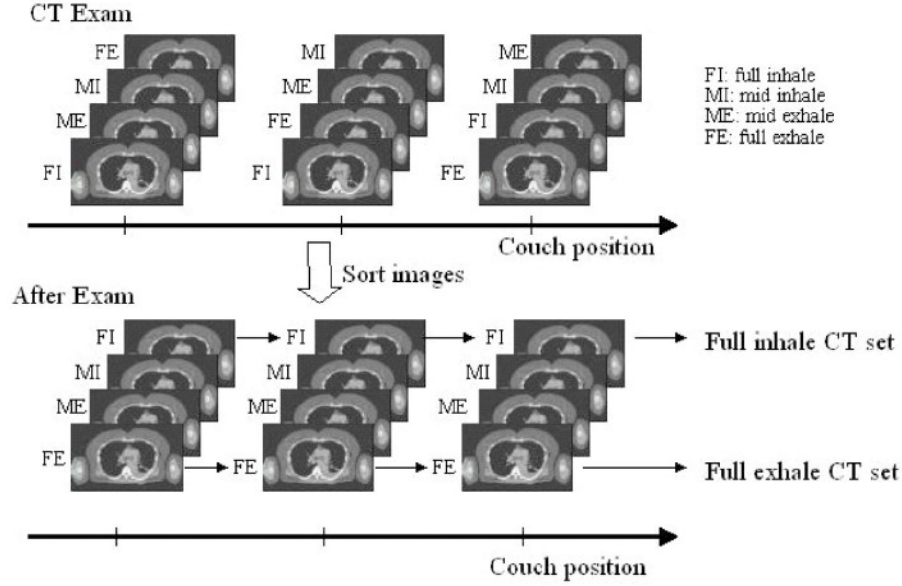
Figure 2.6: Schematic of the 4DCT imaging and sorting procedure by respiratory phase, taken from Keall et al.[26]

2.2.2 Planning at average tumour position

The introduction of 4DCT allows one to obtain multiple CT scans, each corresponding to one of various respiratory phases, in a short amount of time. With the increased acquisition of data, many have investigated which time point in the respiratory cycle is the most advantageous at which to construct the treatment plan. Although many feel that it is safest to design the treatment on exhale as it accounts for the majority of the respiratory cycle, advantages have been demonstrated in designing treatments at the mean position of the tumour in terms of PTV reduction[9]. The main approach in obtaining the appropriate dataset to represent the average tumour position is by choosing the mid-ventilation CT scan[29].

The mid-ventilation scan proposed by Wolthaus *et al.*[29] calculates the time averaged position of the tumour using the tumour motion measured from the 4DCT data. Since the average position of the tumour may not be represented by one of the phase images in the 4DCT

27

data set, the authors selected the 4DCT phases where the tumour position is closest to the time averaged position. The advantage of the midventilation planning technique is that it allows a reduction of the required PTV margin by minimization of the systematic component of respiratory motion which will be further explained in *Section 2.3.2*.

2.2.3 Respiratory gating

Respiratory gating involves the delivery of radiation during a specific portion of the respiratory cycle termed the "gating window"[26]. Tumour positional information is provided through real time imaging of fiducial markers implanted in or near the tumour or by more commonly measuring external movement of the chest wall that can be correlated to the tumour motion. The treatment beam is only turned on during the gating window[26]. The advantage of gated treatments is the large potential for PTV margin reduction as the tumour motion during beam delivery is greatly reduced (*Figure 2.7*). This allows for the sparing of more normal lung tissue as the entire peak-to-peak motion amplitude of the tumour no longer has to be treated. This leaves more opportunity for dose escalation to improve local disease control as well as decreasing the probability of adverse side effects from treatment. Although the idea of gated treatments is very promising, it is still a developing technology and requires a high degree of monitoring[26]. There is also the question of how well external motion measured with a surface marker reflects the position of the tumour. Gated treatments take longer than conventional treatments due to the longer setup time as well as the beam being on for a fraction of the time of the breathing cycle [26].

2.2.4 Breath hold methods

An alternate treatment technique to minimize respiratory motion is to require the patient to hold their breath at a specific point in the respiratory cycle during treatment[26]. This reduces the positional uncertainty of the tumour due to respiratory motion as the beam is only turned on when the patient is holding their breath. There are several different breath hold techniques currently employed including deep-inspiration breath-hold (DIBH), active breathing control (ABC) and self-held breath hold[26]. Each technique has specific patient selection criteria as they must be physically able to control their respirations accordingly.

Deep inspiration breath hold requires the patient to hold their breath at their maximum lung volume which is measured via a spirometer or external motion trace. The patient is coached into a reproducible deep inhale breath-hold and the beam is turned on when the target breath-hold level has been achieved and turned off when it falls below a predetermined tolerance[26]. Active breathing control also known as gated breath hold has the same objective but a predetermined respiratory phase is chosen for breath-hold and the ABC apparatus suspends the breathing. It consists of a spirometer that is attached to a balloon valve which is inflated with an air compressor to hold the patient's breath[26]. The breath-hold method is not applicable to all lung cancer patients because their physical condition limits the duration of breath hold to less than 20 seconds.

2.2.5 Motion management techniques in development

Despite the many options for the management of respiratory motion in radiation therapy, all of the previously described techniques have limits in their applications. Thus, the development of motion management techniques and systems are continuously in progress. Two

novel techniques at the forefront of motion management techniques are real-time tumour tracking and 4D optimization.

Real-time tumour tracking in lung radiotherapy actively repositions the beam during treatment to follow the changing position of the tumour. This can be achieved on a conventional linac by moving of the MLC leaves to adjust the beam aperture to follow the tumour. Other tracking approaches include aligning the tumour with the beam using a robotic couch[30] as well as a specially designed compact linac that is mounted on a robotic arm, called a Cyberknife (Accuray Incorporated, Sunnyvale, CA)[26] capable of real-time adaptation of the beam isocentre to the tumour position. To be successful, a tracking system must include accurate real-time imaging to identify the tumour position. Due to the inevitable lag between the tumour position acquisition and beam adaptation, algorithms that accurately anticipate the tumour position are required. The treatment planning for a tracking treatment must also be altered from conventional planning as now one must account for the dose delivered to the tumour at all points in the respiratory cycle. The plans need to account for the changing lung volume and changing positions of the OARs with respect to the tumour[26]. A real-time tracking system is integrated into the Cyberknife robotic linear accelerator as it uses fluoroscopic images for real time imaging of the tumour. However, this is a very specialized treatment that is not widely available. Tracking software is currently under development for conventional linear accelerators and is not a standard practice yet. There is much advancement to be made in predicting the tumour motion more accurately as well as improving image quality for visualizing the CTV without fiducial markers or using a surrogate respiratory signal for tracking. Despite the complex nature of tracking, once perfected it will allow for small to no

PTV margins. It also provides a much shorter treatment time than gating as the linac is on for an entire duty cycle (the ratio of the beam-on treatment time to the total treatment time) [26].

4D optimization is another area of research that shows much promise in respiratory motion mitigation. 4D optimization is a method that incorporates the tumour motion information gained from 4DCT into the IMRT inverse planning step of treatment [26]. There are many different approaches to solving the advanced optimization algorithms required for the successful construction of a 4D IMRT plan[31-35]. The objective of 4D optimization is to optimize the dose delivered over all respiratory phases simultaneously. This concept provides great advantages in terms of giving the tumour the highest dose possible and while sparing the healthy tissue. Although some 4D IMRT techniques are being developed to be fairly robust to deviations in respiratory motion[31], many will require some form of gating and real time tracking to synchronize the MLC pattern with the patient's breathing.

2.2.6 Impact of respiratory motion management on PTV margins

The ultimate goal of all of the above mentioned techniques is to reduce the uncertainty of the tumour position as it moves with respiratory motion. If one has more knowledge of the tumour location with respect to time, PTV margins can ultimately be reduced leading to more accurate treatments that can yield higher doses. *Figure 2.7* depicts the difference in PTV construction for the above mentioned treatment techniques and demonstrates the volume reduction for the gating and midventilation approaches. Although, the diagram below shows that a gated treatment allows for the smallest PTV margin, gating is a very labour intensive and complicated treatment as explained in *Section 2.2.3* that it is still a developing technology and requires a high degree of monitoring.
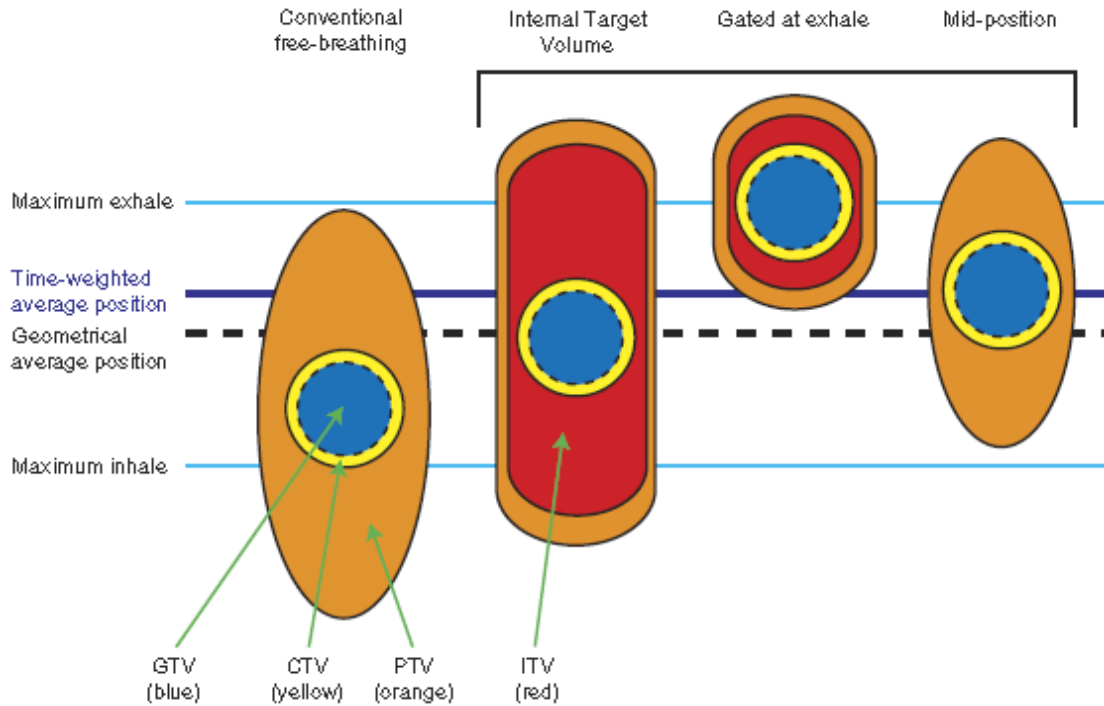
Figure 2.7: Illustration of the PTV construction techniques for various methods of respiratory motion management. Taken from Wolthaus et al. [9]

2.3 Introduction to margin recipes in radiation therapy

To date, motion encompassing methods such as the use of ITVs is the most common form of respiratory motion management as they do not require extra resources and additional advanced equipment such as gating or tracking. However, it has also been shown that ITV margins are the largest and most conservative.[7] Thus, they do not leave room for PTV margin reduction and dose escalation like some of the more labour intensive motion management options.

An alternative approach to an ITV is to use a margin recipe which generates smaller but still effective PTV margins based on statistical models that limit how the dose distribution is affected by respiratory motion. Most margin recipes have random and systematic error

components. Accurate patient and population-specific data characterizing these errors is required for the confident and safe application of these margin recipes. The following subsections describe the two categories of geometric uncertainties and their implications on a static dose distribution. It should be noted that the term "error" refers to any deviation of the target position from its planned position.

2.3.1 Random Errors

Random errors, also termed treatment execution errors are stochastic amongst patients and individual treatment fractions[36]. Random variations in patient setup occur during treatment due to a variety of reasons that occur normally and are difficult to pin-point and remove. The patient position may not be reproduced exactly during each treatment due to co-morbidities or other situational differences[17]. The CTV position also randomly varies due to respiratory motion. Thus random errors are divided into organ motion and setup errors. Since random errors cause different positional errors for each treatment they induce a blurring effect on the planned dose distribution[17].

2.3.2 Systematic Errors

Systematic errors, also termed treatment preparation errors, are stochastic amongst patients but are systematic for a single radiotherapy treatment regime for each patient[17]. They can be due to imprecision in equipmentt or individual biases in the application of a procedure. Examples of systematic errors include setup errors, delineation errors and organ motion errors. Setup errors have a systematic component in addition to the random component discussed previously. The systematic component exists if a setup error occurs during the simulation process, which will offset the patient in the same manner during every fraction of treatment.

Respiratory motion introduces an error if the treatment is not planned on the tumour's time average position[17]. Thus, if a lung radiotherapy plan is designed on the exhale phase which is a common practice, a systematic error is introduced. The delineation error occurs if the tumour is not properly contoured and the error persists for the whole treatment. Since these errors occur in the planning phase, they are propagated to the treatment phase and occur in an identical manner during each fraction for the entire duration of the treatment. Therefore, the dosimetric implication of systematic errors is a displacement of the dose distribution by a given preparation error with respect to its original position[17]. Because they can affect the entire treatment course, systematic errors are the more important of the two types of geometrical uncertainties.

2.4 The van Herk margin formula

The VHMF was introduced in *Section 1.5* as formalism for calculating the PTV margin required to provide full CTV dose coverage by 95% of the prescribed dose to 90% of the population in the presence of known random and systematic errors[17]. Noted earlier with equation (1) in *Section 1.5*, the VHMF is repeated here:

$$M = 2.5\Sigma + 1.64(\sigma - \sigma_p) \qquad (1)$$

Where Σ is the standard deviation (SD) of all systematic errors, σ is the SD of random errors and σ_p is the width of the treatment beam penumbra. The SD of the random and systematic errors at individual treatment facilities can be obtained from measured tumour position data obtained on a daily basis for a number of patients and fractions. The mean and SD of the daily measurements are computed for each patient. The SD of the daily measurements represents the SD of random error, σ. The SD of systematic error, Σ, is simply the SD of all the

means measured for each patient[37]. Therefore, margin formulas can only be applied to patient populations for which this data exists. Fortunately, this data exists for lung Radiation Therapy and has been reported.

The margin derivation relies on a model which provides an analytical description of the influence of random and systematic geometrical deviations on the dose distribution. The first step of the derivation is to create a model of the planned dose distribution ($D_{planned}$) by convolving a top hat function spanning the CTV with a Gaussian distribution in order to produce a clinically realistic dose profile *(Figure 2.8)*. A convolution is the integral of the product of two functions after one is reversed and shifted to produce a third function that is a blurred representation of the original function. In this case is, the Gaussian is flipped (even though it is a symmetrical function) and shifted across the top hat function to create the planned dose profile. The mathematical definition of convolution ($\otimes$) is:

$$A(y) \otimes B(y) = \int_{-\infty}^{+\infty} A(z)\, B(y-z)\, dz \qquad (2)$$

The Gaussian distribution convolved with the top hat function is centred on the tumour and a SD describing the width of the beam penumbra (σ_p). The value of σ_p was assumed to be 3.2 mm by van Herk, approximating the width of the penumbra in soft tissue and has shown to be 6.4 mm for lung tissue due to the wider penumbra in low density media[38, 39]. However, these numbers may not be valid for IMRT where the dose distributions may possess much steeper dose gradients.
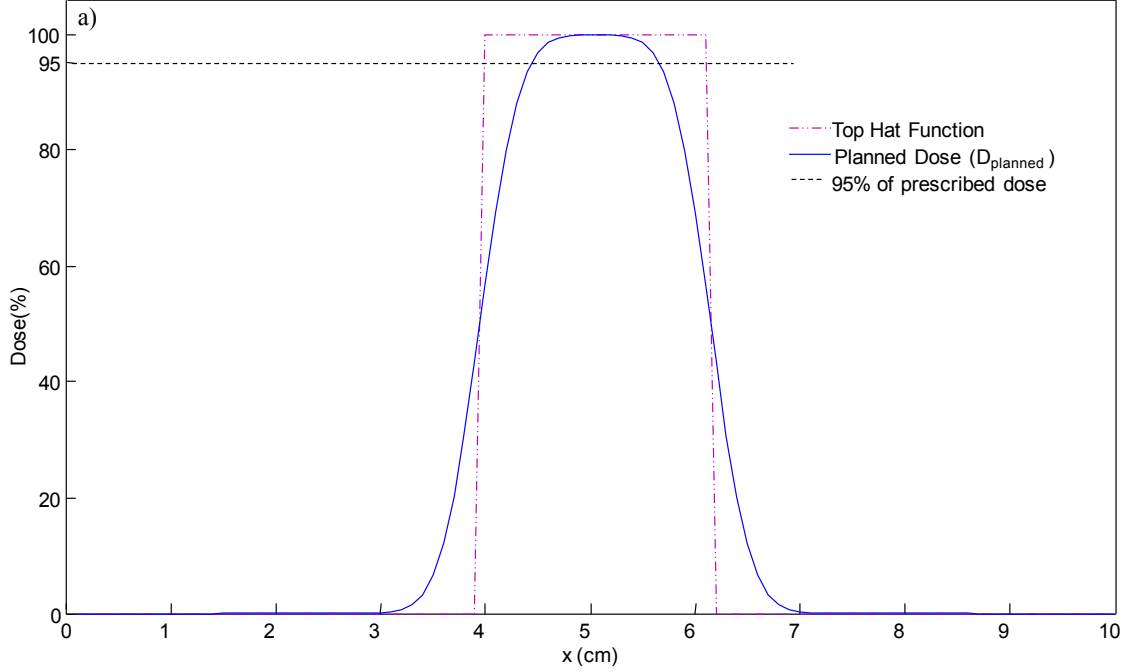
Figure 2.8: The solid blue profile curve indicates $D_{planned}$ which was constructed by convolving the top hat function with a Gaussian of SD = σ_p.

Next, it is assumed that the impact of random errors on the dose distribution can be modelled by blurring the planned dose profile, yielding the blurred dose profile ($D_{blurred}$) depicted in *Figure 2.9*. Assuming that the dose distribution does not change as it is shifted, blurring of the dose can be modelled by convolution. $D_{blurred}$ is constructed by convolving $D_{planned}$ with a Gaussian distribution that has a mean of 0 and a SD of σ_{random}. σ_{random} can be divided into its individual components of random organ motion (σ_m) and setup error (σ_s). $D_{blurred}$ can be obtained directly by convolving a top hat function with a Gaussian function with a SD of σ, where:

$$\sigma = \sqrt{\sigma_m{}^2 + \sigma_s{}^2 + \sigma_p{}^2} \qquad (3)$$

According to van Herk, the PTV margin required for adequate CTV coverage in the presence of random error is equivalent to the distance between the planned and blurred dose distributions at the 95% dose level as indicated in *Figure 2.9* by the black arrows. It should also

36

be noticed that the 50% level of blurred dose coincides with the width of the original top hat function. The slope of the edge of the blurred dose profile is fitted to a linear function from which the distance between the 50% dose level and the 95% dose level is derived to be 1.64σ. Thus, the 95% level of blurred dose is situated 1.64 standard deviations (σ) from the beam edge. Since the distance between the 50% and 95% dose levels of the planned dose profile is $1.64\sigma_p$, the distance between the 50% and the 95% dose levels of the blurred dose profile is 1.64σ and the 50% dose level is invariant to blurring, the distance between the blurred and planned dose profiles at the 95% level is $1.64\sigma_p$-1.64σ which reduces to equation (4). Therefore, the van Herk PTV margin accounting for random geometrical uncertainties only, can be calculated by applying the reduced equation:

$$M_{random} = 1.64(\sigma - \sigma_p) \tag{4}$$
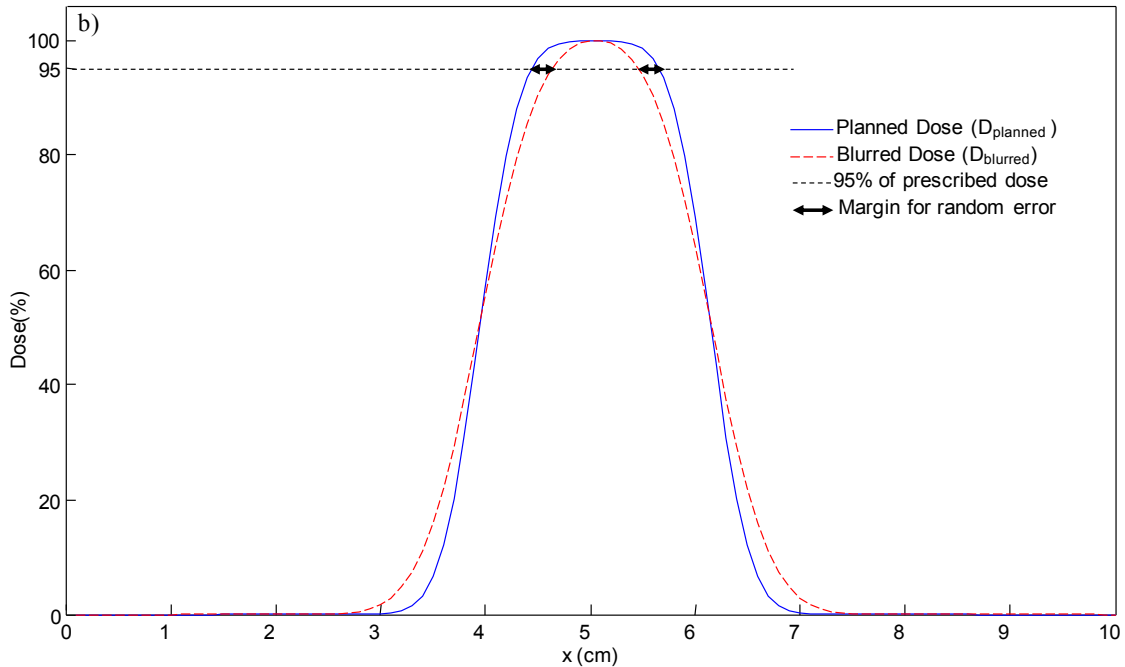
Figure 2.9: The hatched red profile indicates $D_{blurred}$ which was constructed by convolving the blue $D_{planned}$ profile with a Gaussian of SD = σ_{random}. The black arrows indicate the distance between the two profiles at the 95% dose level which is the PTV margin required for random error.

As mentioned previously, the dosimetric effect of systematic errors is effectively a shifting of the dose distribution. Therefore, the margin to account for systematic uncertainties is calculated based on the probability that a systematic error results in the displacement of the CTV outside the region bounded by the 95% dose level in the blurred dose profile $D_{blurred}$. The component of the PTV margin for systematic errors is chosen based on an objective set by the physician which is most commonly that 90% of the patient population receives a minimum CTV dose of 95% of the prescribed dose. Assuming that systematic errors are normally distributed, the 3D volume that encompasses 90% of all positions is given by 2.5Σ, where Σ is the SD of the Gaussian distribution describing systematic errors. It should be noted that the PTV margin for systematic errors is an entirely geometrical concept that does not depend on the shape of the CTV or dose distribution. Σ can be divided into its individual components of systematic organ motion (Σ_m), setup error (Σ_s) and the delineation error (Σ_d) where:

$$\Sigma = \sqrt{\Sigma_m{}^2 + \Sigma_s{}^2} \qquad (5)$$

The combination of the separate random and systematic components of margin leads to equation (1):

$$M = 2.5\Sigma + 1.64(\sigma - \sigma_p).$$

According to this formula, the contribution of systematic errors is roughly one and a half times greater than random errors and therefore contributes to a larger portion of the PTV margin. Therefore, more emphasis is placed on minimizing systematic errors in because reducing the Σ value has a much greater shrinking affect on the PTV. It is also much more clinically practical to reduce systematic errors with the use of motion management techniques

such as those described in *Section 2.2.5* as well imaging during treatment and IGRT (see *Section 1.4.3*). Reducing random errors is less of a clinical focus as they account for a much smaller portion of the PTV margin, are much harder to predict and therefore account for. However, the dosimetric effects of random errors are still important to characterize for accurate PTV construction, especially for lesions with large motion amplitudes.

2.4.1 Limitations of the VHMF

Despite the logic behind the derivation of the VHMF, certain assumptions were made that may limit it applicable to all treatment sites and situations. For example, it is assumes that the planned dose distribution, $D_{planned}$, conforms exactly to the CTV, representing a perfectly conformal dose distribution in a homogeneous medium[38, 40].

The term "homogeneous" refers to the assumption that all tissues in the body are water equivalent. However, in reality, tissues such as bone and lung have significantly different radiobiological properties compared to water and the dose distribution will be altered if these tissues are present in the path of the treatment beam. Dose distributions calculated in a homogeneous medium do not account for these differences and therefore do not accurately represent the dose for lung malignancies in a clinical setting[18]. Heterogeneity corrections are required for accurate dose calculation in lung radiotherapy as they take into account the different properties of tissue within the body and account for lateral electronic disequilibrium. The homogenous assumption results in a shift invariant model, meaning the movement of the CTV and deformation of the surrounding organs such as the lung during respiration do not influence the dose distribution. Thus, the dose distribution can be thought of as a stationary

dose cloud within the lung and the CTV moves independently through it. In reality, the difference in density between the CTV and surrounding lung alters the dose distribution.

Although the concept of lung cancers challenges this assumption, shift invariance is assumed by the use of convolution to model respiratory motion. The use of a convolution model to describe respiratory motion may not be an accurate representation of the blurred dose distribution for a lung malignancy[41, 42]. It assumes that the blurred dose is equivalent to shifting the planned dose distribution to a series of random points along the respiratory cycle and computing the weighted sum of the shifted doses. However, in actuality the shifted dose distributions are perturbed by tissue inhomogeneities and surface curvature.

The perfectly conformal nature of the van Herk dose model is also unrealistic as is not physically achievable in radiation therapy due to the dose fall off at the beam periphery characterized by the beam penumbra. Although with the advancement of IMRT highly conformal treatments are available, for a realistic treatment planning scenario the ICRU specifies that the 95% dose volume must encompass the entire PTV which results in the volume of the 95% isodose being slightly larger than the PTV. Perfectly conformal plans are even more difficult to realize in lung radiotherapy as many tissue inhomogeneities such as the ribs and bronchioles lie in the path of the beam and may cause areas of increased or decreased dose compared to a homogeneous plan. Also, the penumbra is wider in lung tissue as discussed previously in *Section 1.2.4*

Finally, the use of convolution to model the planned dose distributions assumes that the CTV is large in comparison to the width of the beam penumbra. However, for small lesion sizes, the isodose surfaces can become sharply curved and therefore may alter the assumed

penumbra shape[38] so that they cannot be modeled by convolution with a Gaussian. Therefore, PTV margins derived from the VHMF may not be reasonable for small targets.

2.4.2 VHMF modifications and application to lung malignancies

Recognizing the assumptions of the dose model employed in the Van Herk margin recipe, others have attempted to update the formula to address these limitations.

Witte *et al*[38] introduced an updated dose model to compensate for variations in the dose profile for different target sizes and tissue densities. The change to the original van Herk model involved the replacement of the Gaussian penumbra with a more adaptable penumbra model consisting of two Gaussians as shown in *Figure 2.10b*. Various profile models were then generated for square fields ranging from 2x2 cm^2 to 17x17 cm^2 by fitting the penumbra models to dose profiles generated by clinical treatment planning software. This was done for water, to mimic soft tissue, and cork, which has a similar density to lung, yielding a more realistic representation of dose profiles for several target sizes in lung and water. The fitting parameters of the profiles were then used in a dose distribution model to derive the random error margin required to provide full coverage of the CTV by the 95% isodose level for 90% of the population via an iterative approach. Results showed a size and density dependence of the minimum margin necessary to account for random error. Larger margins were required for small targets in soft tissue and large targets in lung tissue. Interestingly, despite the demonstrated relationship between target size, density and the required margin; it was shown that the original formula proposed by van Herk always covers the CTV with the 95% dose level with the exception of small targets in water and denser media.

It should also be noted that although the authors updated the van Herk dose model to better represent realistic dose distributions, some underlying assumptions were made that could still limit the applicability of the revised margin recipe to lung cancer. Even though the penumbra shape was derived for a low density medium, the *Witte et al.* model still assumed that the dose distribution is shift invariant as a uniform density was still assumed. Like the original model, the fact that the tumour itself is a higher density than the surrounding medium was not accounted for and this has the potential to change the penumbra shape as well. Therefore, this model cannot portray variations in profile shape from different tissue densities (inhomogeneities) in the path of the beam. It is also important to note that in this study the PTV margins were calculated with the VHMF to compare to the proposed model. However, a σ_p value of 3.2 mm was used for all calculations which describes the penumbra width in soft tissue where a σ_p of 6.4 mm which should have been used for the lung tissue results. Therefore, a direct comparison cannot be made to the derived lung margins unless a more appropriate σ_p value describing the penumbra width in lung tissue is used.
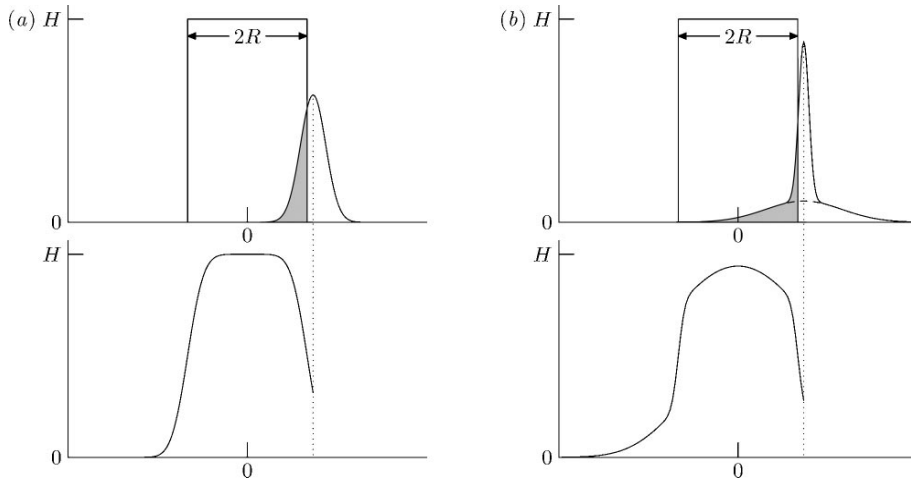
Figure 2.10: The top panels show of the convolution calculation performed by Witte et al. with the resulting dose models in the bottom. The original van Herk model with a single Gaussian is depicted in a) where b) illustrates the Witte model utilizing the sum of two Gaussians. Taken from Witte et al.[38]

The VHMF was also adapted by McKenzie *et al.*[40] to account for the impact of the number of treatment beams and their configuration on the dose distribution. Their argument was that the dose blurring effects at the edge of the beam which define the PTV margin are reduced when multiple coplanar and opposing beams are employed due to their overlap in the lateral and anterior-posterior plane. Thus, the study suggested that the size of appropriate PTV margin is inversely proportional to the number of beams present in the treatment plan. This is because the additional beams reduce the distance between the blurred 95% dose level and the 50% dose level which is invariant to blurring. This concept is based on the assumption that the margin in a realistic treatment plan with multiple beams is defined by a single beam in each plan whose edge is situated closest to the CTV. Therefore the dose gradient of the other beams at this point is much smaller in comparison and their sum at the edge of the single margin defining beam is comparatively flat. According to this hypothesis, the blurred dose level for an entire multi-beam plan with *n* number of beams that corresponds to the equivalent blurred dose level of a single beam plan can be calculated by:

$$(100 - 5n)\% \tag{6}$$

For example, this equation indicates that for a treatment plan containing three beams, the dose level of the single blurred beam that delimits the target is 85% which is only 1.04σ away from the beam edge instead of 1.64 as proposed by van Herk. *Figure 2.11* depicts the dose profile of the previously mentioned example, demonstrating that the 95% level of the total dose corresponds to the 85% level of the blurred single beam. Therefore in this case, the VHMF becomes:

$$2.5\Sigma + 1.04(\sigma - \sigma_p) \tag{7}$$

43

It should also be noted that this value remained 1.64 for margins in the superior-inferior direction since treatment the beams overlap in the lateral direction only.
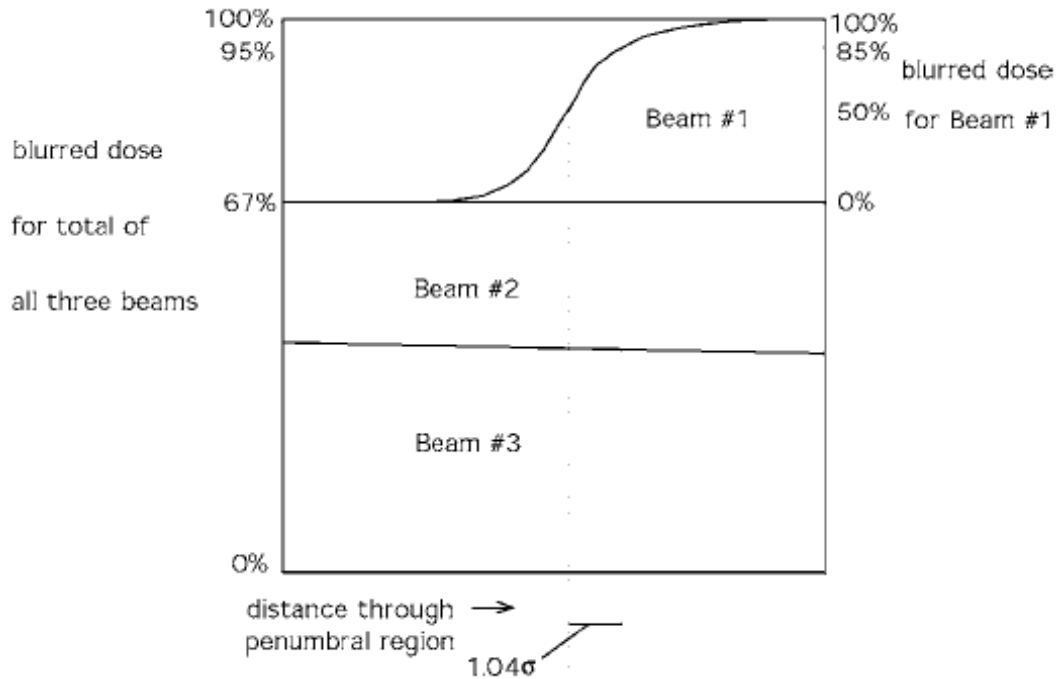
Figure 2.11: Profile of the blurred dose distribution of a 3 beam treatment plan. The 95% dose level for the margin defining beam is equivalent to the 85% dose level of the entire dose distribution which is 1.04σ away from the beam edge. Taken from McKenzie et al.[40]

2.5 Hypothesis

Prior to the completion of the experiments outlined in the following chapters, it was hypothesized that the dose model utilized by the VHMF contained too many simplifying assumptions to be valid for all treatment scenarios in lung radiotherapy. As summarized in the previous sections, the VHMF does not take into account the size of the tumour, variations in tissue density along the path of the treatment beams as well as the type of treatment. The dose model also assumes a perfectly conformal treatment which is not practically achievable in radiation therapy planning, especially in low density media such as the lung due to the widened penumbra. Therefore, it was anticipated that the VHMF may need to be adjusted to account for

lesion size, tissue density, and treatment type as theoretically proposed by others to compensate

for the heterogeneous nature inherent in lung radiotherapy planning.

CHAPTER 3
MATERIALS AND METHODS

In this chapter, the software used to generate patient images and all of the treatment planning software utilized in this study is described along with the different experiments executed to test the systematic and random components of VHMF. Within the described experiments, the influence of tissue density, tumour size and motion amplitude as well as plan conformity are investigated. Finally, possible modifications to VHMF are explored.

3.1 Materials

3.1.1 XCAT virtual phantom

The XCAT virtual phantom program[44, 45] was used to generate the 4DCT datasets required for treatment planning and dose accumulation in this study. This 4D virtual phantom is categorized as a "hybrid" phantom which combines the anatomical accuracy of a voxelized phantom with the precise modelling of tissue deformation and motion of a mathematical phantom. This is done through the use of non-uniform rational B-splines (NURBS)[46] and subdivision surfaces which can accurately model the complex curves and 3D surfaces of human anatomy and are also quite flexible to model anatomical motion. The XCAT NURBS surfaces are based on the Visible Male and Female anatomical datasets from the National Library of Medicine [47] whose measurements were scaled to fit a 50th percentile adult. The NURBS surfaces are defined based on a set of control points that model the surface of all anatomical structures within the phantom. Anatomical variations are achieved by applying transformations to the control points as depicted in *Figure 3.1*.
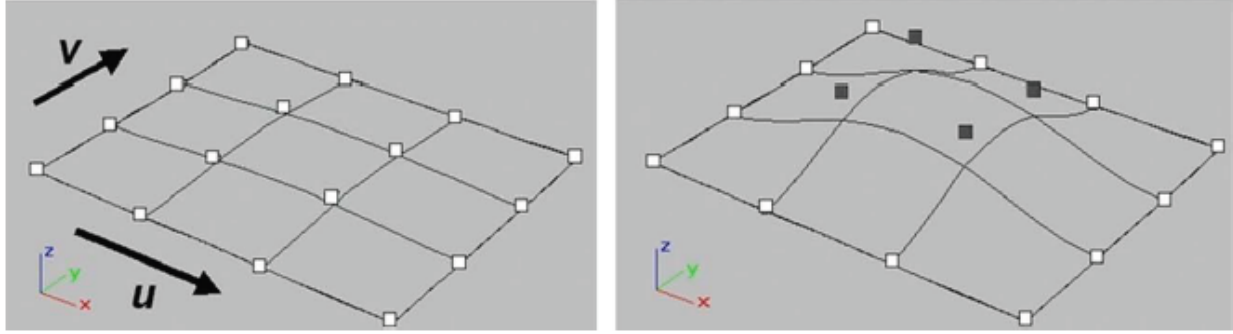
Figure 3.1: Depiction of NURBS surface modelled by a set of control points. The shaded control points on the right are translated upward, altering the shape of the surface. Taken from Segars et al [48].

The XCAT virtual phantom was extended into 4D to model cardiac and respiratory motion. Motion vs. Time curves for anatomical motion are applied to select control points, for example on the diaphragm for respiratory motion. The motion curves for cardiac rhythm and respiration were created from the gated CT images by tracking the 3D position of each control point defining cardiac or respiratory structures. These time curves can be manipulated by the user to simulate motion variations.

The XCAT virtual phantom program is able to produce CT images of the specified phantom via an analytical projection algorithm that creates planar images by projecting diagnostic energy x-rays from a source through the phantom. XCAT then reconstructs the projection data into a CT 3D volume image via filtered backprojection[41]. The output is a voxelized phantom representing a 3D distribution of attenuation coefficients saved as a raw binary image with no header. Examples of coronal and saggital views of CT images created in XCAT and their corresponding Radiation Therapy coordinate system are depicted in *Figure 3.2.*

The user also has the ability to set numerous parameters in order to customize the XCAT phantom for study specific purposes. This includes voxel size, respiratory motion amplitude, phantom size, energy of diagnostic x-ray source, etc. It also may be operated in different modes to simulate the user-defined male or female phantoms, heart lesions and spherical lung lesions, the latter of which were used for this study.
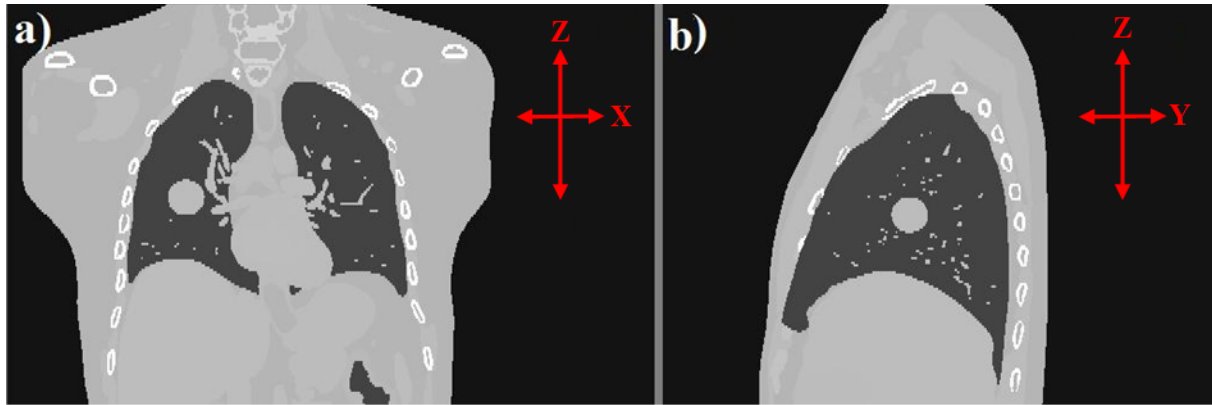
Figure 3.2:a) coronal and b) sagittal view of an XCAT phantom image used for planning with 3cm lesion diameter (1mm in-slice resolution with 2mm slice thickness).With the standard Radiation Therapy coordinate system designated.

3.1.2 Pinnacle treatment planning system

The commercial treatment planning system Pinnacle Version 9.0 (Philips Healthcare, Andover, MA) was used as an intermediate treatment planning platform for CT image importing, contouring and 3DCRT treatment planning. Pinnacle is a widely used Health Canada approved clinical 3D treatment software system. A screenshot from a Pinnacle planning GUI is shown in *Figure 3.3*. It offers a variety of advanced tools for forward and inverse treatment planning, optimization, CT image registration, automatic contouring (auto-contouring) for delineating structures and more. However, only the contouring tools and

forward planning tools such as dose calculation as well as positioning the treatment beams and

isocentre were utilized for this study.
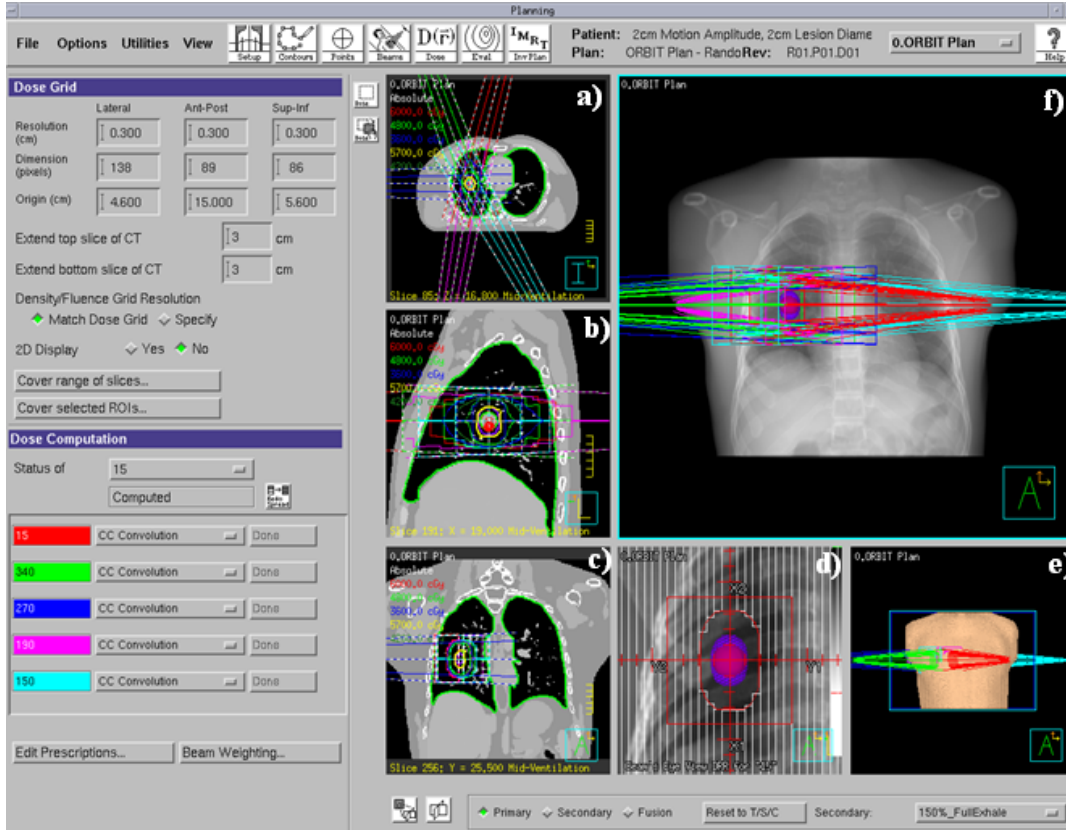
Figure 3.3: Screenshot of the Pinnacle GUI for forward planning in the view for dose calculation where the user sets the dose grid size and dose calculation algorithm for each beam using the menu on the left. The patient views on the right display a) an axial, b) saggital, c) coronal, d) beams eye view with the CTV and PTV contours e) surface rendering and f) Digital Reconstructive Radiograph. All views are shown with the beams angles on.

3.1.3 ORBIT treatment planning platform

ORBIT Workstation (Raysearch Laboratories, Stockholm Sweden) was the treatment

planning software used for the construction and analysis of the treatment plans in this study.

ORBIT is a stand-alone Windows-based treatment planning software developed in C++ for

Radiation Therapy research. Its main purpose is to provide an environment for development of

IMRT optimization, biological models, proton therapy and adaptive radiation therapy. ORBIT

possesses a GUI for IMRT optimization as seen in *Figure 3.4*. The GUI also provides access to tools for adaptive radiation therapy planning, including deformable image registration and dose accumulation based on images acquired at the time of planning and/or treatment. It should be noted that the ORBIT Workstation is compatible with the Pinnacle treatment planning system and treatment plans. Patient images may be imported and Pinnacle treatment plans may be recalculated and analyzed within the ORBIT software.

Only the standard direct-aperture IMRT optimization techniques were utilized in this study although ORBIT is also capable of changing the gantry, couch and collimator angles in a given treatment plan. The inverse planning process may be based on standard dose constraints as well as biological constraints and models that are in development. A homogeneous singular value decomposition based dose calculation algorithm is available as well as a heterogeneity corrected collapsed cone algorithm[49].
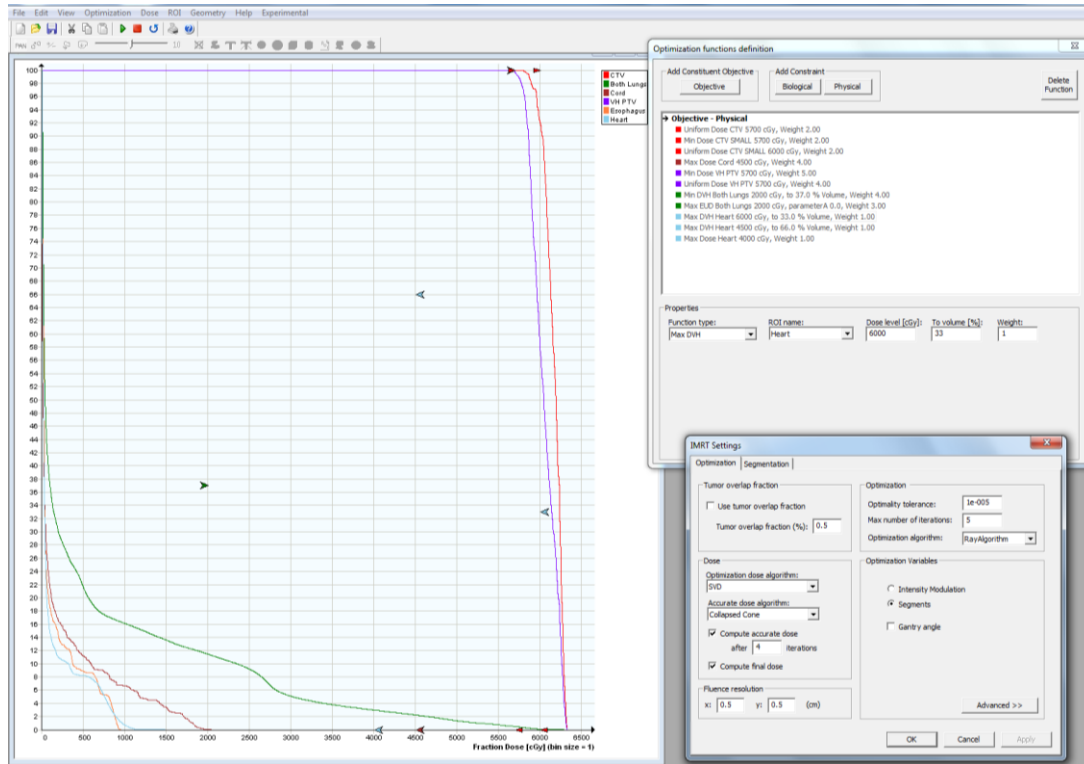
Figure 3.4: Screenshot of the ORBIT GUI for IMRT optimization for the 2cm lesion with 2cm motion amplitude. The final DVH is displayed (left) along with the IMRT objective functions (top right) and IMRT settings (bottom right) which remained constant for all plans.

The deformable image registration and dose accumulation tools available in ORBIT were used for this study to assess dose distributions within a patient undergoing respiratory motion during treatment delivery. The deformable dose accumulation uses surface meshes created from contours made in Pinnacle on CT images of the patient acquired during different treatment fractions. These images are loaded into ORBIT where the contours from the planning geometry are deformed to fit the current images. This establishes a point-to-point correspondence between the planning and treatment patient geometries and allows for the creation of deformation vector fields. ORBIT then calculates the dose on the new geometries represented by the 4DCT scans and the dose distributions calculated on the images corresponding to respiratory phases are deformed back to the original planning image using the deformation vector field information.[50] This allows the cumulative dose to the target and

51

surrounding OARS to be calculated as they are all mapped to the same reference frame. The specific accumulation process that was used in this study will be described again later in *Section 3.4.2* and is summarized in *Figure 3.5*.
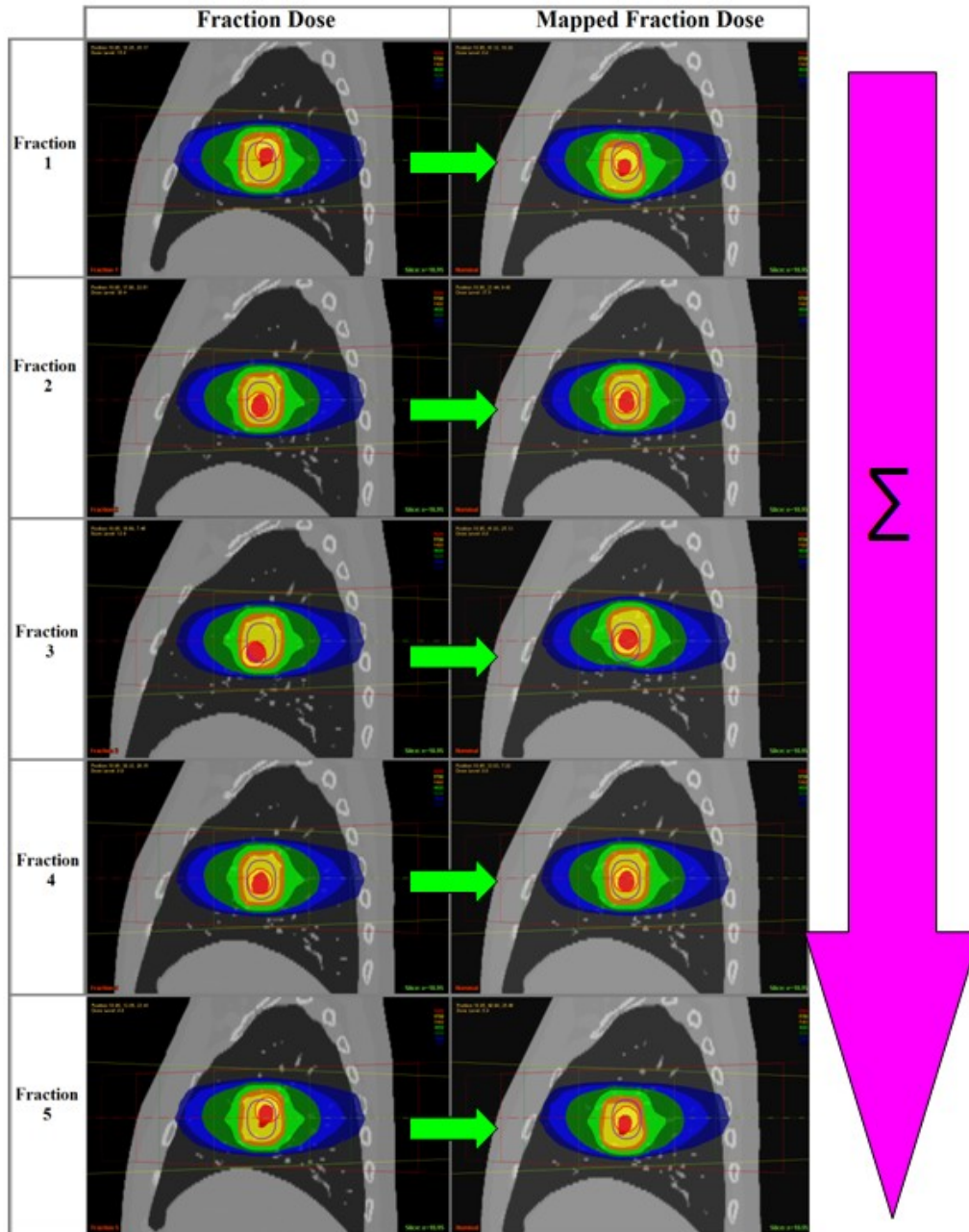
Figure 3.5: Summary of the dose accumulation process in ORBIT.

3.2 Generation of 4DCT data and image processing

The XCAT phantom program was used to generate the 4DCT datasets required for treatment planning and dose accumulation in this study. The following section describes the processes of creating each 4DCT dataset, including a midventilation CT required for the experiments performed in this thesis.

3.2.1 Creation of the 4DCT datasets required for planning

The XCAT program was executed in the standard phantom generation mode to produce three phantoms of a 50th percentile male with a respiratory period of 5 seconds and maximum diaphragm motion amplitude of 1, 2 and 3cm. The 4DCT images produced by the XCAT phantom consisted of five 3DCT datasets at 1.135 second intervals and corresponded to specific respiratory phases including full exhale, 50% inhale, full inhale, 41% exhale and 83% exhale. The temporal resolution was chosen to ensure the full inhale and full exhale phases were captured so an accurate sample of the full range of respiratory motion was obtained. All images produced for this study had a 512 x 512 pixels and a 1 mm^2 in-slice resolution. The slice spacing was 2 mm.

The XCAT images created following the procedure above corresponded to a healthy patient without any tumour. To add a tumour into the lung, the same process as outlined above was executed with the XCAT phantom program in the spherical lesion generator mode to generate images of a spherical lesion at the different respiratory phases. The lesion location corresponded to the centre of the right lung away from any density interfaces. Lesions phantoms were generated having a diameter of 1, 2 and 3 cm and peak-to-peak motion amplitudes of 1, 2 and 3 cm in the Z plane (cranial-caudal direction) for each lesion size.

Motion amplitudes in the X an Y planes were identical for all phantoms and consisted of 0 cm and 1.2 cm respectively. The lesion images for each respiratory phase were then added with the corresponding phantom images generated earlier. In total, 9 phantoms were created which in turn produced 9 4DCT datasets of a 50th percentile male with a lesion in the centre of his right lung (*Figure 3.6*).

3.2.2 Creation of the Midventilation dataset

In addition to a standard 4DCT dataset, an additional CT dataset corresponding to the time averaged position of the lesion was required for treatment planning. A midventilation CT image was constructed using XCAT for each of the 9 phantoms by the following procedure. The position of the lesion at each of the five respiratory phases for each 4DCT dataset created through the process outlined in *Section 3.2.1* was measured in AMIDE[51] which is a free and open source tool for viewing and registering medical images. The coordinates of the centre of mass of the contour. Using the coordinates of the lesion at each phase, the time-averaged position was calculated. XCAT was used to generate a CT image at a respiratory phase where the lesion position matched the calculated midventilation position. This was found to correspond to the 52% exhaled phase. A midventilation image was created for each of the 9 phantoms described in *Section 3.2.1*.
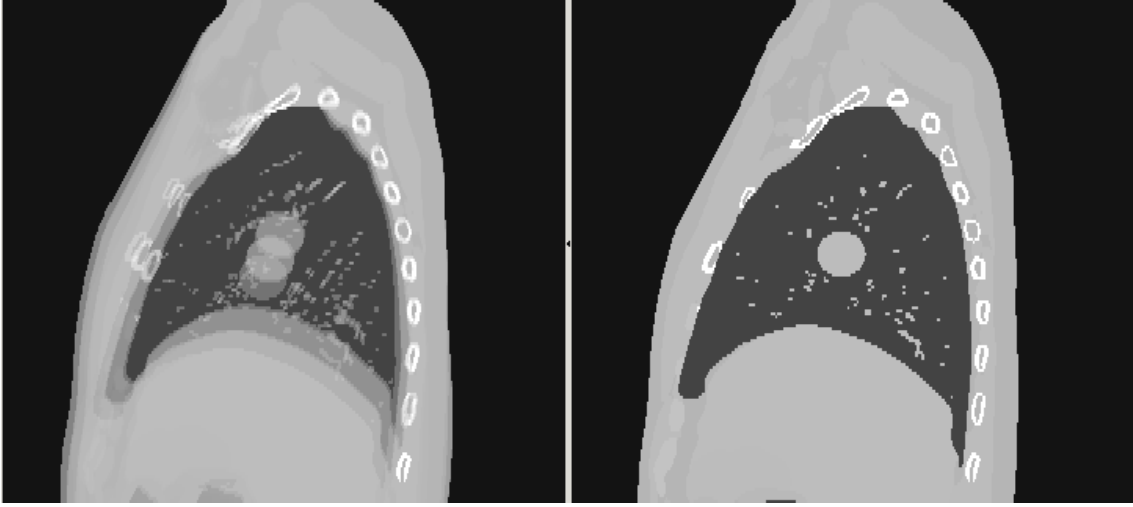
Figure 3.6: a) Sagittal view of the 5 4DCT respiratory phases overlaid demonstrating the lesion motion path. b) Sagittal view of the midventilation image.

3.2.3 Image processing for import to Treatment Planning System

The XCAT phantom program outputs a voxelized phantom representing a 3D distribution of attenuation coefficients saved as a raw binary image with no header. Therefore, further image processing was required to transform each 3D dataset into a standard 16-bit CT scan format to import these images into PINNACLE and ORBIT. To accomplish this, a C code was written which performed the task of converting the attenuation coefficientof each voxel into its corresponding Hounsfield Unit (HU). This is done via the formula:

$$HU = 1000 \times \frac{\mu_x - \mu_{water}}{\mu_{water}} \tag{8}$$

Where μ_x is the attenuation coefficient in question and μ_{water} is the average attenuation coefficient of water.

3.3 Treatment Planning

3DCRT and IMRT treatment plans were created for each of the 9 phantoms in the ORBIT Workstation. However, the Pinnacle treatment planning software was first required as

an intermediate platform for image importing, contouring as well as the 3DCRT treatment plan construction.

3.3.1 Image importing and contouring

The 4DCT datasets were imported into a Pinnacle Version 9.0 treatment planning workstation by creating a Pinnacle version of a DICOM image header file for each 4DCT dataset so that the raw image files would be recognized by the treatment planning system.

Once the images were imported, the organs at risk (OARs) and target volumes were contoured on the midventilation scan of each 4DCT dataset. All contouring of the OARs and the GTV was done using an auto-contouring tool to ensure consistency in the way contours were generated. The radiation therapy planning protocol from RTOG 0839[52] was followed for all OAR contouring and dose tolerances as seen later in *Table 3.1*. The GTV-CTV margin was set to 0 mm. Thus the CTV is equivalent to the GTV in this study. The PTV was created using an auto-expansion tool that expands upon a designated contour independently in the X, Y and Z plane, which in this case was the CTV. However, it should be noted that the size of the expansion and number of voxels is constrained by the resolution of the CT image set. As a result, the software must round the requested expansion to the nearest integer number of voxels. To account for this, all PTV calculated margins were rounded up to accommodate the scan resolution (*Table 3.2*).

A surface mesh was generated from the CTV contours for input into ORBIT where it is required for deformable image registration. The meshing procedure divides the surface area of the entire organ volume into a number of triangular elements with known vertices termed nodes. Surface meshes of the PTV contours were also generated to give the PTV a more

realistic smooth shape as the original PTV contours had a pixilated appearance *(Figure 3.7)* due to the contour resolution in Pinnacle being limited to 1 voxel [53].
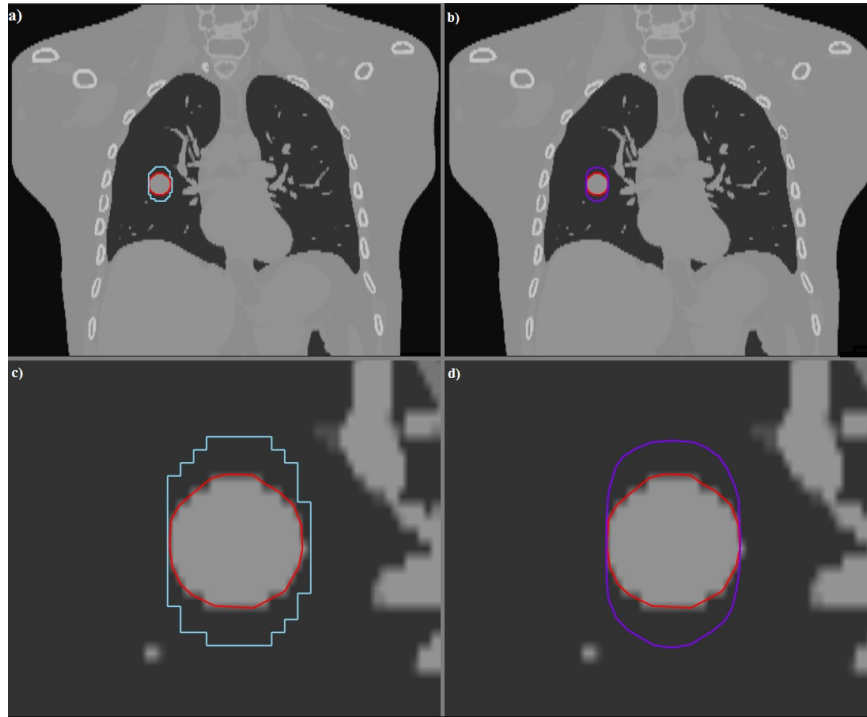
Figure 3.7: Coronal view of the coarse PTV contour (blue) in a) and c) (close-up) and the smooth PTV contour achieved with a mesh (purple) in b) and d) (close-up). The CTV is defined by the red contour.

3.3.2 Treatment planning parameters

Although it is impossible to produce identical treatment plans on the different phantoms, many steps were taken to ensure that the 3DCRT and IMRT treatment planning processes were consistent across all datasets. It was important that all plans possessed the same conformity and a similar distribution of dose within and outside of the PTV so that an accurate comparison could be made across all lesion sizes, motion amplitudes and planning techniques.

The dose coverage and avoidance goals from RTOG 0839[52] was followed with the exception of the acceptable plan variation parameters. In our study, the PTV had to be fully

covered by the 95% isodose volume whereas RTOG 0839 allowed for 93% coverage. All treatment plans in this study prescribed 60 Gy in 30 fractions to the isocentre, which was located within the CTV, and the maximum dose for a volume of at least $0.03cm^3$ within the PTV of no more than 125%.

All plans possessed the same beam arrangement of five beams at angles of 15⁰, 340⁰, 270⁰, 190⁰, and 150⁰ (*Figure 3.8*) and a 6 MV treatment beam energy.
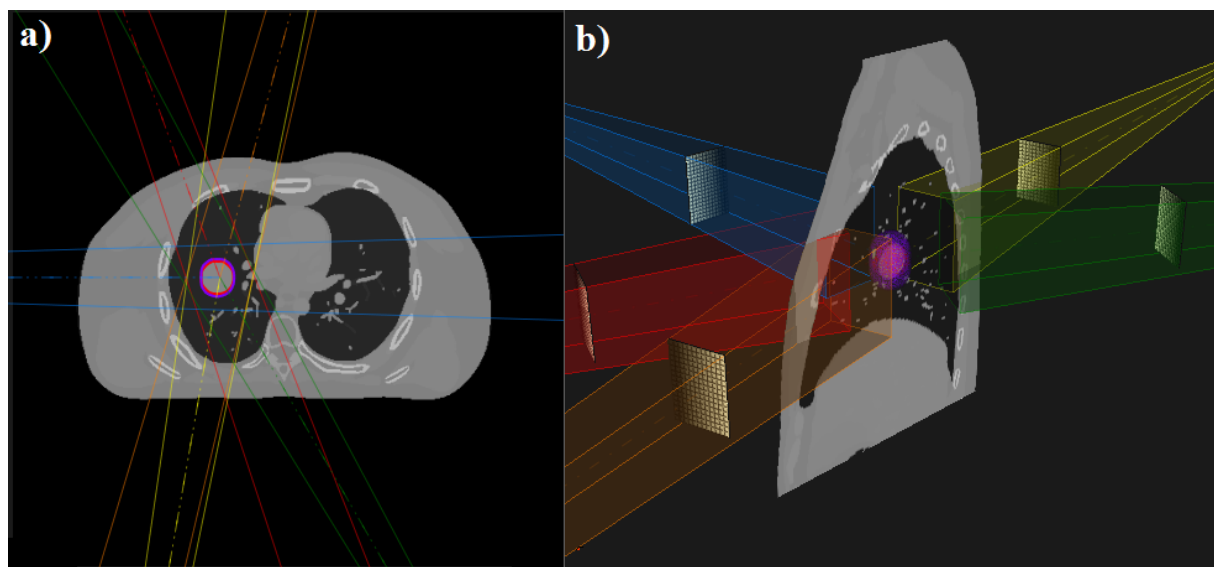
Figure 3.8: a) 2-D axial view and b) 3-D sagittal view of the 3cm lesion with 3cm motion amplitude displaying the beam angles, CTV and PTV.

All plans adhered to ICRU planning criteria[6, 7] and the OAR tolerance doses as per RTOG 0839[52] are displayed in *Table 3.1*. It should be noted that we omitted the restrictions on the brachial plexus as the location of the lesion was not close enough to pose a threat of toxicity. The priorities listed in *Table 3.1* are based on the severity of the toxicities associated with exceeding the dose parameters and are used in treatment planning to guide the planner on which dose constraint can be sacrificed at the expense of saving a more critical organ if all objectives cannot be achieved.

Organ	Priority	Dose parameter	Volume Parameter
Spinal cord	1	D_{max} < 50.5 Gy	
Lungs	2	D_{mean} < 20 Gy	V20Gy < 37%
Esophagus	3	D_{mean} < 40 Gy	
Heart	4	<60 cGy <45 cGy <40 cGy	V33% < 60 Gy V66% < 45 Gy V100% < 40 Gy

Table 3.1: OAR tolerance doses used for treatment planning[52].

All treatment plans were designed with the same level of conformity for the 95% isodose line around the PTV. Plan conformity was quantified using a metric called the Conformation Number (CN)[54] which measures how well a specified isodose level conforms to the edge of the target, in this case the PTV. The CN is calculated with the equation (9) where V_{95} is the volume of the target volume (TV) covered by the 95% isodose value and IV_{95} is the volume of the 95% isodose.

$$CN = \frac{V_{95}}{TV} \times \frac{V_{95}}{IV_{95}} \qquad (9)$$

A CN of 1 implies that the plan is perfectly conformal (*Figure 3.9a*). A CN of less than 1 implies that the target is either not covered by the reference isodose value, which in our case is 95% (*Figure 3.9b*), or the IV_{95} is far larger than the target (*Figure 3.9c*) or a combination of both.
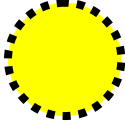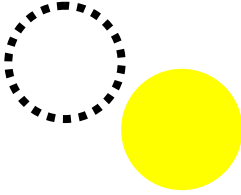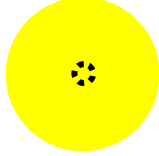
$CN = 1$	$CN = 0$	$CN \approx 0$
a)	b)	c)
TV: IV$_{95}$:	TV: IV$_{95}$:	TV: IV$_{95}$:
TV = 5 cm^3 IV$_{95}$ = 5 cm^3 V$_{95}$ = 5 cm^3	TV = 5 cm^3 IV$_{95}$ = 5 cm^3 V$_{95}$ = 0 cm^3	TV = 5 cm^3 IV$_{95}$ = 1600 cm^3 V$_{95}$ = 5 cm^3
$\dfrac{V_{95}}{TV} \times \dfrac{V_{95}}{IV_{95}} = 1$	$\dfrac{V_{95}}{TV} \times \dfrac{V_{95}}{IV_{95}} = 0$	$\dfrac{V_{95}}{TV} \times \dfrac{V_{95}}{IV_{95}} \approx 0$

Figure 3.9: Illustration of treatment planning scenarios that produce CNs of 1 a) and 0 b), c). Adapted from Feuvret et al.[54]

All of the treatment plans in this study were designed to achieve a Conformation Number (CN) of 0.6 with the exception of the 1 cm lesion diameter plans which had a CN of 0.5. It was not possible to construct a plan with full PTV dose coverage and a CN higher than 0.5 for the 1 cm lesion diameter as the MLC leaves were 1cm wide and the dose grid voxels were 3 mm in each plane (0.027 cm^3), which accounted for a larger fraction of the target volume compared to the other lesion sizes. Therefore, it only took a small MLC leaf adjustment and few dose grid voxels receiving less than 95% of the prescribed dose within the PTV to achieve an unacceptable V$_{95}$ value.

This investigation accepted a minimum V$_{95}$ value of 98.5% as the ICRU requires the target volume to receive at least 95% of the prescribed dose. Reducing the minimum V$_{95}$ value to 98.5% from the theoretically acceptable value of 100% was necessary to compensate for dose coverage artifacts caused by the position and resolution of the dose grid. *Figure 3.10* demonstrates that a target fully covered by the 95% when the isodose lines are interpolated

between voxels (*Figure 3.10a*) will have a V_{95} value less than 100% if even one dose grid

voxel of the target is covered by a dose of less than 95% of the prescribed dose.
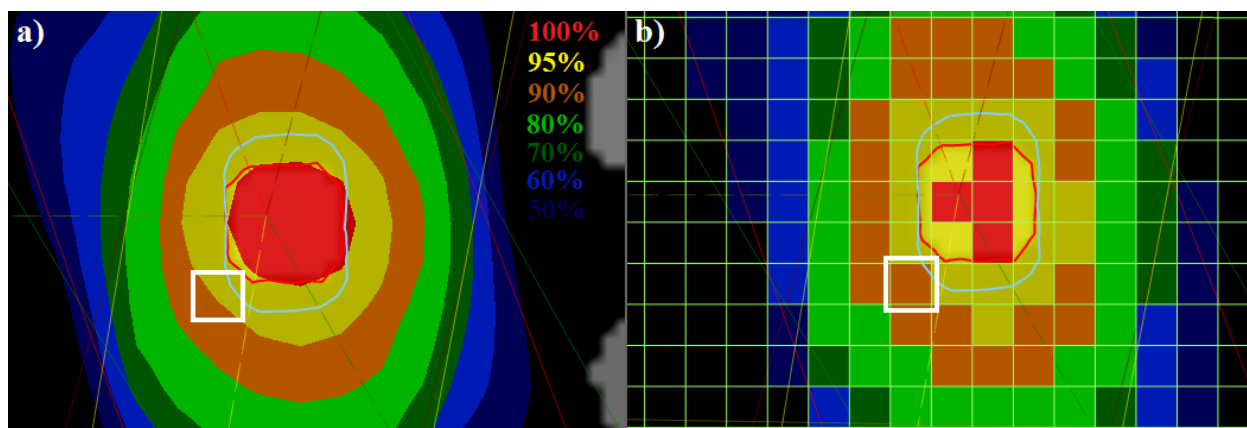
Figure 3.10: Axial view of the planned dose distribution on the 1cm lesion phantom. a) with the isodose lines interpolated between dose grid voxels and b) showing the dose in each voxel. The dose grid voxel that is not covering the PTV is highlighted in both views.

3.3.3 3DCRT Treatment planning process

The 3DCRT treatment plans were constructed with a Pinnacle version 9.0 treatment

planning workstation as ORBIT functions only as an IMRT planning platform. The treatments

were planned for a Varian Clinac 2100iX medical linear accelerator (Varian Medical Systems,

Inc., Palo Alto, CA). All dose distributions were calculated with the collapse-cone convolution-

superposition (CCCS) dose calculation algorithm in Pinnacle. Once an optimal dose

distribution was achieved, the treatment plan was imported into ORBIT and the dose

distribution was recalculated using the Collapsed Cone Convolution dose calculation

algorithm. One difficulty encountered in the transition between Pinnacle and ORBIT was that

they did not possess a common linear accelerator model which resulted in modest discrepancies

between dose distributions calculated for the same plan in the different treatment planning

platforms. The 3DCRT plan was recalculated using the beam model for a Varian Clinac 2100C

linear accelerator in ORBIT which was the closest match to the Varian Clinac 2100iX model in

PINNACLE. Due to this obstacle, once imported and recalculated in ORBIT, each 3DCRT plan had to be adjusted to produce an optimal dose distribution. The plans were adjusted by scaling the MUs, adjusting the location of the isocentre within the CTV and editing the treatment plan files to manually adjust the MLC positions.

3.3.4 IMRT Treatment planning process

Since ORBIT is an IMRT specific treatment planning platform, Pinnacle was only needed for importing the raw image formats and contouring for the IMRT planning process (unlike the 3DCRT planning process which required full plan construction in Pinnacle). The IMRT treatment plans were designed directly within ORBIT for the Varian Clinac 2100C linear accelerator through standard inverse planning techniques. All plans used the IMRT direct-aperture optimization technique and were given a limit of 25 segments per plan (5 segments per beam). Optimization objectives varied slightly between plans; however, common ones included full PTV coverage, a lung V_{20} of $\geq 37\%$ (all plans yielded much lower V_{20} values) and spinal cord doses under 40 Gy.

3.4 Evaluation of the VHMF in lung for random error

This section describes the methods used to investigate the ability of the VHMF to account for the random error component of respiratory motion. Realistic simulations of a changing dose distribution in the presence of respiratory motion were performed within the ORBIT treatment planning platform. All 3DCRT and IMRT treatment plans used in the simulations were constructed and optimized using the methods described in S*ection 3.3* on the 4DCT data acquired via the methods outlined in S*ection 3.2.*

3.4.1 Calculation of PTV Margin for random error

Since the peak-to-motion amplitude of the lesion within each of the 9 phantoms was known, the PTV margin required to account for respiratory motion could be calculated using the VHMF. In order to examine the random error component of respiratory motion alone, there was assumed to be no systematic error. This was accomplished by adopting a setup error of zero and using the mid-ventilation dataset for treatment plan construction. Planning on mid-ventilation eliminated the systematic error component of respiratory motion that results from the treatment being planned on a CTV location that deviates from its time-averaged position. By fully removing the systematic error, random dosimetric effect of respiratory motion from the CTVs motion through the planned dose distribution with breathing was isolated to accurately assess this component of the van Herk PTV margin.

Equation (10) calculated the margin required to account for random error alone:

$$Mrandom = 1.64(\sigma - \sigma_p) \tag{10}$$

Where σ is total the standard deviation of random motion and σ_p is the width of the penumbra. σ is calculated from the quadratic sum of the standard deviations of organ motion (σ_m), setup error (σ_s) and the width of the penumbra as outlined in *Section 2.4*. For this study, a perfect setup was assumed ($\sigma_s = 0$) to isolate the effects of respiratory motion, the standard deviation of organ motion was assumed to be one third of the lesion`s peak-to-peak amplitude[36] and a value of 6.4 mm was used as the width of the penumbra in lung[38].

Motion plane	Motion amplitude (cm)	σ_s (cm)	σ_p (cm)	σ_m (cm)	σ	van Herk margin (cm)	Margin rounded to scan resolution (cm)
Z	1	0	0.64	0.33	0.72	0.13	0.2
	2			0.67	0.92	0.47	0.6
	3			1.00	1.19	0.90	1.0
Y	1.2			0.40	0.75	0.19	0.2
X	0.1			0.03	0.64	0.00	0.0

Table 3.2: Summary of PTV margins used for random error calculated with the VHMF.

3.4.2 Simulation of random error - dose accumulation

ORBIT workstation was used to simulate the dosimetric effects of intrafractional respiratory motion for each 3DCT and IMRT treatment plan through dose deformation and accumulation based on surface meshes as outlined in *Figure 3.11*[50]. The surface meshes of the CTV created within Pinnacle on the midventilation CT used for planning were propagated and deformed to each of the five respiratory phases represented within each 4DCT dataset. This establishes a point to point correlation between the vertices (nodes) of the surface meshes so their movement from the reference image used for planning can be tracked. To accumulate the dose along the respiratory cycle, ORBIT applies the midventilation treatment plan to each of the five imported respiratory phases and recalculates the dose. It then deforms the image of each phase back to the nominal geometry along with the dose, based on the displacement of the nodes of the surface meshes. Thus, the dose distribution for each of the five respiratory phases may be displayed on the patient geometry for each respiratory phase or on the initial planning geometry as well, which in this case is the midventilation CT. The ability to map the dose back to the same patient geometry allows for the summation of each fractional dose as they are in the same reference system, thus enabling dose accumulation. The display of the fractional and accumulated dose on the planning patient geometry is extremely advantageous as it allows for

a direct comparison of CTV dose coverage between the planned dose and the dose in the presence of respiratory motion.
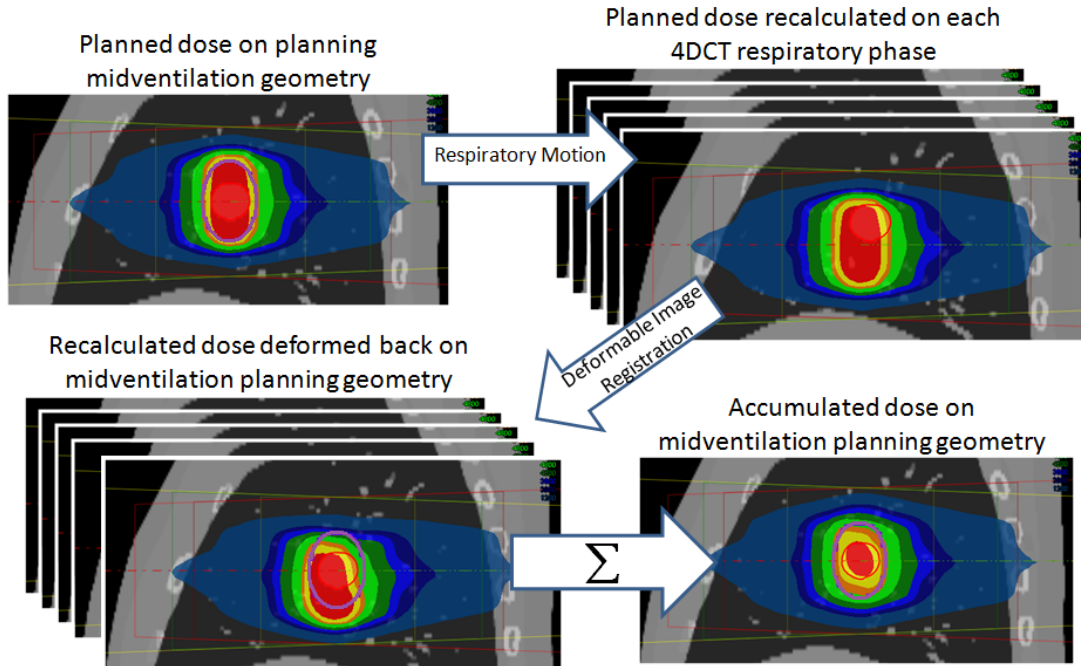
Figure 3.11: Illustration of the dose accumulation process used in ORBIT.

The number of images required for accurate dose accumulation was tested prior to the execution of these experiments. 4DCT datasets with 2 (inhale and exhale), 5 and 10 respiratory phases were generated with XCAT and accumulated on a 3DCRT treatment plan generated in ORBIT. The difference in the 95% dose volume from the original to accumulated plan between 5 and 10 phase 4DCT datasets was within 1%. Thus, accumulation over 5 phases was chosen as half the computational time was required. Accumulating over inhale and exhale only did not provide an adequate sample of the motion detail for accurate results as there was a large discrepancy of the 2 image accumulation results from 5 and 10 image tests.

3.5 Evaluation of the VHMF in lung for systematic error

The systematic error component of respiratory motion occurs in the CT simulation process and is the result of the CTV position being offset in the planning scan from its time averaged position. Since the dose model used for margin derivation is homogeneous, it is assumed by van Herk that rigidly shifting the dose distribution is equivalent to the CTV moving from its average position. The validity of this assumption was tested for lung malignancies by simulating a rigid shift scenario as well as a more realistic scenario where the patient's anatomy deforms in ORBIT to see how well they resembled each other. Although IGRT has shown to greatly reduce the effects of systematic error[55], we chose to simulate a treatment without daily imaging to represent a worst case scenario. For correct usage of the VHMF with image guidance, centre specific systematic error data for IGRT treatments should be obtained which would result in smaller $\sum$ values and in turn a smaller PTV margin.

3.5.1 Treatment Planning and PTV margin construction

The systematic error employed a single 3DCRT and IMRT treatment plan for each of the 9 phantoms which was constructed via the process described in *Section 3.3*. The treatment plan was then copied within ORBIT so that the plan isocentre could be shifted, as is assumed by the van Herk dose model, and compared to the realistic situation of the CTV moving within a stationary dose cloud. For this investigation, only one CT scan corresponding to the exhale phase was loaded into ORBIT for dose calculation. The exhale phase was chosen since it corresponds to the limit of CTV motion and also because many current planning protocols are performed on exhale. This is due to the fact that it is the respiratory phase where the CTV spends the most time, and where the lung volume is smallest so it ensures tolerance doses are conservative for the lung volumes[56]. The PTV margin for each plan was equal to the CTV

motion between the midventilation and exhale phase in each plane which is consistent with the formulation of the VHMF. For this portion of the study, the systematic setup error (Σ_s) and delineation error (Σ_d) were set to 0 (*i.e.* perfect setup and organ delineation).

Motion plane	Motion amplitude (cm)	Σ_s (cm)	Σ_d (cm)	Σ_m (cm)	van Herk margin (cm)	Margin rounded to scan resolution (cm)
Z	1			0.46	0.46	0.6
	2			0.88	0.88	1
	3	0	0	1.36	1.36	1.4
Y	1.2			0.53	0.53	0.5
X	0.1			0.04	0.04	0

Table 3.3: Summary of PTV margins used for the systematic error simulations.

3.5.2 Simulation of respiratory motion induced systematic error

The systematic shift invariant assumption made by van Herk was simulated by simply shifting the isocentre of each treatment plan by the distance the CTV travelled between the midventilation and exhale phases. The second scenario models the respiratory motion more accurately and models the displacement of the CTV and surrounding anatomy with deformation. This was achieved by applying the treatment plan to the exhale phase only and then mapping it back to the midventilation image for a direct comparison to the shifted plan within the same reference frame. Since dose is accumulated on a single image, this technique does not produce any motion blur and therefore isolates the systematic error component of the VHMF. The resulting dose distributions of the two scenarios depicted in *Figure 3.12* were then compared to assess the validity of the shift invariant assumption of the systematic component of the VMHF.
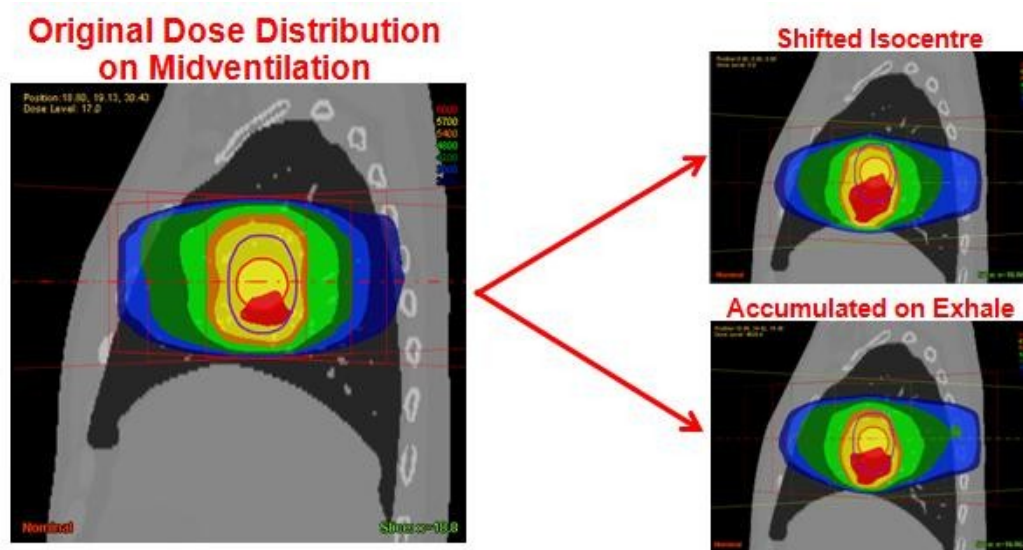
Figure 3.12: Illustration of the two scenarios used to simulate the systematic error component of respiratory motion in ORBIT.

3.6 Investigation of tissue density

It was initially hypothesized that the VHMF may not be applicable to all lung lesion sizes and motion amplitudes due to the loss of electronic equilibrium seen at the field edges in low density medium. To assess such effects an investigation was conducted that focused on the ability of the inputted penumbra width (σ_p) to adjust the van Herk margin for density effects. A second set of treatment plans were designed in the same manner as the random error investigation described in *Section 3.4*, but no heterogeneity correction was used for the dose calculation. Thus, the density all incident tissues were taken to be that of water. This was accomplished by employing the Singular Value Decomposition (SVD) dose calculation algorithm which assumes all incident tissue is water equivalent. Therefore, the σ_p value for soft tissue (3.2 mm) was used for the margin calculation phase of the experiment. A summary of the PTV margins used and their inputted parameters for calculation may be found in *Table 3.4*.

Motion plane	Motion amplitude (cm)	σ_s (cm)	σ_p (cm)	σ_m (cm)	Σ (cm)	van Herk margin (cm)	Margin rounded to scan resolution (cm)
Z	1			0.33	0.46	0.23	0.2
	2			0.67	0.74	0.69	0.8
	3	0	0.32	1.00	1.05	1.20	1.2
Y	1.2			0.40	0.51	0.32	0.3
X	0.1			0.03	0.32	0.00	0.0

Table 3.4: Summary of PTV margins used for random error calculated with the VHMF assuming the density of water.

According to the VHMF, decreasing the σ_p value increases the size of PTV margin required for random error to compensate for the steeper dose gradients in the penumbra regions of denser tissue. The accumulated dose was compared to the results of the random error simulations in lung density tissue to assess how the simulations differ if performed in standard soft tissue as opposed to lung and assess the ability of the σ_p value to account for density changes.

3.7 Evaluation of VHMF dose model

The accuracy of the VHMF ultimately relies on the ability of the dose model to correctly represent realistic static and blurred distributions. This was tested by comparing the actual dose distributions constructed for the random and systematic error simulations to their corresponding model. The following investigations evaluate the static and blurred dose profile models separately in order to determine if convolution can accurately mimic the real dose distributions. All of the data analysis for the following experiments was conducted in MATLAB (10.11, The MathWorks Inc., Natick, MA, 2010.)

3.7.1 Investigation of the van Herk static profile model

The ability of the static van Herk dose distribution model to mimic the dose distributions constructed in ORBIT was assessed through the comparison of their subsequent profiles. The ORBIT dose distributions were first imported into MATLAB via a series of files provided by RaySearch Laboratories for the reading and visualization of dose distributions, A MATLAB code was then constructed that finds the maximum value of the 3D dose matrix located within the CTV and plots a profile along the cranial-caudal direction (Z direction) *(Figure 3.13)*. All profiles present in this study were constructed in the cranial-caudal direction because the steepest dose gradients are present along the Z direction[40] as the treatment beams are incident perpendicular to this axis. The Z direction also corresponds to the dominant direction of respiratory motion.
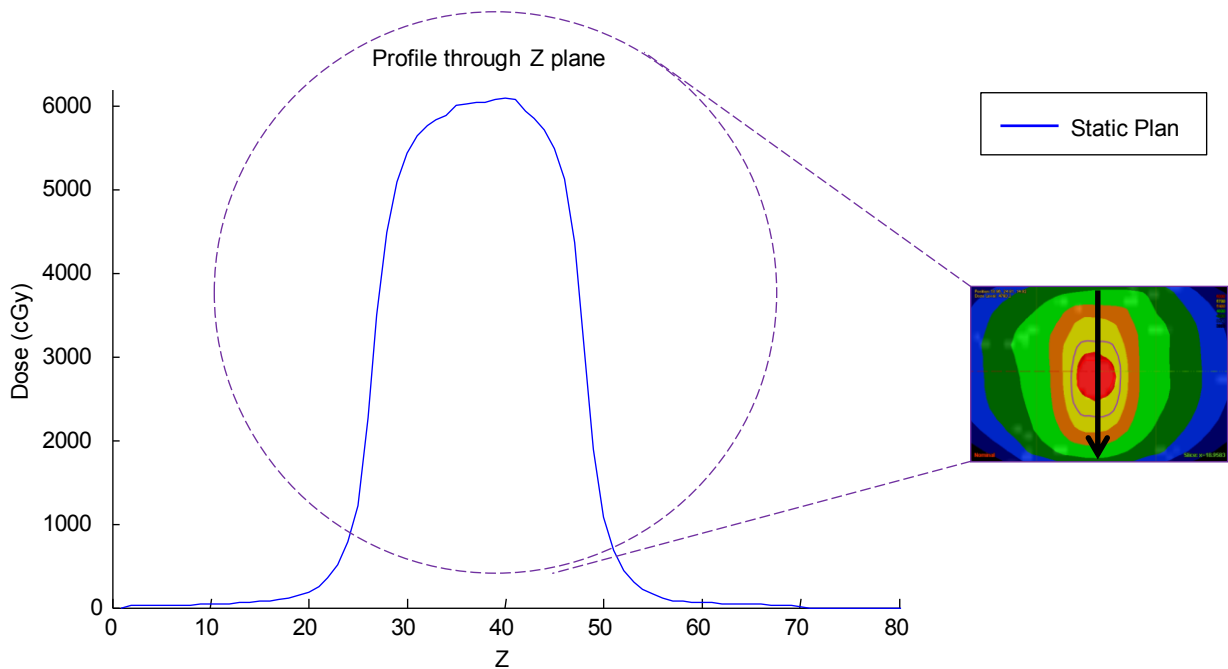
Figure 3.13: Depiction of the process executed in MATLAB for plotting the ORBIT dose profiles.

After the dose profiles were plotted, the corresponding van Herk profile models were constructed with a σ_p value of 6.4 mm for comparison. This was done with a MATLAB script that determines the width of the ORBIT profile at 30 Gy or 50% of the prescribed dose and constructs a top hat function of equal width. The profile model is then achieved by convolving the top hat function with a Gaussian function of 0 mean and SD of σ_p which is 6.4 mm in lung tissue according to the literature.

3.7.2   Accuracy of σ_p value

The first step in the derivation of the VHMF is the construction of the planned dose profile, $D_{planned}$, by convolving a top hat function with a Gaussian function with standard deviation σ_p. This method relies heavily on the accuracy of the σ_p value as it determines the slope of the penumbra defining the high and low dose regions that govern the PTV dose coverage. Thus in this case, one must be confident that the actual penumbra width in lung does not vary too far from the 6.4 mm value reported in literature. Higher σ_p values create broader penumbras and therefore smaller PTV margins are required as per the VHMF. A MATLAB code was created to find the optimal σ_p value that yields the van Herk dose profile model that most accurately resembles the corresponding ORBIT dose profile. The code plots the static ORBIT profile and uses it to plot the top hat function. It then iteratively convolves the top hat with series of Gaussians of SD within a fixed interval and finds the SD (σ_p value) which yields the smallest sum of squared residuals (SSR) to the data. The SSR is a statistical tool that measures the discrepancy between a model that has a single independent variable and any corresponding data. A small SSR implies that the model fits the data very well. The code yielded σ_p values that best fit the whole ORBIT profile as well as the top 5% of the profile.

3.7.3 Investigation of the van Herk blurred profile model

The second step in the derivation of the VHMF is the construction of the blurred dose profile, $D_{blurred}$, through convolving the static dose profile model with a Gaussian function of 0 mean and SD of σ. Since the random error experiments assumed no setup error, the σ ended up to be the SD of motion, $σ_m$, which is equal to one third of the peak-to-peak motion amplitude[38]. In order to test if this convolution can accurately model the dose in the presence of motion, the original static ORBIT profiles were convolved with a Gaussian function of 0 mean and SD of σ in MATLAB. These convolved profiles were then compared to the profiles of the accumulated ORBIT plans which realistically simulate the dose distribution in the presence of motion.

3.8 Investigation of plan conformity

One assumption of the VHMF is that it presumes perfect plan conformity, i.e. the 95% isodose line is the exact same size and shape as the PTV. However, in a realistic treatment planning scenario it is not possible for the prescription isodose to be tailored exactly to the shape to the PTV and therefore, in order to satisfy the ICRU planning criteria, the prescription isodose ends up being larger than the PTV. Therefore, the PTV margin calculated using the VHMF may be larger than required due to its inability to account for plan conformity. Relating this back to the derivation of the VHMF, without perfect plan conformity the initial top hat function in practice is larger than the derivation and thus the 95% dose level of the static dose model will not coincide with the edge of the PTV (*Figure 3.14*).
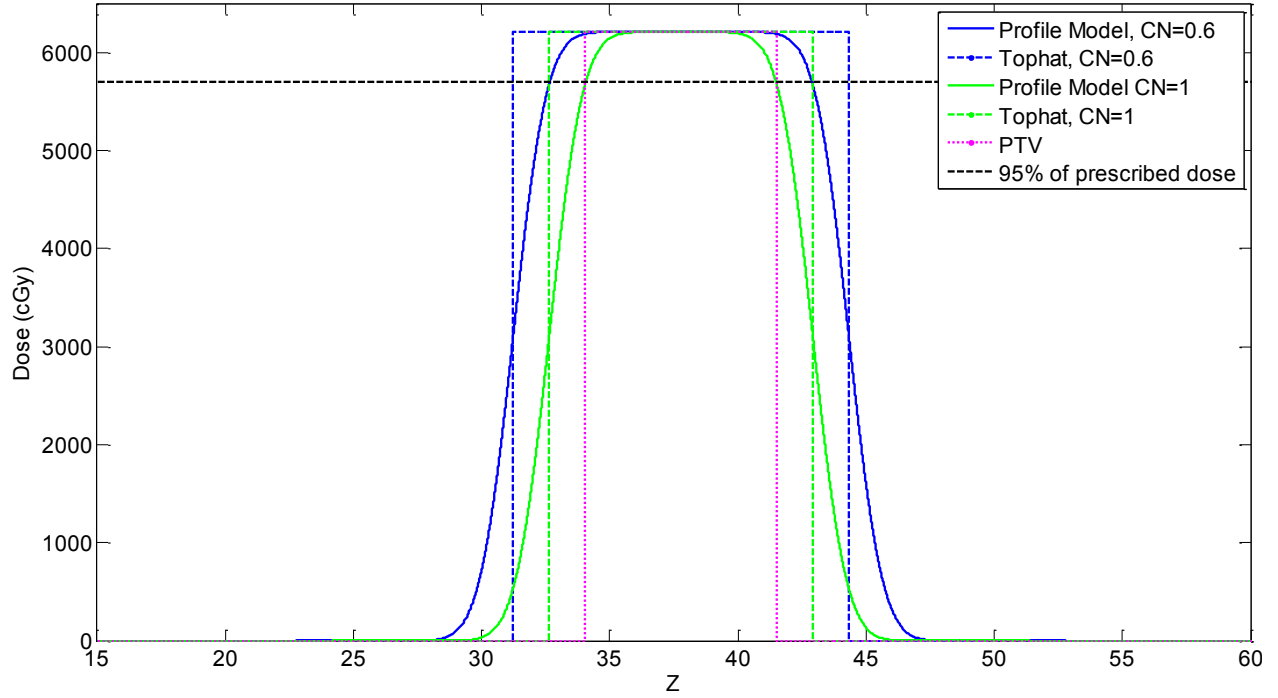
Figure 3.14: The van Herk models using a σ_p value of 6.4 mm for a 3cm lesion with 3cm motion with CNs of 1, 0.6 and their corresponding top hat function.

The influence of the plan conformity assumption was tested by performing the random error investigation described in S*ection 3.4* with two more 3DCRT treatment plans possessing higher CNs of 0.7 and 0.8, indicating more conformal plans. The 3 cm lesion with 3cm motion-amplitude was used for planning as it is easier to produce plans of high conformity with larger volumes due to the lesser impact of the dose grid size and MLC leaf width outlines in *Section 3.3.2*. It should be noted that 0.8 was the highest CN achievable while still maintaining adequate PTV dose coverage.   The goal of this study was to assess how the initial plan conformity affects the CTV coverage and if conformity restrictions should be placed on the safe use of the VHMF.

3.9 Suggested Improvements to the VHMF

One of the shortcomings of the PTV margins constructed with the VHMF identified early in this study was its inability to account for the lesion-specific motion trajectory. Specifically, a PTV margin expansion along the cranial-caudal, left-right and anterior-posterior direction may not be optimal for a tumour whose main axis of motion does not coincide with one of these axes. *Figure 3.15* demonstrates that a realistic CTV motion trajectory results in the movement through only a portion of the van Herk PTV. Thus, constructing a margin based on the vector components of the lesion peak-to-peak amplitude creates a target volume that expands into areas where the lesion does not travel. This provided adequate grounds for the hypothesis that the van Herk PTV may be larger than required and could result in the treatment of excess normal lung tissue.
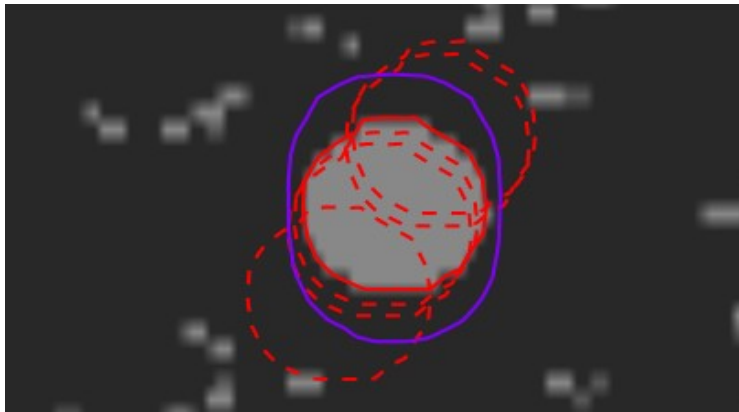
Figure 3.15: Close up sagittal view of a 2cm lesion with a 2cm peak-to-peak motion amplitude. The PTV is defined by the purple contour and the CTV is represented by the red contour with the dotted red contours showing the motion trajectory of the CTV.

3.9.1 Application of the VHMF to the ITV concept

In order to improve upon this shortcoming of the VHMF, a modification was applied to the existing coordinate system so it coincides with the CTV motion trajectory. This modified van Herk PTV was evaluated for the 2cm lesion diameter with 2cm motion amplitude. The new

coordinate system was constructed by simply rotating the old coordinate system so the Z plane (originally in the cranial-caudal direction) coincides with the dominant direction of motion of the CTV and was renamed as Z'. This new PTV was constructed in Pinnacle by fusing the inhale and exhale CTV contours and scaling the resulting ITV to match the dimensions of the calculated van Herk PTV.
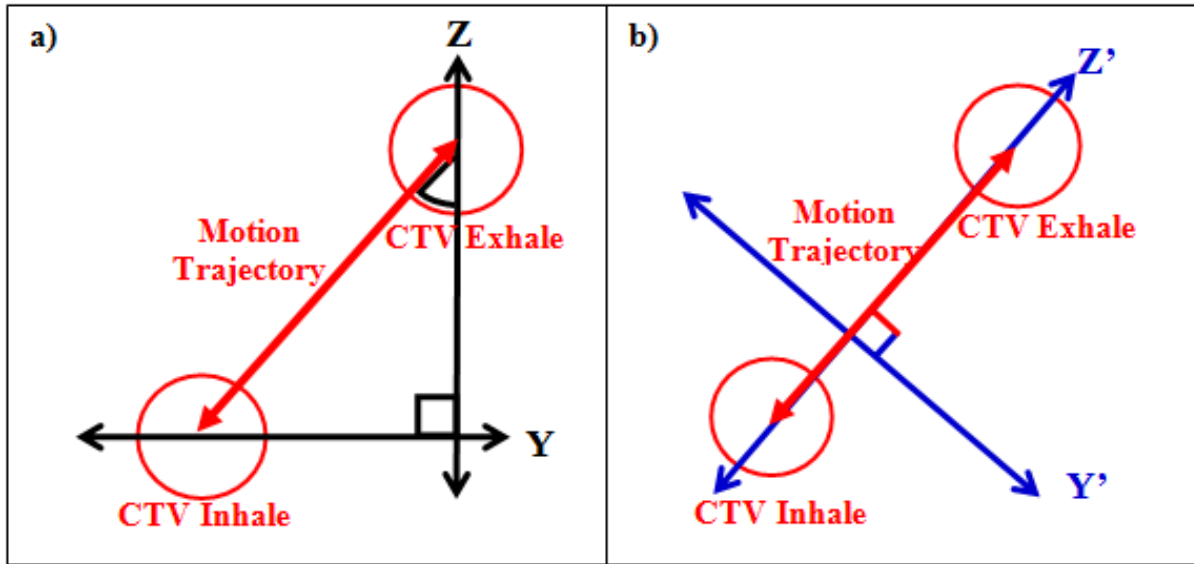
Figure 3.16: Depiction of a) the standard and b) modified coordinate systems

The random error investigation described in *Section 3.2* was repeated for the PTV margin within the new coordinate system for the 2cm lesion with the 2cm motion amplitude. Hence, the treatment plan was accumulated along the respiratory cycle to test the PTV for random error. The peak-to-peak motion amplitude for each new plane was calculated through similar triangles as depicted *Figure 3.17*. Since the location of the CTV was known within the original standard coordinates, the Z' trajectory was found by calculating the hypotenuse of the triangle in *Figure 3.16a* and the Y' trajectory was found via the opposite angle created by the intersection of the Z and Z' axes which is the same for both triangles depicted in *Figure 3.17*.

The same process was carried out in a coronal view to find the peak-to-peak motion amplitude in the X' plane.
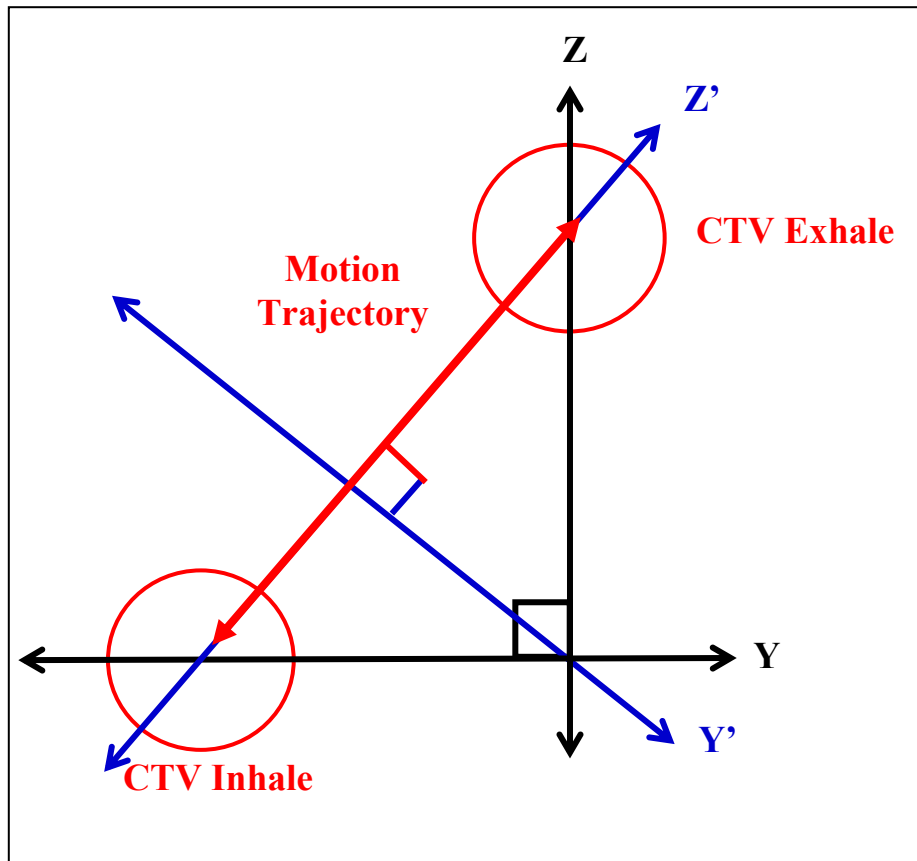
Figure 3.17: Diagram of the relationship of the two coordinate systems through similar triangles

CHAPTER 4

RESULTS AND DISCUSSION

4.1 Evaluation of the VHMF in lung for random error

This section summarizes the results of the dose accumulation experiments outlined in *Section 3.4* investigating the ability of the VHMF to compensate for the random error component of respiratory motion.

4.1.1 CTV dose coverage for the accumulated plans

The accumulated treatment plans yielded adequate CTV dose coverage by the 95% isodose volume for all lesion sizes and motion amplitudes for both the 3DCRT and IMRT treatment techniques (*Table 4.1*). The PTV margin constructed using the VHMF was deemed adequate if, on the accumulated dose distribution, the CTV volume receiving 95% of the prescribed dose or more (V_{95}) was 98.5% or above.

Lesion Diameter	Motion Amplitude	3DCRT	IMRT
		Accumulated V_{95} (%)	
	1cm	99.3	99.1
1 cm	2cm	99.6	99.9
	3cm	100	100
	1cm	99.9	99.9
2 cm	2cm	99.9	100
	3cm	99.6	99.7
	1cm	100	100
3 cm	2cm	100	100
	3cm	100	100

Table 4.1: V_{95} values for the accumulated 3DCRT and IMRT treatment plans

4.1.2 Accumulated plan conformity

Figure 4.1 demonstrates the shape of the 95% isodose before and after dose accumulation along the respiratory cycle. All of the accumulated plans demonstrated the characteristic shrinking of the 95% isodose as predicted by the van Herk model. All plans particularly showed the shrinkage in the direction of the CTV motion trajectory which is displayed by the dotted red contours in *Figure 4.1b*.
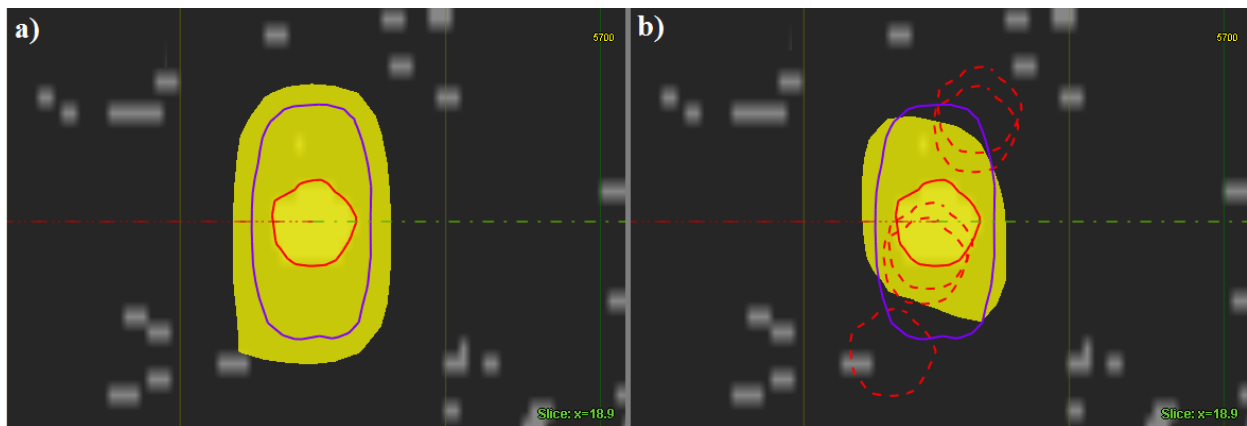
Figure 4.1: Close-up sagittal view of the 3DCRT dose distribution for a 1cm lesion with 3 cm motion amplitude. The 95% dose volume is represented by the solid yellow colourwash, the PTV is defined by the outer purple contour, and the CTV is represented by the inner red contour. a) Depicts the original static plan b) Illustrates the plan after dose accumulation with the dotted red contours showing the motion trajectory of the CTV.

Table 4.2 displays the calculated conformity number (CN) of all treatment plans before and after dose accumulation. It should be noted that the PTV was the target volume of interest used to calculate the CN in the static plans as opposed to the accumulated plans where the CTV became the target volume used for the calculations. The CN of the accumulated plan is affected by both a reduction in volume from the PTV to the CTV, which should lower the CN, as well as the reduction in the volume of the 95% isodose between the static and accumulated dose distributions, which should increase the CN. In this case, the decrease in volume of the CTV

compared to the PTV is larger than the 95% isodose shrinkage and therefore the net effect is a reduction in CN.

Lesion Diameter	Motion Amplitude	Initial CN*	3DCRT		IMRT	
			Accumulated Plan CN†	Reduction in 95% Volume (%)	Accumulated Plan CN†	Reduction in 95% Volume (%)
1 cm	1cm	0.5	0.45	33	0.42	36
	2cm		0.25	38	0.21	21
	3cm		0.20	49	0.21	51
2 cm	1cm	0.6	0.55	26	0.55	28
	2cm		0.43	27	0.48	33
	3cm		0.37	39	0.39	41
3 cm	1cm	0.6	0.49	13	0.55	19
	2cm		0.45	23	0.45	22
	3cm		0.40	28	0.40	30
*PTV is the target volume used for the CN calculation						
† CTV is the target volume used for the CN calculation						

Table 4.2: CN values of the static and accumulated 3DCRT and IMRT treatment plans.

An interesting trend displayed within this data is the inverse relationship between the 95% isodose volume shrinkage and the accumulated plan conformity for a given lesion diameter. Although the 95% percent shrinkage increased with peak-to-peak motion amplitude as anticipated, the plan conformity decreased *(Figure 4.2).* To investigate this further, a visual comparison of the static and accumulated dose distributions was performed because although the CN is a useful metric for treatment plan evaluation, it lacks spatial information. Upon analysis of the accumulated dose distributions, it was evident that the reduction in the 95% dose volume was only in the direction of motion, which in this case was in the posterior-superior and anterior-inferior directions. In other words, the tumour moved diagonally along the Z-Y plane which is most easily observed in a sagittal view *(Figure 4.1b).*
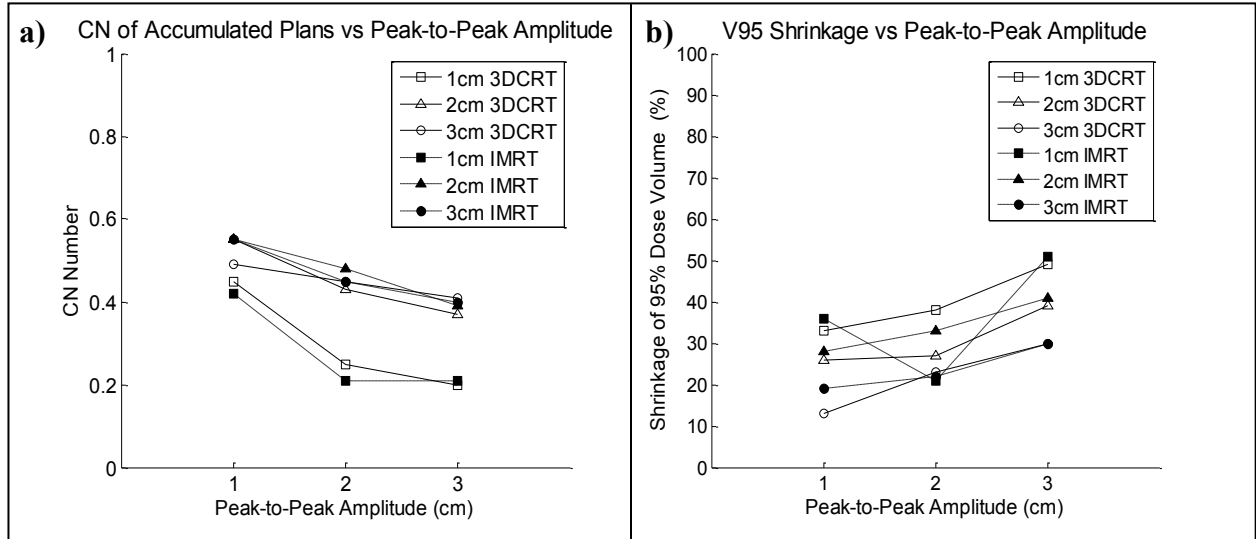
Figure 4.2: Plots of a) the CN and b) the shrinkage of the 95% dose volume as a function of peak-to-peak motion amplitude, demonstrating their inverse relationship.

This explains the lower CN value of the accumulated plans compared to their nominal plan value of 0.6 (or 0.5 for the 1cm diameter lesions) as the VHMF can only address motion independently within each plane. In reality, the tumour motion trajectory occurs simultaneously in multiple planes determined by the patient specific respiratory motion. Since the CTV moved diagonally through only a portion of the PTV, an unnecessarily treated volume of healthy tissue is left at the periphery of the CTV in the areas that did not experience any motion blur indicated by the white arrows in *Figure 4.3*. This volume increases with the motion amplitude yielding less conformal plans for greater motion amplitudes, thus explaining the inverse relationship between the peak-to-peak motion amplitude and the CN of the accumulated plans. The deviation from this pattern seen with the IMRT plan for the 1cm lesion diameter with 2cm motion amplitude is an artifact due to the fact that the volume of one dose grid voxel accounts for a greater portion of the 95% dose volume. Thus a difference of 1 voxel appears to have a larger impact on the results.

80
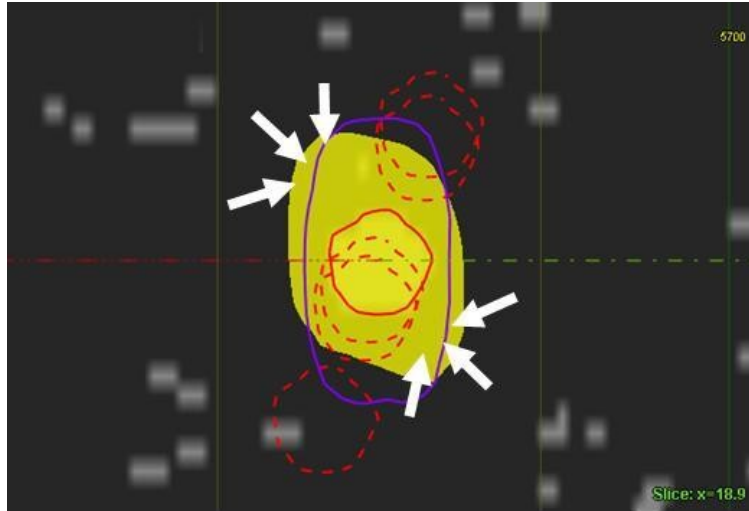
Figure 4.3 Close-up saggital view of the accumulated 3DCRT dose distribution for a 1cm lesion with 3 cm motion amplitude. The white arrows indicate the excess healthy tissue contained within the 95% dose volume at the periphery of the CTV.

4.1.3 IMRT vs. 3DCRT planning techniques

It was originally thought that IMRT planning techniques may result in poorer accumulated CTV dose coverage compared to 3DCRT plans due to the steeper dose gradients in the IMRT plan. However, the previous results show that there was not a significant difference in coverage, accumulated CN or any apparent trends observed between the two plan types as demonstrated in *Table 4.1*. Steeper dose gradients were observed for the IMRT plans, particularly in the cranial-caudal direction illustrated in *Figure 4.4*. However, the VHMF was still robust enough to compensate for this and provide equal dose coverage for both types of plans, provided they possess same initial CN.

81
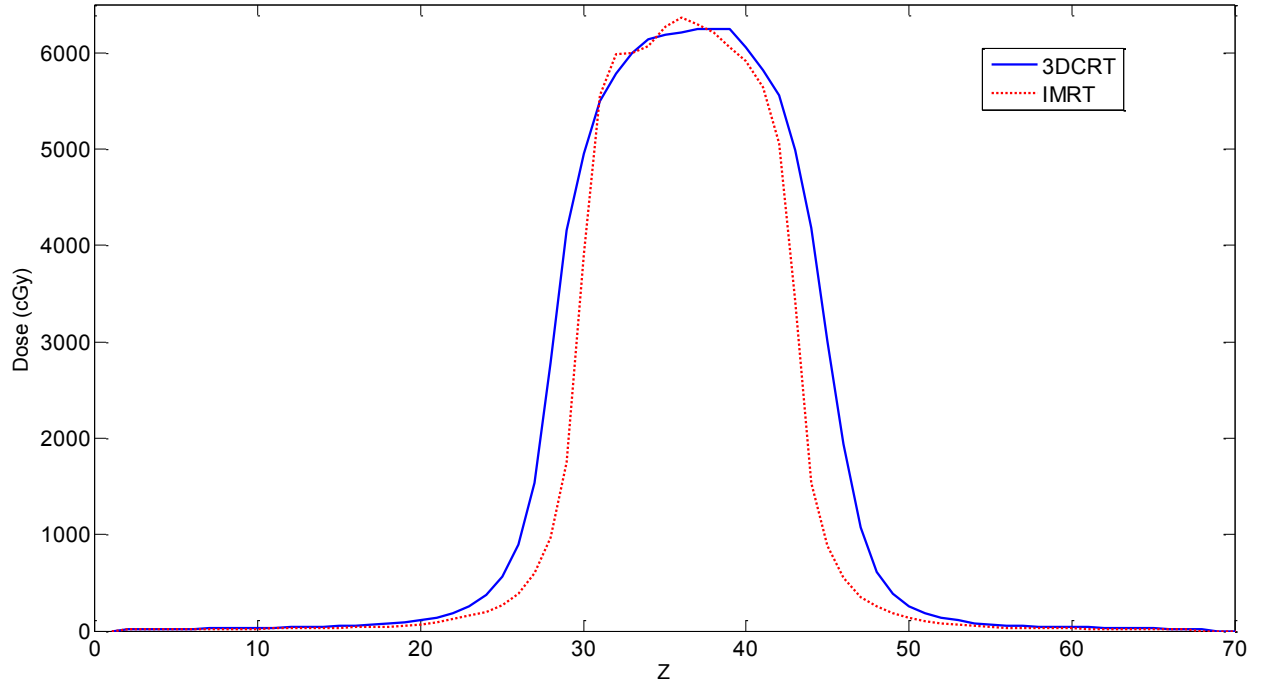
Figure 4.4: The sharpness of dose gradients observed in the IMRT plans compared to the 3DCRT plans using the 2cm lesion with 1cm of peak-to-peak motion profiles as an example.

4.2 Evaluation of the VHMF in lung for systematic error

This section summarizes the results of the experiments performed investigating the ability of the VHMF to compensate for the systematic component of respiratory motion. In the following results, the shift invariance assumption of the VHMF was investigated to assess if rigidly shifting the dose distribution could accurately model the systematic offset of the CTV. It should also be noted that the rigid shift approach resembles the effect of a setup error, compared to the accumulation approach which models a systematic difference in the tumour position as a result of respiratory motion. In a realistic planning scenario, both these contributions must be taken into account.

4.2.1 Comparison of shifted and accumulated plans

For both the shifted and accumulated treatment plans, adequate CTV dose coverage by the 95% isodose volume was achieved for all lesion sizes and motion amplitudes for both the 3DCRT and IMRT treatment techniques as demonstrated in *Table 4.3*. In fact, all V_{95} values for the two scenarios were within 2% of each other and the CN differed by a maximum value of 0.03 across all pairs of plans. Thus, for these experiments the assumptions related to the systematic error component of the VHMF has been shown to be safe. However, it should also be noted that the lesions were located in the centre of the lung and therefore cannot represent all lung cancer cases.

Lesion Diameter	Motion Amplitude	3DCRT				IMRT			
		V_{95} (%)		CN around CTV		V_{95} (%)		CN around CTV	
		S	A	S	A	S	A	S	A
1 cm	1cm	99.2	99.1	0.12	0.13	98.5	99.5	0.11	0.13
	2cm	99.9	100	0.07	0.06	100	99.8	0.06	0.07
	3cm	99.9	100	0.05	0.06	98.7	99.5	0.05	0.06
2 cm	1cm	100	100	0.23	0.25	99	99.1	0.23	0.24
	2cm	99.8	99.7	0.17	0.20	99.8	99.2	0.17	0.20
	3cm	98.4	99.9	0.16	0.15	99.5	99.6	0.34	0.33
3 cm	1cm	100	100	0.29	0.30	100	100	0.29	0.30
	2cm	99.9	100	0.23	0.25	99.9	99.9	0.24	0.25
	3cm	99.9	100	0.19	0.21	99.8	99.8	0.19	0.20
"S" stands for the shifted plans, where "A "stands for the accumulated plans									

Table 4.3: V_{95} and CN values for the shifted and accumulated 3DCRT and IMRT treatment plans

Despite the similarities seen between the shifted and accumulated plans, there were some differences observed as well. The 95% isodose volume varied between the two scenarios with no apparent pattern as demonstrated in *Table 4.4*.

		3DCRT		IMRT	
Lesion Diameter	**Motion Amplitude**	**Difference in Shifted & Accumulated 95% Dose Volumes**		**Difference in Shifted & Accumulated 95% Dose Volumes**	
		(cm^3)	**Dose Grid Voxels**	**(cm^3)**	**Dose Grid Voxels**
1 cm	1cm	0.70	25.93	0.86	31.85
	2cm	2.62	97.04	1.92	71.11
	3cm	2.65	98.15	0.71	26.30
2 cm	1cm	1.97	72.96	0.43	15.93
	2cm	5.62	208.15	6.16	228.15
	3cm	4.48	165.93	0.79	29.26
3 cm	1cm	4.29	158.89	1.16	42.96
	2cm	6.64	245.93	5.40	200.00
	3cm	7.43	275.19	4.75	175.93

Table 4.4: Difference in the 95% dose volumes for the shifted and accumulated 3DCRT and IMRT treatment plans.

This was more prominent for the large CTVs with large motion amplitudes that differed up to 7.43 cm^3 which is equivalent to approximately 275 dose grid voxels as shown in *Figure 4.5*. The discrepancy between these two scenarios is due to the inherent differences in their surface curvature and tissue inhomogeneities in the path of the beams. The larger target volumes displayed more variation as they required larger fields. This increases the probability for differences in inhomogeneities and surface contour changes which subsequently increases the variation of the 95% isodose volume between the two scenarios.
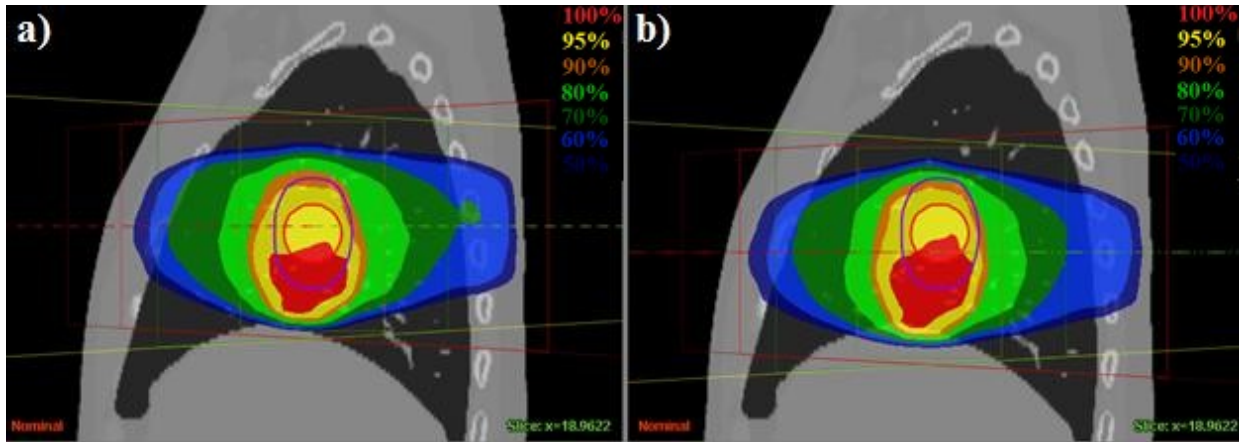
Figure 4.5: Sagittal view comparing the 3DCRT a) accumulated and b) the shifted treatment plans for the 3cm lesion with 3cm motion amplitude.

This is further illustrated in *Figure 4.6* where the original, shifted and accumulated dose profiles of the 3DCRT plans constructed for the 3cm lesion diameter with the 3cm motion amplitude are displayed. The shifted and accumulated plans appear to be stretched along the x axis, which corresponds to the cranial-caudal direction. This can be observed upon visual inspection of the plans as demonstrated in *Figure 4.5*. There is also an obvious offset between the static and accumulated plans which was observed for all lesion sizes, motion amplitudes and treatment types. This illustrates that the shifted plans overestimate movement of the dose distribution in the inferior direction, implying that the van Herk assumption could lead tolarger margins than necessary. However, the 95% dose regions of the shifted and accumulated profiles do agree at the edge of the CTV along the direction of the systematic offset for these experiments.
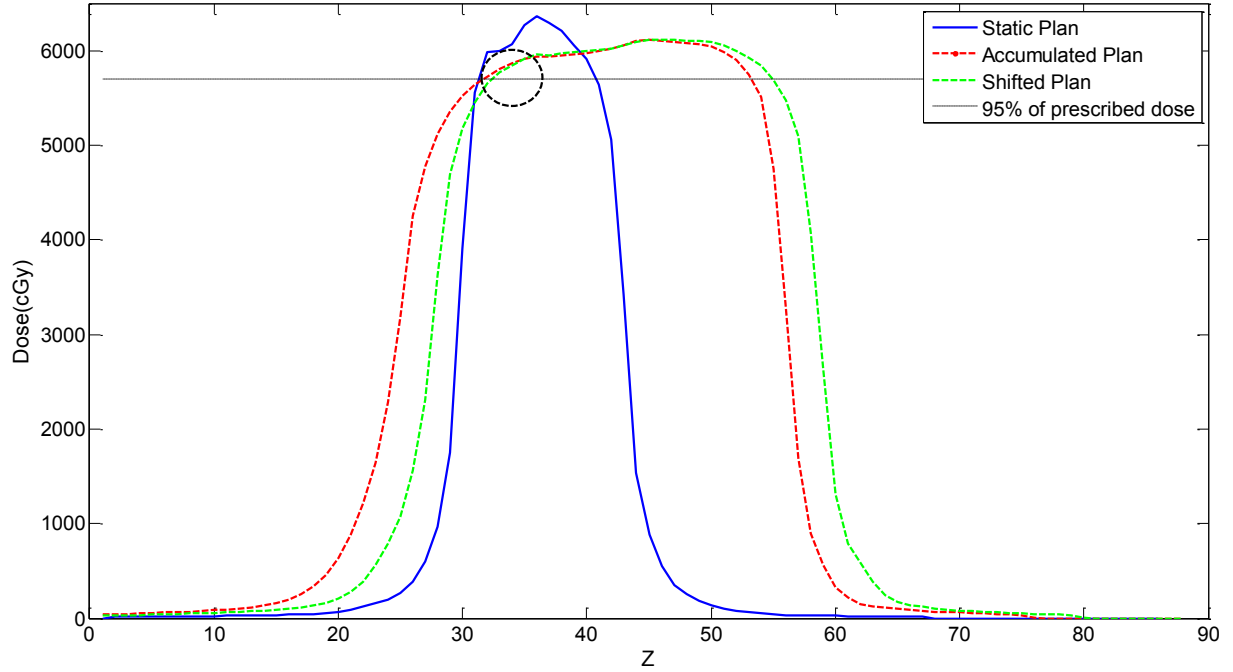
Figure 4.6: Profiles of the 3DCRT plans for the 3cm lesion with 3cm motion amplitude.

4.3 Investigation of tissue density

The CTV coverage for all accumulated 3DCRT and IMRT treatment plans designed with the homogeneous dose calculation algorithm and van Herk PTV margin constructed for soft tissue was comparable to the coverage of the heterogeneously calculated plans discussed in *Section 4.1.2*. However, discrepancies were seen with the 1cm lesion size with 1cm motion amplitude. All of the other lesion sizes, motion amplitudes and treatment types produced accumulated plans with full CTV 95% dose coverage and similar CNs to the heterogeneous results as seen in *Table 4.5*. This is consistent with the findings of *Witte et al.*[38] who claimed the VHMF was safe for clinical use except for small targets in soft tissue.

		3DCRT	IMRT
Lesion Diameter	Motion Amplitude	Accumulated V_{95} (%)	
1 cm	1cm	97	94
	2cm	100	100
	3cm	100	100
2 cm	1cm	99.9	99.9
	2cm	100	100
	3cm	99.9	100
3 cm	1cm	100	100
	2cm	100	100
	3cm	100	100

Table 4.5: V_{95} values for the accumulated 3DCRT and IMRT treatment plans, with no heterogeneity correction.

Decreasing σ_p from 6.4 mm to 3.2 mm increases the required PTV margin calculated with the VHMF compared to lung tissue. This is due to steeper dose gradients that occur in denser tissue due to the decreased range of secondary electrons. Hence, the CTV would move into a lower dose region more quickly if displaced. Upon further analysis of the treatment plans for the 1cm lesion size with 1cm motion amplitudes the σ_p value of 3.2 mm did a good job of mimicking the planned profile as seen in *Figure 4.7a.* However, the convolution assumption did not hold for this small PTV size as a reduction in the maximum dose was observed for both the IMRT and the 3DCRT plan as demonstrated in *Figure 4.7b*.
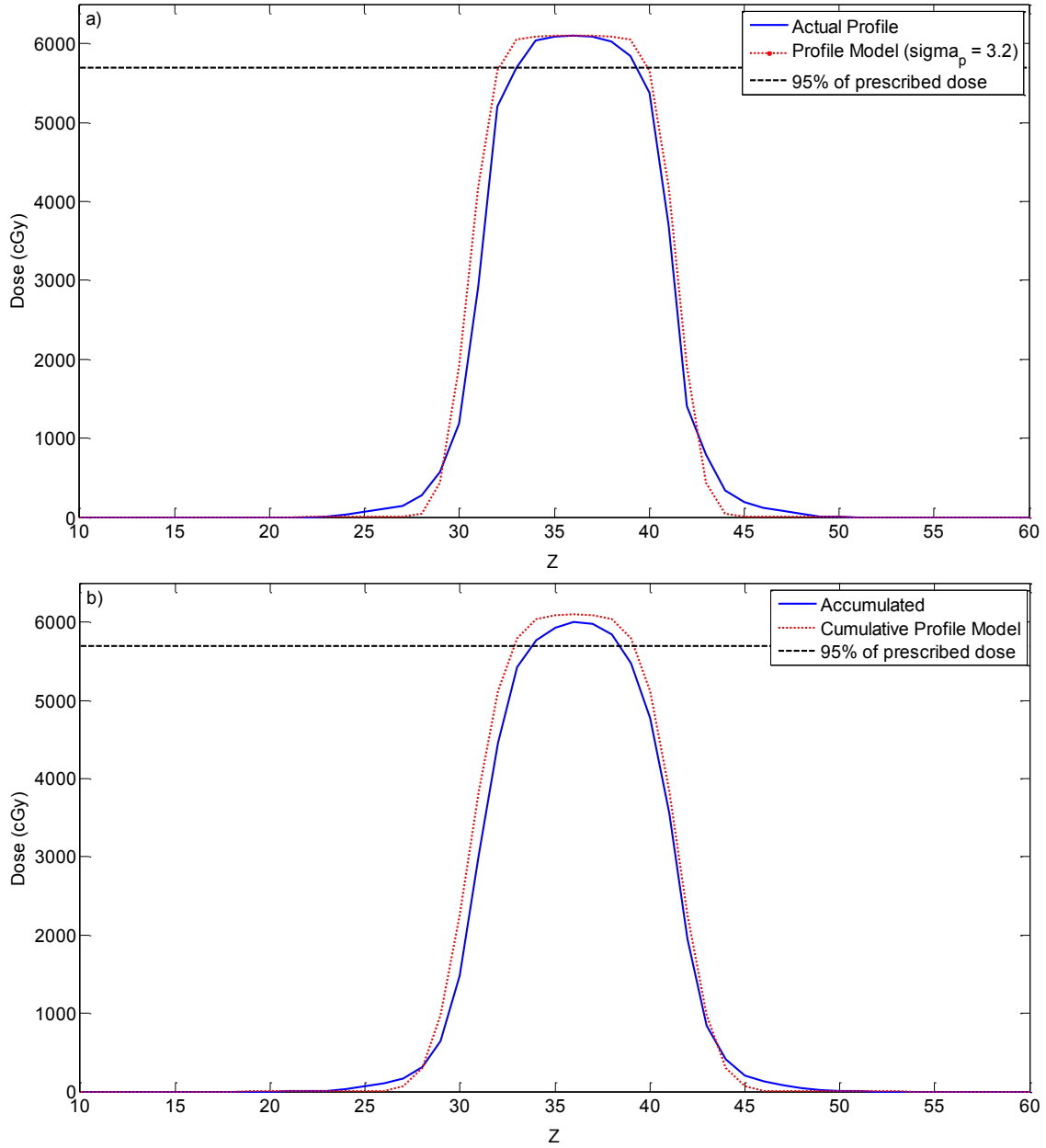
Figure 4.7: Comparison of a) the static VHMF dose model and corresponding 3DCRTORBIT plan and b) the accumulated 3DCRT ORBIT plan profile and the static profile convolved with a Gaussian of SD= σ_m for the 1cm lesion size with 1cm motion amplitude

These results show that accurately selecting the σ_p value that describes the penumbra width adequately compensates for variations in dose with tissue density except for very small targets in denser medium as also found by *Witte et al.*[38].

4.4 Evaluation of VHMF dose model

The VHMF is derived using analytical models of the static and blurred dose distributions. The first step to model the static profile is the convolution of a top hat function with a Gaussian function of SD equal to σ_p. This convolution models the dose falloff at the edge of the beam due to the penumbra. The blurred dose profile is modeled by a second convolution of the static profile model with a Gaussian function of SD equal to σ_{random}, which is the square root of the SDs of all random errors added in quadrature. This is equivalent to shifting the static dose profile to a series of random points along the respiratory cycle and computing the weighted sum of all of the profiles. However, the resulting models are idealized as they represent a perfectly conformal homogeneous treatment plan. Thus, the top hat function is designed so the resulting static dose distribution conforms perfectly to the edge of the CTV, which is not achievable in realistic treatment planning. The accuracy of this double convolution method was addressed with two separate experiments outlined in *Section 3.7* separating each convolution required for the derivation of the static and blurred plan models in hopes to justify or annul the underlying assumptions made by van Herk. We also plan treatment with wider beams than the VHMF assumes as high conformity is difficult to manage.

4.4.1 Investigation of the van Herk static profile model

The width of the penumbra represented by the σ_p value in the VHMF for lung tissue was found to be 6.4 mm in the literature. This value was used to derive the PTV margins for the random error investigation. In *Figure 4.8*, a dose profile which was extracted along in the Z direction through the maximum dose value within the CTV of the static dose distribution in ORBIT, is compared to its equivalent profile model which was generated by convolving its corresponding step function with a Gaussian function possessing a σ_p value of 6.4 mm
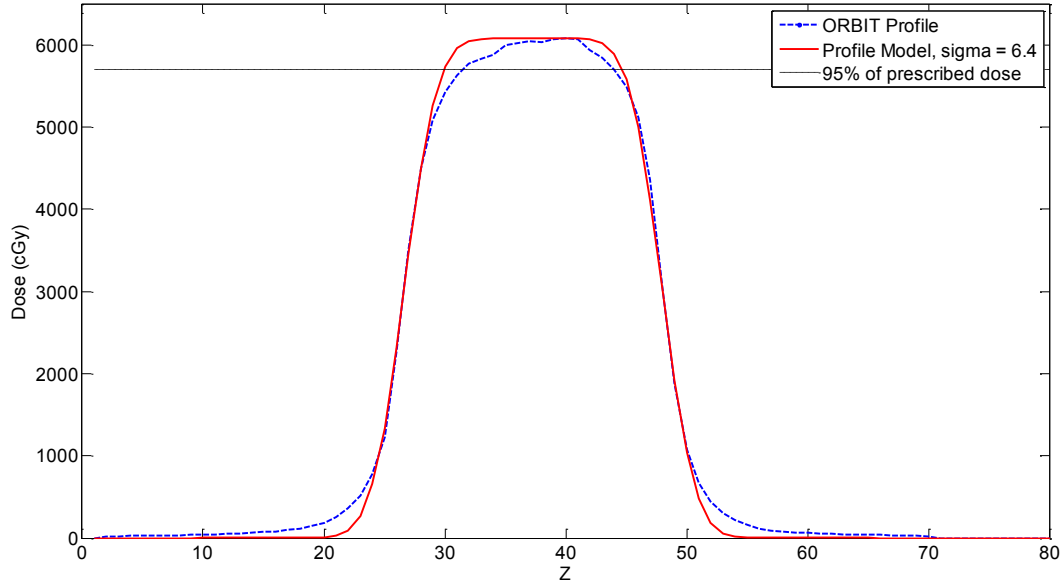
Figure 4.8: Comparison of static van Herk profile model constructed with a σ_p value of 6.4 mm to the ORBIT static dose profile for a 2cm lesion with 2cm peak-to-peak motion amplitude.

Although the general shapes of the two profiles are similar, there are distinct differences in the high dose region and the tails in the low dose region as seen with all of the 3DCRT and IMRT plans. This implies that 6.4 mm may not be the ideal σ_p value for every plan and should be further evaluated. For the above example, performing the convolution with a greater σ_p value may improve the fit of the model to the data as a narrower peak and wider bottom region of the profile would be produced. However, it is important to mention that the model fit in the 95% dose region in particular is of most importance as that is the level required for margin derivations. It should also be mentioned that a convolution of a top hat function is unable to model any non-uniformities in the beam profile, such as the asymmetry in the ORBIT profile shown in *Figure 4.8*. Non-uniformities generally occur due to the properties of the treatment beams or dose perturbations from variations in tissue density inside the patient.

4.4.2 Accuracy of σ_p value

Results for the experiments to find the σ_p values that best fit the static 3DCRT and IMRT profiles from the random error investigation described in *Section 3.1.7* are shown in *Table 4.6*. The does profile model with the σ_p value that yielded smallest SSR value between its corresponding ORBIT profile was determined to be the best fit. The general trend of the data illustrates an increase in the required σ_p value when fitting the 95% dose region as opposed to fitting all dose levels simultaneously. Interestingly, the IMRT plans possessed lower σ_p values than the 3DCRT plans on average indicating that slightly larger margins are in fact required to compensate for the steeper dose gradients. No statistically significant trends were noted between the σ_p values and lesion diameters.

Lesion Diameter	Motion Amplitude	3DCRT - σ_p value (mm)		IMRT - σ_p value (mm)	
		All points	D ≥ 95%	All points	D ≥ 95%
1 cm	1 cm	7.3	10.1	6.3	11.8
	2 cm	8.9	12.3	6.3	19.4
	3 cm	7.4	9.7	5.2	6.4
2 cm	1 cm	6.9	8.0	4.7	5.7
	2 cm	7.1	8.7	5.3	7.2
	3 cm	7.2	8.3	5.4	6.4
3 cm	1 cm	8.2	9.2	5.4	5.0
	2 cm	6.6	8.2	5.8	6.7
	3 cm	6.3	7.6	5.5	8.2

Table 4.6: σ_p values that best fit the 95% dose region and above as well as the entire dose profile for all 3DCRT and IMRT plans.

When comparing the fitted profile models to the actual profiles of each treatment plan, the single Gaussian assumption from the van Herk model is unable to simultaneously reproduce the high and low dose regions. The σ_p value that best fits the 95% dose region does not adequately model the lower dose regions, especially below 50% of the prescribed dose.

This can be observed in *Figure 4.9* which compares dose profiles created with various σ_p values to the dose profile of the actual treatment plan. In this example, the σ_p value of 8.7 mm was found to best fit the top 5% of the profile ($\geq$95% dose region) and fits the data best in the regions above 50% of the prescribed dose. However, the 7.1 mm σ_p value was found to be the best fit for the whole profile and more closely resembles the regions below. Since margins are derived based on the 95% dose region, choosing a σ_p value that accurately fits the high dose region should be made a priority. Based on the example in *Figure 4.9* depicting the 3DCRT plan for the 2cm lesion with a 2cm motion amplitude, the 8.7 mm σ_p value most closely resembles the 95% dose region while the other values are slightly larger, thus overestimating the margin. These results indicate that the approach proposed by Witte *et al.*[38] where the penumbra was modelled with the sum of two Gaussians described in *Section 2.4.2,* may be a better and more realistic approach when looking to represent the full dose profile more accurately.
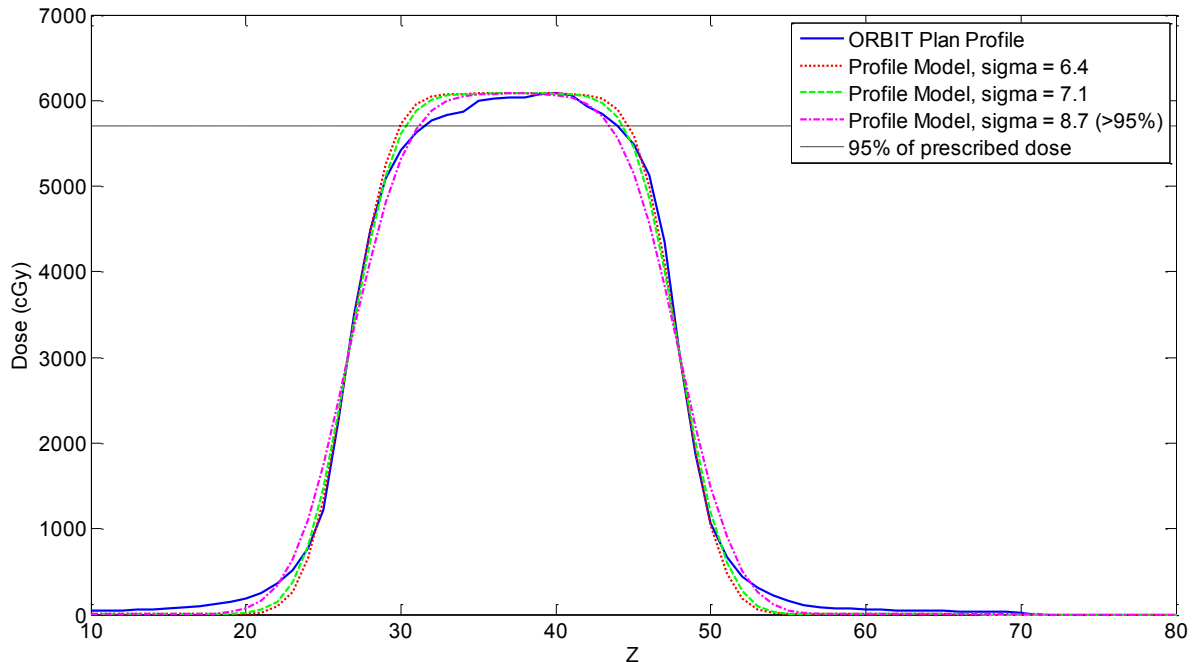

Figure 4.9: Comparison of static van Herk profile models constructed with various fitted σ_p values of a 2cm lesion with 2cm peak-to-peak motion to the actual static profile.

The convolution method's inability to model artefacts due to field inhomogeneities was especially encountered with the 1cm lesion diameters where heterogeneities had most effect. The density of the CTV compared to the surrounding lung within the small field sizes produced a bulge in the resulting dose profiles as demonstrated in *Figure 4.10*. Thus, fitting a simple Gaussian function proves to be difficult especially in the high dose regions which may result in unrealistically large σ_p values from the narrow peaks caused by the dense CTV. This was the case for the IMRT plan of the 1cm lesion with the 2cm peak-to-peak motion amplitude, which was observed to have a σ_p value of 19.4 mm (*Table 4.7*) and whose profile is shown in *Figure 4.10* as well. This issue has potential to become amplified with IMRT planning as the technique is capable of producing unconventional and irregularity shaped dose profiles.
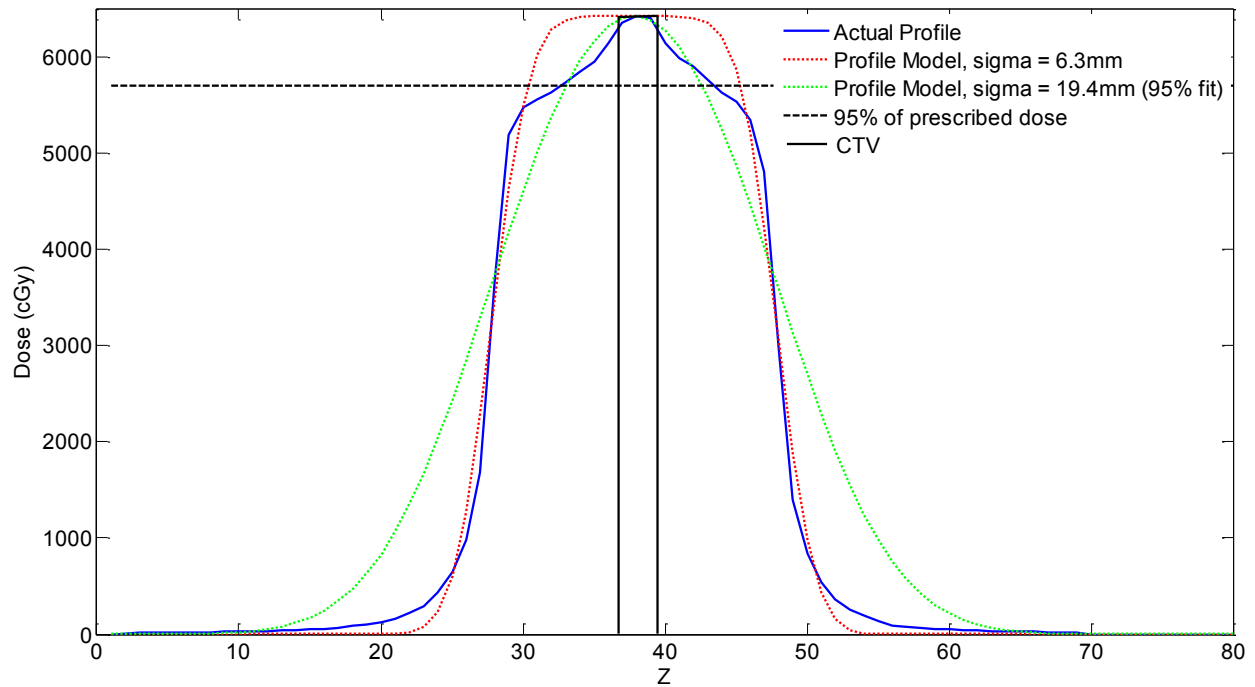
Figure 4.10: Profile of IMRT plan for the 1cm Lesion with 2cm motion amplitude compared to the van Herk models for the σ_p values fitted to the whole profile and top 5%. The bulge at the peak occurs at location of the CTV which is indicated by the purple top hat.

Although the σ_p value is crucial for margin derivations, the discrepancies between the full profile and $\geq$95% fit as well as the variation between plans may prove to be less clinically

93

relevant than anticipated. *Figure 4.11* plots the calculated margin for all three CTV motion amplitudes used in this study as a function of σ_p. It may be noticed that for many of the measured values of σ_p, the difference in the resulting PTV margin is less than the planning image resolution (2 mm slice thickness). Therefore, in these cases the PTV margin will not change with variations of σ_p as treatment planning systems are not able to contour between slices. In fact, it may be observed that for a 1 cm motion amplitude, the margin does not vary outside the scan resolution for the measured σ_p values and thus does not change. However, *Figure 4.11* also demonstrates that as the motion amplitude increases the PTV margins become more sensitive to variations in σ_p. Therefore, extra care should be taken for lesions with intermediate to large motion amplitudes.
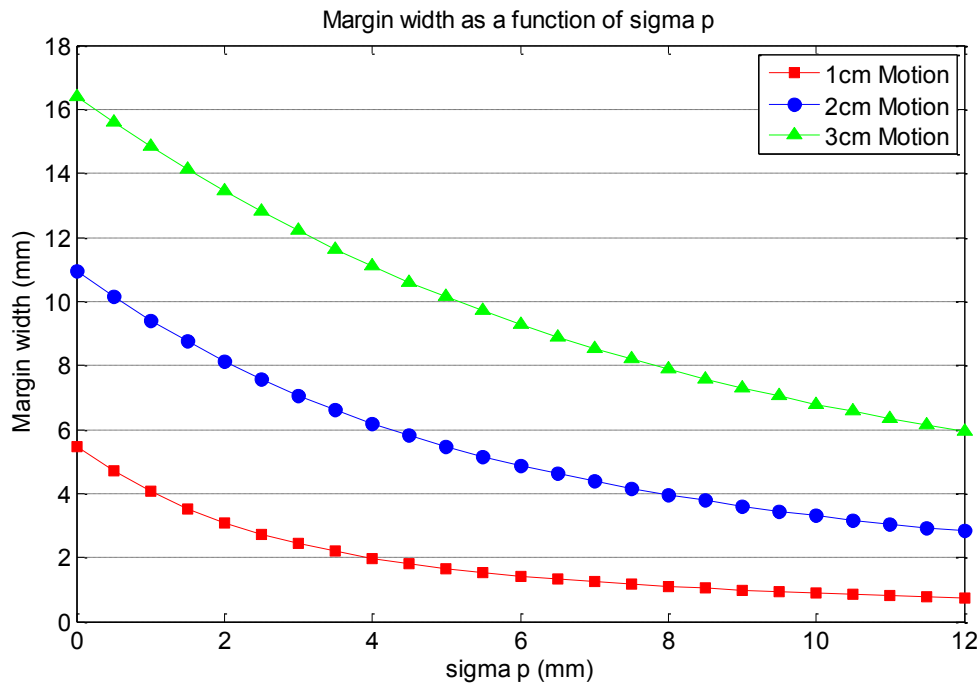

Figure 4.11: *Plot of the van Herk margin as a function of σ_p for the motion amplitudes used in this study. The horizontal axis is shown to indicate the σ_p value for which the margin will change in a plan with a 2mm slice thickness.*

## 4.4.3 Investigation of the van Herk blurred profile model

The second step in the VHMF derivation to achieve the blurred profile is the convolution of the static profile model with a Gaussian function of SD equal to σ_{random} which is the square root of the SDs of all random errors added in quadrature[17]. The accuracy of this blurred model was tested by convolving the ORBIT dose profiles with their corresponding Gaussian function with SD equivalent to one third of the peak-to-peak motion amplitude (σ_m) as described in Section 3.7.3. The resulting profile was then compared to its corresponding treatment plan constructed in the random error investigation (*Section 3.4*) that was accumulated over the respiratory cycle. As demonstrated in *Figure 4.12*, the convolution method is unable to simultaneously model the high and low dose regions of the accumulated profile extracted from ORBIT. This is very similar to the results of the previous two sections as convolution does a fairly good job at modelling the shrinkage of the high dose area and regions above 50% of the prescribed dose but fails in the regions below. This is because the dose accumulation method differs from convolution in that it employs deformable image registration techniques to map the dose back from each respiratory phase to the planned reference conditions. Thus, we do not see the same spread in the low dose region predicted by the van Herk model as the convolution approach is equivalent to shifting a dose profile to a series of random points along the respiratory cycle and computing the weighted sum of the profiles. Hence, the observed overestimation of the dose received at the ends of the motion ranges by the convolution method was also seen to increase as the peak-to-peak motion amplitude increased which can be observed by comparing *Figure 4.12 a)-c)*. Although we are more concerned with the reduction in the V_{95} for margin recipes, the convolution method's inability to accurately model lower

dose regions should be kept in mind during blurred dose evaluation, particularly with large

motion amplitudes.
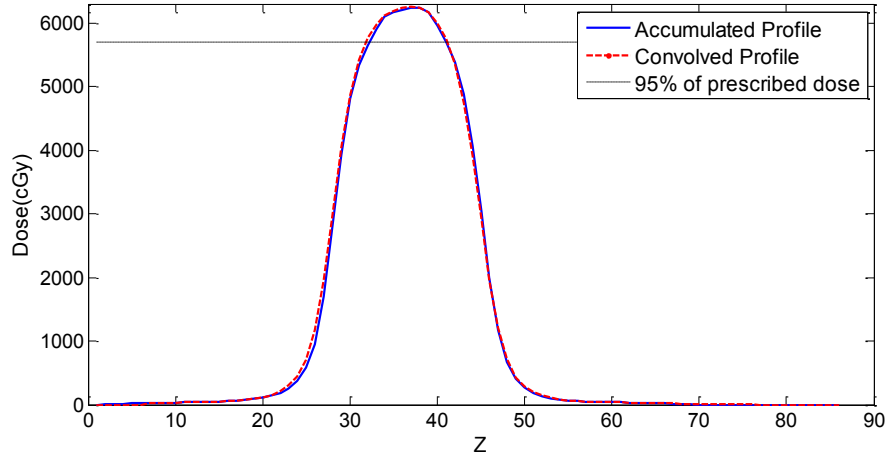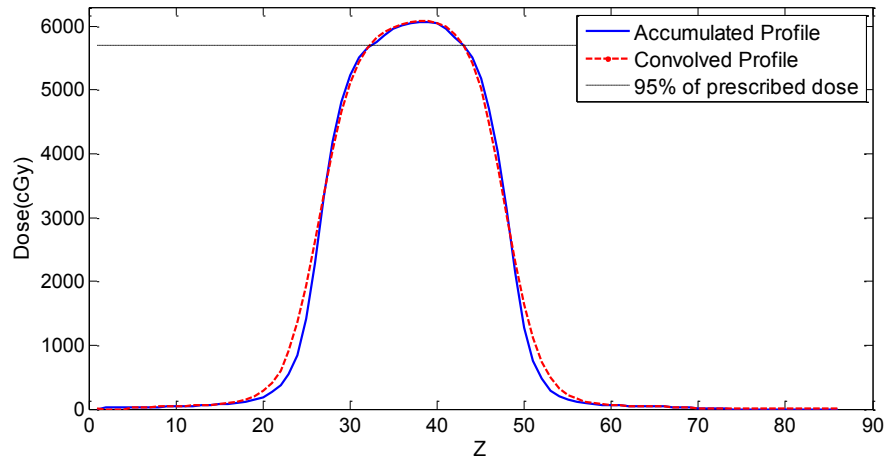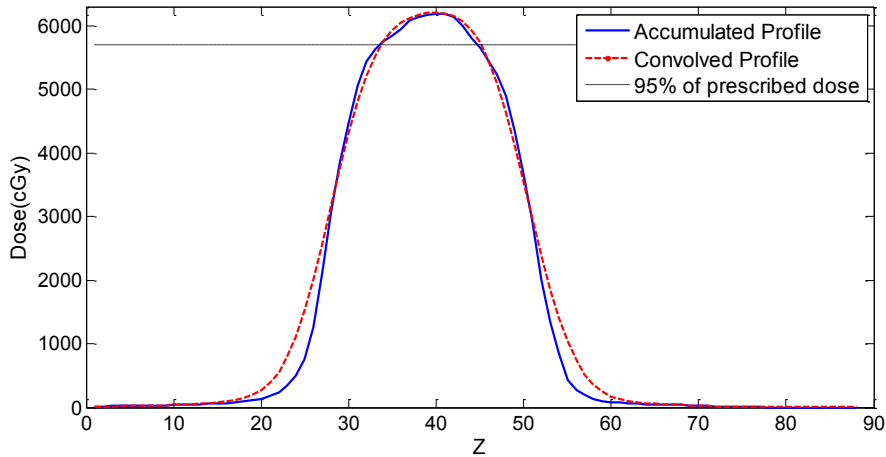
Figure 4.12: Comparison of the convolved static 3DCRTplan profiles to the accumulated plans for the 2cm lesion with a) 1cm b) 2cm and c) 3cm motion amplitude.

4.5 Investigation of plan conformity

The impact of the initial plan conformity was investigated by conducting the random error experiment described in *Section 3.4* for the 3cm lesion with 3cm motion amplitude again with more conformal plans. *Table 4.7* summarizes the results of the accumulated plans for the experiments and are displayed in *Figure 4.13*.

Initial Static Plan CN*	Accumulated V_{95} (%)*	Accumulated Plan CN†	Reduction in 95% Volume (%)
0.6	100	0.40	28
0.7	99.6	0.50	32
0.8	99.5	0.60	35
*PTV is the target volume used for the CN calculation			
† CTV is the target volume used for the CN calculation			

Table 4.7: Accumulated treatment plan data for the CN investigation.

It is apparent that all resulting accumulated plans provided adequate V_{95} values for the CTV. Although the accumulated plan conformity approached more acceptable values with more conformal plans, the highest CN possible was only 0.6 implying the VHMF constructs margins that are too large for realistic plan conformities.

Figure 4.13: Close-up saggital view of the static and accumulated 3DCRT plans constructed on the 3cm lesion with 3cm motion amplitude with initial CNs of a) 0.6, b) 0.7 and c) 0.8.

4.6 Suggested Improvements to the VHMF

4.6.1 Application of the VHMF to the ITV concept
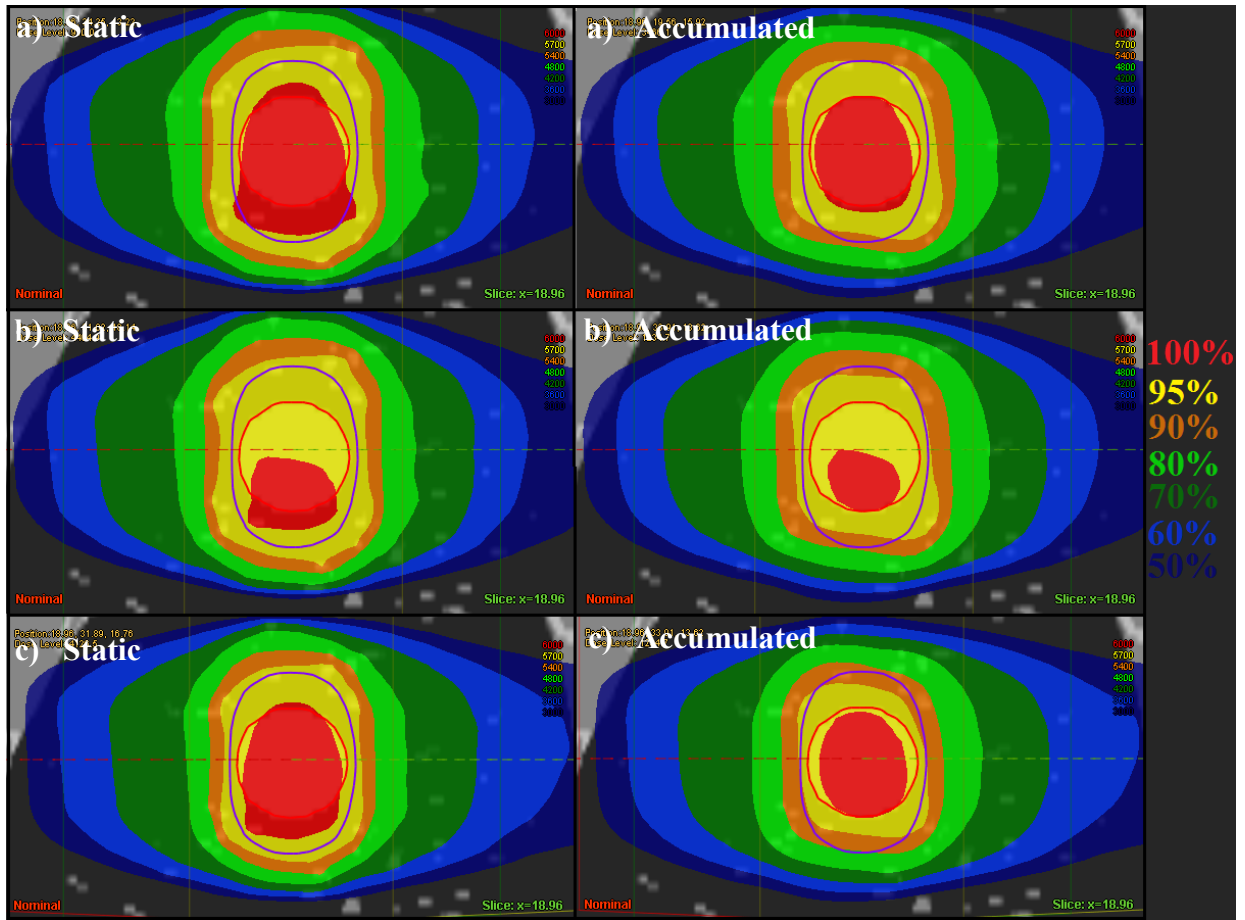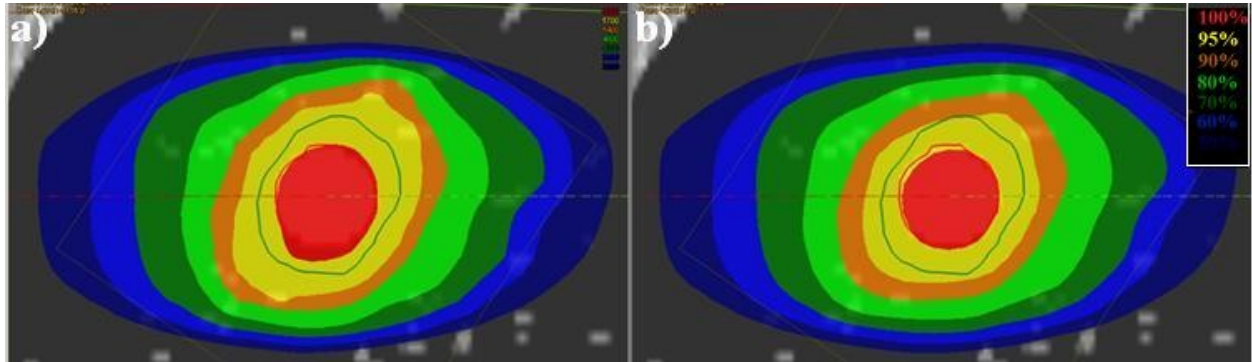

Figure 4.14: Close-up saggital view of the a) static and b) accumulated 3DCRT treatment plans with the PTV constructed in the rotated coordinate system for the 2cm lesion with 2cm motion.

In S*ection 4.1.2* the inability of the VHMF to account for the motion trajectory of the CTV was established. The accumulated plans possessed poor CNs due to an unnecessarily treated volume of healthy tissue left at the periphery of the CTV when it does not move along the cardinal axis as illustrated earlier in *Figure 4.3*. In order to improve upon this shortcoming of the VHMF, a modification was applied to the existing coordinate system so it coincides with the CTV motion trajectory and was evaluated for the 2cm lesion diameter with 2cm motion amplitude.

A sagittal view of the accumulated treatment plan for the 2cm lesion with 2cm motion amplitude is depicted in *Figure 4.15b* which yielded 100% target coverage of the 95% dose volume and a CN of 0.35 around the CTV. It may be recalled that the accumulated V_{95} and CN values constructed in the original coordinate system were 99.9% and 0.43 respectively, as previously displayed in *Table 4.1 and 4.2*. Thus, the rotated coordinate system yielded a less

conformal accumulated plan compared to the original experiment conducted with the original

van herk PTV margin (*Figure 4.15*).
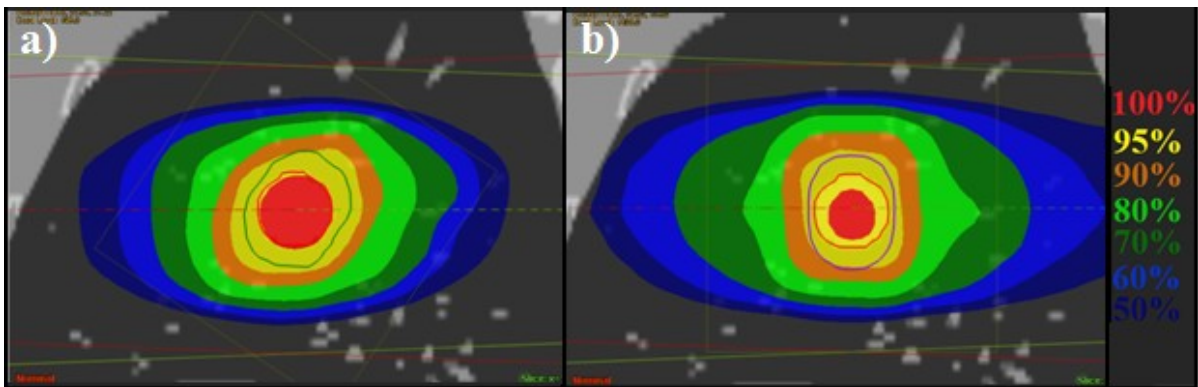
Figure 4.15: Close-up saggital view of the accumulated 3DCRT treatment plans in a) the rotated coordinate system and b) the original coordinate system for the 2cm lesion with 2cm motion.

Upon further analysis, it was revealed that the 95% dose volume in the rotated coordinate system shrunk by 23% of its original size whereas the plan constructed in the original coordinate system shrunk by 27% as previously revealed in *Table 4.2*. This explains the lower accumulated plan conformity of the rotated PTV as the 95% dose volume shrank 4% less than the original plan, constituting a 9 dose grid voxel difference. The reason behind this reduced shrinkage is due to the fact that the high dose region is now designed along the motion trajectory of the CTV. Therefore, for the plan with the rotated PTV, the CTV stays in the high dose region for a larger portion of the respiratory cycle and in turn shrinks less compared to the original plan. Now that the motion trajectory has been accounted for and yielded even lower accumulated plan conformities, our suspicion that the VHMF predicts PTV margins that are in fact larger than required for adequate CTV dose coverage is further reinforced.

CHAPTER 5

SUMMARY OF RESULTS, CONCLUSIONS AND FUTURE WORK

5.1 Summary of Results and Conclusions

In this work we have simulated the random and systematic variations in respiratory motion using treatment planning software utilizing realistic dose calculation algorithms, deformable dose accumulation algorithms and respiratory motion modelling. This allowed us to compare realistic dose distributions to their corresponding dose model assumed by the VHMF. We investigated the VHMF's ability to account for variations in tissue density, lesion size and motion amplitude. The results of these experiments confirmed the robustness of the VHMF for random and systematic respiratory motion errors in lung radiotherapy, despite the adoption of certain assumptions that some feel limit its clinical application. The VHMF succeeded in maintaining adequate CTV coverage by 95% of the prescribed dose for both 3DCRT and IMRT dose distributions and for the realistic lesion sizes and motion amplitudes investigated with the exception of small targets in soft tissue. These results are consistent with those of *Witte et al.*[38]and supports the safe clinical application of the VHMF for the successfully tested cases. However, we did not demonstrate a size dependence as did Witte *et al.* due to the fact that we only tested the original VHMF which showed to be conservative. A size dependence may have been shown if we found the smallest possible PTV margin for each lesion size.

Although there has been a clear demonstration of the VHMF's ability to account for the various lesion sizes and motion amplitudes, we also revealed some disagreements between the

VHMF dose profile models and realistic lung radiation therapy treatment plan profiles. This was apparent for both the random and systematic error simulations as the van Herk model is unable to account for tissue density changes in the path of the beam. Despite this, the simplified dose model and realistic treatment plans agreed at the 95% dose level for all tested cases which is pertinent for margin derivations. Therefore, the ability of the VHMF to produce adequate CTV coverage in the presence of random and systematic errors was not compromised. Nevertheless, these limitations should be recognized if the convolution method is utilized for plan evaluation as it yields inaccurate results particularly in the low dose regions for large motion amplitudes.

Additional limitations encountered in this study were inherent in the resolution of the dose grid and CT data. Firstly, when testing the VHMF, all PTV margin widths were rounded up to the nearest voxel as treatment planning software cannot contour smaller than the resolution. The dose grid resolution also limited the dose coverage accuracy for the small lesions as one slightly under dosed voxel could account for a large percentage of the target volume. This means a coarse dose grid has potential to overestimate the under dosage of small lesions in comparison to larger lesions with the same distribution dose within the target. The dose grid resolution also limits the initial plan conformity for small lesion sizes, as seen with the 1cm CTV diameter treatment plans. Although these effects can be minimized by increasing the spatial resolution of the images and dose grid, we kept all parameters at realistic values to best represent how these situations would be handled in a clinical setting, maintain reasonable computational times and avoid situations where software stops responding.

We developed a novel planning approach using the VHMF applied to the ITV concept which solves the problem of the VHMF's inability to account for realistic CTV the motion trajectories during respiratory motion.

In conclusion, we showed that although the dose model and convolution assumption do fall short in creating realistic profile shapes for lung, it is able to accurately predict the 95% dose level required for margin derivation provided the correct penumbra width is chosen. Thus, it can predict full CTV dose coverage in the presence of random and systematic geometrical uncertainties. However, the VHMF does not need to be adjusted for lesion size, treatment type and tissue density as originally hypothesized. In fact, we confirmed that the VHMF is insensitive to lesion size and treatment type with realistic plan conformities and can adequately compensate for low density media by inputting an accurate σ_p value. Instead, the VHMF should be adjusted to account for more realistic plan conformities.

The assumption of perfect plan conformity in the derivation predicted PTV margins than were slightly larger than required in practice and should be. Therefore, we can classify constructing PTV margins with the VHMF as a conservative planning approach. Despite this, the application of the VHMF and the modified ITV techniques do provide some opportunity for dose escalation over the traditional ITV concept which is commonly used and yields a larger PTV margin.

5.2 Future work

Future work continuing from this study should include further modification of the VHMF to account for the assumption of perfect plan conformity. Theoretically, reducing the PTV margin by the distance of the 95% isodose line from the edge of the PTV is the simplest option. However, in practice, this approach is limited by the dose grid resolution and requires

the construction of a preliminary treatment plan for the measurement. Instead, guidelines should be established on how much PTV margins calculated with the VHMF can be safely reduced for specific plan conformities and metrics that will aide in safely making these judgements should be established. The modified ITV approach should also be evaluated while simultaneously simulating random and systematic errors which is more representative of a real treatment. Finally, a comprehensive study comparing the modified margin recipe with current clinical lung planning protocols on patient planning and treatment images is needed to assess the safety of its clinical application and potential for dose escalation.

REFERENCES

1 Canadian Cancer Society's Steering Committee on Cancer Statistics, "Canadian Cancer Statistics 2011," (2011).

2 Murat Beyzadeoglu, Gokhan Ozyigit and Cuneyt Ebruli, Basic Radiation Oncology, (Springer, Berlin/Heidelberg, DEU, 2010).

3 C. J. Karzmark, C. S. Nunan and E. Tanabe, Medical electron accelerators, (McGraw-Hill, Inc, Health Professions Division, 1993).

4 E. B. Podgorsak, editor, Radiation oncology physics : a handbook for teachers and students., (International Atomic Energy Agency, Vienna, 2005).

5 Philips Medical Systems, "Pinnacle Planning Reference Guide: Release 9." Document number 4535 604 45201 A, (2009).

6 International Commission on Radiation Units and Measurements (ICRU), Prescribing, recording and reporting photon beam therapy. ICRU-50, (ICRU, Bethesda, MD, 1993).

7 International Commission on Radiation Units and Measurements (ICRU), Prescribing, recording and reporting photon beam therapy (Supplement to ICRU Report 50) ICRU-62, (ICRU, Bethesda, MD, 1999), .

8 B. Emami et al., "Tolerance of normal tissue to therapeutic irradiation," Int.J.Radiat.Oncol.Biol.Phys. 21 (1), 109-122 (1991).

9 J. W. H. Wolthaus *et al.*, "Comparison of Different Strategies to Use Four-Dimensional Computed Tomography in Treatment Planning for Lung Cancer Patients," Int.J.Radiat.Oncol.Biol.Phys. 70 (4), 1229-1238 (2008).

10 James A. Purdy, "Dose to normal tissues outside the radiation therapy patient's treated volume: a review of different radiation therapy techniques." Health Phys. 95 (5), 666-676 (2008).

11 R. R. Patel and M. Mehta, "Three-dimensional conformal radiotherapy for lung cancer: promises and pitfalls," Curr.Oncol.Rep. 4 (4), 347-353 (2002).

12 Faiz M. Khan, <u>The physics of radiation therapy</u>, 3rd ed. ed. (Lippincott Williams & Wilkins, Philadelphia, 2003).

13 Bongile Mzenda *et al.*, "Determination of target volumes in radiotherapy and the implications of technological advances: a literature review," Journal of Radiotherapy in Practice 8 (01), 41 (2009).

14 L. Xing *et al.*, "Overview of image-guided radiation therapy," Med.Dosim. 31 (2), 91-112 (2006).

15 F-F Yin *et al.*, "The role of in-room kV X-ray imaging for patient setup and target localization. Report of AAMP Task Group 104," AAMP 104, (2009).

16 D. A. Jaffray and J. H. Siewerdsen, "Cone-beam computed tomography with a flat-panel imager: initial performance characterization," Med.Phys. 27 (6), 1311-1323 (2000).

17 M. van Herk *et al.*, "The probability of correct target dosage: dose-population histograms for deriving treatment margins in radiotherapy." Int.J.Radiat.Oncol.Biol.Phys. 47 (4), 1121-1135 (2000).

18 P. J. White, R. D. Zwicker and D. T. Huang, "Comparison of dose homogeneity effects due to electron equilibrium loss in lung for 6 MV and 18 MV photons." Int.J.Radiat.Oncol.Biol.Phys. 34 (5), 1141-1146 (1996).

19 R. C. Miller, J. A. Bonner and R. W. Kline, "Impact of beam energy and field margin on penumbra at lung tumor-lung parenchyma interfaces." Int.J.Radiat.Oncol.Biol.Phys. 41 (3), 707-713 (1998).

20 M. A. Hunt *et al.*, "Effect of low-density lateral interfaces on soft-tissue doses." Int.J.Radiat.Oncol.Biol.Phys. 37 (2), 475-482 (1997).

21 K. E. Ekstrand and W. H. Barnes, "Pitfalls in the use of high energy X rays to treat tumors in the lung," Int.J.Radiat.Oncol.Biol.Phys. 18 (1), 249-252 (1990).

22 R. O. Kornelsen and M. E. Young, "Changes in the dose-profile of a 10 MV x-ray beam within and beyond low density material." Med.Phys. 9 (1), 114-116 (1982).

23 Hiroki Shirato *et al.*, "Intrafractional tumor motion: lung and liver," Semin.Radiat.Oncol. 14 (1), 10-18 (2004).

24 Yvette Seppenwoolde *et al.*, "Precise and real-time measurement of 3D tumor motion in lung due to breathing and heartbeat, measured during radiotherapy," Int.J.Radiat.Oncol.Biol.Phys. 53 (4), 822-834 (2002).

25 L. Ekberg *et al.*, "What margins should be added to the clinical target volume in radiotherapy treatment planning for lung cancer?" Radiother.Oncol. 48 (1), 71-77 (1998).

26 P. Keall *et al.*, "The management of respiratory motion in radiation oncology report of AAPM Task Group 76," Med.Phys. 33 (10), 3874-3900 (2006).

27 R. W. Underberg *et al.*, "Use of maximum intensity projections (MIP) for target volume generation in 4DCT scans for lung cancer," Int.J.Radiat.Oncol.Biol.Phys. 63 (1), 253-260 (2005).

28 P. Keall, "4-Dimensional Computed Tomography Imaging and Treatment Planning," Semin.Radiat.Oncol. 14 (1), 81-90 (2004).

29 J. W. Wolthaus *et al.*, "Mid-ventilation CT scan construction from four-dimensional respiration-correlated CT scans for radiotherapy planning of lung cancer patients," Int.J.Radiat.Oncol.Biol.Phys. 65 (5), 1560-1571 (2006).

30 I. Buzurovic, Y. Yu and T. K. Podder, "Active Tracking and Dynamic Dose Delivery for robotic couch in radiation therapy," Conf.Proc.IEEE Eng.Med.Biol.Soc. 2011, 2156-2159 (2011).

31 Timothy C. Y. Chan, Thomas Bortfeld and John N. Tsitsiklis, "A robust approach to IMRT optimization," Phys.Med.Biol. 51 (10), 2567-2583 (2006).

32 M. Gui *et al.*, "Four-dimensional intensity-modulated radiation therapy planning for dynamic tracking using a direct aperture deformation (DAD) method," Med.Phys. 37 (5), 1966-1975 (2010).

33 X. Li *et al.*, "A 4D IMRT planning method using deformable image registration to improve normal tissue sparing with contemporary delivery techniques," Radiation Oncology 6 (1), (2011).

34 Y. Suh *et al.*, "Four-dimensional IMRT treatment planning using a DMLC motion-tracking algorithm," Phys.Med.Biol. 54 (12), 3821-3835 (2009).

35 Y. Suh *et al.*, "A deliverable four-dimensional intensity-modulated radiation therapy-planning method for dynamic multileaf collimator tumor tracking delivery," Int.J.Radiat.Oncol.Biol.Phys. 71 (5), 1526-1536 (2008).

36 M. van Herk *et al.*, "Biologic and physical fractionation effects of random geometric errors," Int.J.Radiat.Oncol.Biol.Phys. 57 (5), 1460-1471 (2003).

37 M. van Herk, "Errors and margins in radiotherapy," Semin.Radiat.Oncol. 14 (1), 52-64 (2004).

38 M. G. Witte *et al.*, "The effects of target size and tissue density on the minimum margin required for random errors," Med.Phys. 31 (11), 3068-3079 (2004).

39 J. J. Sonke, J. Lebesque and M. van Herk, "Variability of four-dimensional computed tomography patient models," Int.J.Radiat.Oncol.Biol.Phys. 70 (2), 590-598 (2008).

40 Alan L. McKenzie, Marcel van Herk and Ben Mijnheer, "The width of margins in radiotherapy treatment plans," Phys.Med.Biol. 45 (11), 3331-3342 (2000).

41 W. P. Segars *et al.*, "4D XCAT phantom for multimodality imaging research," Med.Phys. 37 (9), 4902-4915 (2010).

42 W. P. Segars *et al.*, "Realistic CT simulation using the 4D XCAT phantom," Med.Phys. 35 (8), 3800-3808 (2008).

43 L. Piegl, "On NURBS: a survey," IEEE Comput.Grap.Appl. 11 (1), 55-71 (1991).

44 National Library of Medicine, "The Visible Human Project[®]," , (April 6th, 2012).

45 W. P. Segars and B. Tsui, "MCAT to XCAT: The Evolution of 4-D Computerized Phantoms for Imaging Research," Proceedings of the IEEE 97 (12), 1954-1968 (2009).

46 T. McNutt , "Dose calculations: collapsed cone convolution superposition and delta pixel beam. Pinnacle White Paper No. 4535 983 02474," Andover, MA: Philips Medical System, (2002).

47 D. Yan, D. A. Jaffray and J. W. Wong, "A model to accumulate fractionated dose in a deforming organ," Int.J.Radiat.Oncol.Biol.Phys. 44 (3), 665-675 (1999).

48 A. M. Loening and S. S. Gambhir, "AMIDE: a free software tool for multimodality medical image analysis," Mol.Imaging 2 (3), 131-137 (2003).

49 M. J. Edelman *et al.*, "Radiation Therapy Oncology Group Protocol 0839: Randomized Phase II Study of Pre-Operative Chemoradiotherapy +/- Panitumumab (IND #110152) Followed By Consolidation Chemotherapy In Potentially Operable Locally Advanced (Stage IIIA, N2+) Non-Small Cell Lung Cancer," RTOG 0839, (Februaru 9th, 2012).

50 L. Wang *et al.*, "Dosimetric advantage of using 6 MV over 15 MV photons in conformal therapy of lung cancer: Monte Carlo studies in patient geometries." J.appl.clin.med.phys. 3 (1), 51-59 (2002).

51 L. Feuvret *et al.*, "Conformity index: a review," Int.J.Radiat.Oncol.Biol.Phys. 64 (2), 333-342 (2006).

52 J. Higgins *et al.*, "Effect of image-guidance frequency on geometric accuracy and setup margins in radiotherapy for locally advanced lung cancer," Int.J.Radiat.Oncol.Biol.Phys. 80 (5), 1330-1337 (2011).

53 M. Rosu *et al.*, "Dose reconstruction in deforming lung anatomy: dose grid size effects and clinical implications," Med.Phys. 32 (8), 2487-2495 (2005).